NON-INVASIVE MONITORING OF MICROBIAL INDUCED OIL DEGRADATION IN BEACH SEDIMENT UNDER HIGH CONDUCTIVITY CONDITIONS USING THE SPECTRAL INDUCED POLARIZATION METHOD

By Christine M. Kimak

A thesis submitted to the

Graduate School-Newark

Rutgers, The State University of New Jersey

in partial fulfillment of requirements

for the degree of

Master of Science

Graduate Program in Environmental Science

Written under the direction of

Assistant Research Professor Dimitrios Ntarlagiannis

and approved by

_____

_____

_____

_____

Newark, New Jersey

October, 2015

Non-Invasive Monitoring of Microbial Induced Oil Degradation in Beach Sediment Under High Conductivity Conditions Using the Spectral Induced Polarization Method

By Christine M. Kimak

Thesis Director: Assistant Research Professor Dimitrios Ntarlagiannis

Massive oil spills, such as the Deepwater Horizon oil spill in April 2010, have prompted increased research and attention on the techniques available to monitor oil spills, including degradation processes, and have highlighted the limitations of existing monitoring methods. Previous research has shown the spectral induced polarization method (SIP) to be sensitive to the biogeochemical changes that occur as a result of microbial oil degradation; however, there is no research on the applicability of the SIP method under high conductivity conditions typical of coastal environments. The purpose of this study is to monitor natural attenuation of microbial oil degradation in brackish coastal sediment. Natural attenuation is of primary importance since in many instances, such as for remote and inaccessible areas, it is the only option available for remediation. This research is based on the hypothesis that biogeochemical changes due to microbially-induced processes can generate detectable SIP signals, even under high conductivity environments.

Five different treatments of heavy oil contaminated sediment were run for 143 days. Results indicated that geophysical signals were more pronounced in the columns with conductivities close to the actual field conditions from where the sediments were collected. Gas Chromatography/Mass Spectrometry analysis showed decreased peaks in

the chromatograms of active columns compared to control columns, as well as the appearance of metabolites, indicating degradation of the substrate (contaminant oil).

The results show that SIP is sensitive to the biogeochemical changes occurring as a result of microbial oil degradation even under high conductivity conditions, indicating that it could be a useful tool to non-invasively monitor natural attenuation within brackish environments.

ACKNOWLEDGEMENTS

My thanks to Dr. Dimitris Ntarlagiannis for all his support, guidance, patience, and advice throughout the duration of this research. He gave me a "crash course" in geophysics and I can't say how much I appreciate all his trust in letting me run this experiment; I certainly learned more than I ever thought I would. Thanks to my thesis committee: Drs. Estella Atekwana, Yves Robert Personna, and Lee Slater for all their time and effort; their advice and recommendations made this project all the better. Thank you also to Dr. Abigail Porter for providing the GC/MS analysis and helping with data interpretation. Special thanks to Ms. Liz Morrin for the logistical and departmental support. I would also like to thank Jan Olechowski who spent an entire summer with me building the columns, setting everything up, and getting us ready to take our first set of measurements. Lastly, thanks to all the faculty, staff, and students of the Earth and Environmental Science Department at Rutgers-Newark.

This work was partially supported by the Chevron Energy Corporation under Grant #433700.

TABLE OF CONTENTS

LIST OF TABLES

LIST OF FIGURES

INTRODUCTION

Background

Microorganisms are very efficient in situ degraders of toxic organic chemicals (Madsen, 1991). Bioremediation of pollutants relies on the innate biodegradative capabilities of microorganisms and exploits those processes in the context of pollutants deemed undesirable (Madsen, 1991). However, efforts to verify biodegradation processes are limited by methodology (Madsen, 1991; Bekins et al., 2001; Allen et al., 2007; Atlas et al., 2009). In addition to the traditional methods, relying on sampling and analyses for monitoring biodegradation, attention has been given to geophysical methods since they offer certain advantages (e.g. non invasive, cost efficient, spatial and temporal resolution). One such method that recent research has shown to have promise in this area is the spectral induced polarization (SIP) method (Abdel Aal; et al., 2004; Abdel Aal et al., 2006; Davis et al., 2006; Heenan et al., 2013). Most biodegradation related SIP research has focused on freshwater environments (Atekwana et al., 2000; Bekins et al., 2001; Werkema et al., 2003; Atekwana et al., 2004; Schmutz et al., 2010; Abdel Aal et al., 2006; Heenan et al., 2013) and since most oil spills commonly occur in marine environments, there is a need to determine the applicability of the SIP technique as an oil degradation monitoring tool in coastal environments.

Oil biodegradation occurs at the oil-water interface and first involves degradation of lower molecular weight constituents, such as single bonded alkanes, due to the minimal energy needed to break them down. The rate of biodegradation then slows with the removal of these more easily degraded components (Personna et al., 2014). Some of the factors that can increase biodegradation include an increase in the surface area to volume

ratio of the oil, increases in microorganisms capable of degrading the oil, and the inherent biodegradability of the contaminant (Personna et al, 2014).

Research into in situ biodegradation has shown how difficult biodegradation is to prove, mainly due to errors involved in assembling mass balances and attempting to distinguish biotic from abiotic processes (Madsen, 1991). Some of these abiotic processes include a variety of physical, chemical, and biological factors such as oil dilution from turbulence and currents (Personna et al., 2014), underground water flows, winds, physical washout, dissolution, and volatilization (Venosa et al., 1996). Additionally, sand contaminated with oil can be moved by tidal action, winds, currents, and human and animal activities (Venosa et al., 1996). The effects of tidal action on hydrocarbon degradation specifically can be significant. Permeability and capillarity both impact subsurface flow and mixing, leading to physical removal of the contaminant (Geng et al., 2014).

In order to ascertain whether hydrocarbon degradation is progressing in a manner sufficient for natural attenuation, information on microbial activity and the resulting biogeochemical reactions is needed. In order to demonstrate the effectiveness of a bioremediation treatment, systematic monitoring and evaluation must be implemented (Heitzer et al., 1993; Phelps et al., 2002; Löffler et al., 2006; Kostka et al., 2011; Liu et al., 2012). After confirmation of geochemical changes in the sediment and surrounding pore space, SIP can potentially be used to non-invasively monitor the natural attenuation.

Some of these geochemical changes are a result of microbial growth; biodegradation can cause chemical changes from variations in Eh and pH, biogenic gas production, and the presence of metabolic by-products such as organic acids and biosurfactants

(Atekwana and Slater 2009). Additionally, microbial activity can cause changes to the oil properties such as wettability, due to the production of biosurfactants (Abdel Aal et al., 2014). Wettability is the tendency of a fluid to adhere or adsorb to a solid surface in the presence of another immiscible fluid; it is a measure of the affinity of the soil mineral surface for the oil or water phase (Abdel Aal et al., 2014). Additionally, microbial biodegradation affects the physical properties and molecular composition of crude oil, leading to a decrease in low molecular weight compounds (Abdel Aal et al., 2014).

Deepwater Horizon (DWH) oil spill

On April 20, 2010, our nation experienced the worst oil spill in its history. The Macondo 252 oil well, located 45 miles off the coast of Louisiana, experienced a blow out that resulted in a major explosion and the ultimate sinking of the Mobile Offshore Drilling Unit Deepwater Horizon (DWH) (Figure 1). For almost three months, the Gulf of Mexico experienced a continuous discharge of crude oil 1500 m below the surface of the ocean. Of the approximately 4.9 million barrels released, a significant portion ultimately made its way to the Gulf shoreline. Efforts to prevent a shoreline impact were in some cases successful; however, a significant amount of this oil remains trapped within the coastal beach sediment (CG ISPR, 2011; Kostka et al., 2011). This incident illustrates the need to improve upon not only oil remediation techniques, but also the technologies that we can employ to monitor oil degradation processes, particularly that of natural attenuation, in various remote and sensitive coastal environments, typically with limited access.

Figure 1. Location of the Deepwater Horizon oil well. Image courtesy of Encyclopedia Britannica.

Following this unprecedented disaster, a large number of studies were undertaken to determine the impact of the spill on the ecosystems within the Gulf of Mexico. One such study by Kostka et al., 2011 examined the in situ response of indigenous bacterial communities within the coastal ecosystems. These coastal ecosystems are dominated by permeable sandy sediments which are covered with biofilms of the various microbial communities (Kostka et al., 2011). These communities thrive because of the high exchange of nutrients and waste products as a result of the highly permeable nature of the sediment (Kostka et al., 2011). As demonstrated previously, oil degradation by microorganisms is the main driver of hydrocarbon removal in seawater, marshlands, and beach sediment (Madsen, 1991; Pritchard et al., 1991; Löeffler et al., 2006; Liu et al., 2012; Kostka et al., 2011). Specifically, biodegradation has a proven track record of successfully remediating oil contamination within shorelines dominated by permeable

beach sediment (Lindstrom et al., 1991; Bragg et al., 1992; Rosenberg et al., 1996). However, limits exist on how we can monitor this progress in brackish environments, save for costly and time consuming field sampling. While point sampling methods cannot be eliminated completely during oil removal operations, geophysical methods can be used complementary to make them more efficient and reduce their frequency. This research aims to study one option for non-invasive geophysical monitoring that could allow for more efficient oil spill evolution monitoring with large spatial coverage.

A precursor study to this experiment deployed an autonomous resistivity monitoring system in Grand Terre, LA in order to monitor natural degradation processes in hydrocarbon contaminated beach sediments (Heenan et al., 2015). This experiment was the first to study the evolution of the subsurface electric properties as a young oil spill matures in a coastal environment. Results indicated a progressive decrease in resistivity partly attributed to microbial induced mineral weathering and oil emulsion (due to biosurfactant production). This decrease was likely driven by the microbial degradation of the contaminant (Heenan et al., 2015). Microbes capable of degrading the oil were confirmed in situ and their degradation processes resulted in alterations in pore-fluid chemistry, the formation and/or removal of solid phases, and the addition of biodegradation by-products, all of which can alter the geophysical signals (Heenan et al., 2015). Additionally, degradation of benzene and toluene in microcosm studies suggested that the microorganisms had recently been exposed to hydrocarbons (likely from the DWH spill) (Heenan et al., 2015).

Geophysical monitoring

Previous research has shown the spectral induced polarization method (SIP) and electrical resistivity imaging (ERI) to be sensitive to the biogeochemical changes that occur as a result of microbial oil degradation (Atekwana et al., 2000; Atekwana et al., 2004; Abdel Aal et al., 2004; Abdel Aal et al., 2006; Schmutz et al., 2010; Heenan et al,. 2013). Electrical geophysical methods can offer almost real time monitoring of degradation processes, with high spatial and temporal resolution (Slater and Atekwana, 2013). Areas contaminated by hydrocarbons are typically found to exhibit an enhanced induced-polarization (IP) response, the result of which can be attributed to oil degradation, in many instances due to microbial processes (Abdel Aal et al., 2006). Biogeochemical changes due to oil degradation can generate distinctive IP signatures that can be used to noninvasively monitor microbial hydrocarbon degradation (Atekwana et al., 2000; Bekins et al., 2001; Werkema et al., 2003; Atekwana et al., 2004; Abdel Aal et al., 2006; Davis et al., 2006). Conceivably, geophysical methods can render oil remediation more efficient by guiding the direct sampling and limiting the volume of point sampling and analysis. Additionally, this real-time analysis will lead to more efficient treatment in the case of enhanced remediation and improve upon recovery efforts.

Geophysical signatures are typically associated with presence of microorganisms and/or their activity. In one study by Heenan et al., 2013, the main driver of SIP signals was found to be related to microbially-induced oil degradation, likely associated with alteration of oil properties, such as the production of biosurfactants and organic acids.

Organic acid production can affect surface roughness and surface area, both of which can cause variations in the SIP response (Heenan et al., 2013).

Additional research on SIP response to microbial oil degradation has shown that wettability, saturation, and the physiochemical properties of the organic contaminant can all affect SIP signatures (Schmutz et al., 2010; Schmutz et al., 2012; Abdel Aal et al., 2014). The wettability alteration is caused by the production of biosurfactants that enhance the solubility and reduce the surface tension of the oil adsorbed on the mineral grain surfaces (Abdel Aal et al., 2014).

Hypothesis

I hypothesize that microbial driven oil degradation will create biogeochemical changes that can generate SIP signals, detectable even under high conductivity environments. This could render the SIP method as the monitoring tool of choice for monitored natural attenuation (MNA) in brackish environments, such as marshes and wetlands.

Objectives

The main objective of this experiment is to determine whether the SIP method is sensitive to biogeochemical changes, as a result of oil degradation, under high conductivity conditions. To achieve this, a laboratory experiment was performed to monitor natural attenuation of microbial oil degradation in brackish beach sediment. During this experiment, SIP measurements were recorded and linked to microbial oil degradation as evidenced by microbiological and geochemical monitoring. To our knowledge, this is the first such study to geophysically monitor this process under high conductivity conditions.

Biogeochemical Changes

Microbial breakdown of contaminants can be related to geophysical signatures due to changes in fluid conductivity (Atekwana et al., 2000; Atekwana et al., 2004). Furthermore, geophysical signals can be associated with the activity of microorganisms within the medium (Atekwana and Slater, 2009; Ntarlagiannis et al., 2005a; Ntarlagiannis et al., 2005b; Davis et al., 2006). Figure 2 (Heenan et al., 2013) summarizes the interactions between microbes and the sediment and pore space, and the resulting biochemical changes that these interactions induce. When microbes are utilizing oil as the carbon source, changes in chemistry, such as organic acid, biogenic gas, and biosurfactant production, and changes in Eh and pH take place. This in turn leads to the dissolution and precipitation of minerals, further causing both chemical (in the electrical double layer and organic acid production that alters the ion concentration) and physical (wetting phase, surface area, roughness, porosity, and pore size/shape) changes that could lead to changes in the SIP response. Additionally, the microbes can produce biofilms that can serve as a conduction pathway, further altering the SIP signal. All mentioned physical changes could result in changes in the SIP response. Lastly, microbial growth can occur, leading to alterations in charge or potential along the cell membrane and grain surface due to the microbial build-up (Atekwana and Slater, 2009; Kemna et al., 2012; Slater and Atekwana, 2013; Heenan et al., 2013).

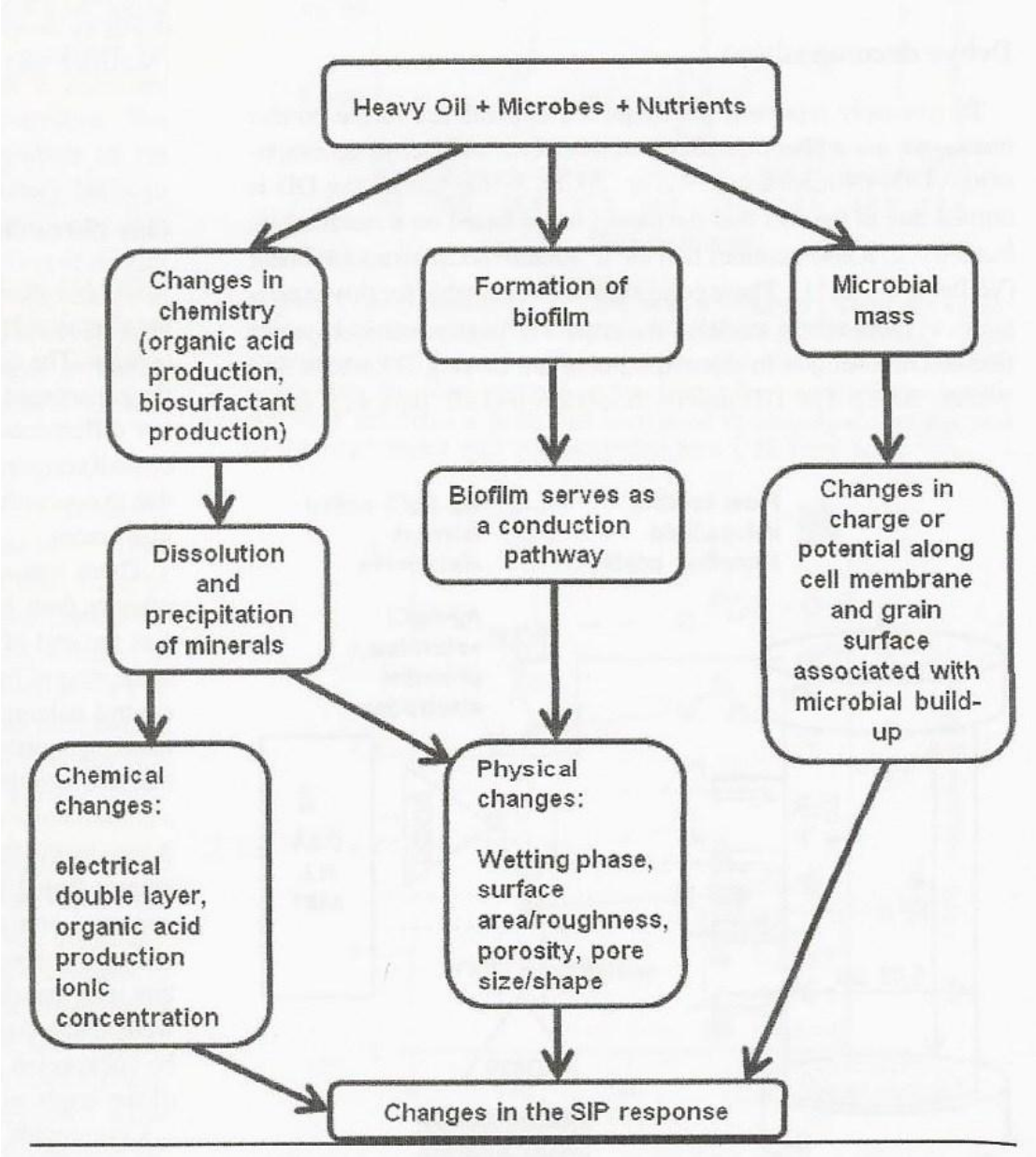

Figure 2. Flow chart outlining the geophysical response as a result of microbial activity. Microbial growth and interaction with the surroundings causes geochemical changes that can be monitored with geophysical techniques (from *Heenan et al., 2013*).

SIP signatures can be related to active degradation processes, with the driver of such signatures resulting from the microbial-induced oil degradation. Studies have shown a direct link between SIP measurements and biodegradation associated with microbial

induced hydrocarbon degradation; the observed signal likely being a result of the alteration of the oil properties, including wettability, by means of the production of biosurfactants and organic acids (Atekwana et al., 2000; Schmutz et al., 2010; Personna et al., 2013a; Personna et al., 2013b; Heenan et. al., 2013). This study aims to use this previous work as a reference point, and to try to extend the SIP research on monitoring natural attenuation under more saline conditions.

METHODOLOGY

Experiment Design

The experimental set up involved eight columns with identical geometric characteristics: columns were fabricated from a 15.24 cm thick-walled clear PVC pipe, capped at each end with inflow and outflow valves. Potential electrodes were placed at the center of each column with approximately 4 cm spacing (Figure 3). Each electrode holder was packed with a 1 M potassium chloride and montmorillonite paste preventing the direct contact of the electrode with column materials, while maintaining the electrolytic conduction pathway. Electrode holders were repacked as necessary throughout the experiment in order to decrease the contact resistances to ensure an unimpeded flow of electric current. The Ag-AgCl coiled current electrodes were housed in each end cap. A separate port was drilled into each top cap and sealed with a rubber stopper to allow for the collection of outflow fluids for further analysis. See Figure 3 below for a schematic of the column set up.

Columns were wet packed with an equal weight Ottawa sand/microbial sediment mixture (taken from a beach in Grand Terre Island (GTI), LA known to be impacted by the DWH spill) and then mixed with 5% crude oil by weight. The only exception to this

is Column 4. Due to insufficient sediment, Column 4 was packed only with an Ottawa sand and 5% crude oil by weight mixture; as such, Column 4 functioned as an additional control, not enhanced with microbial activity from the GTI sediments.

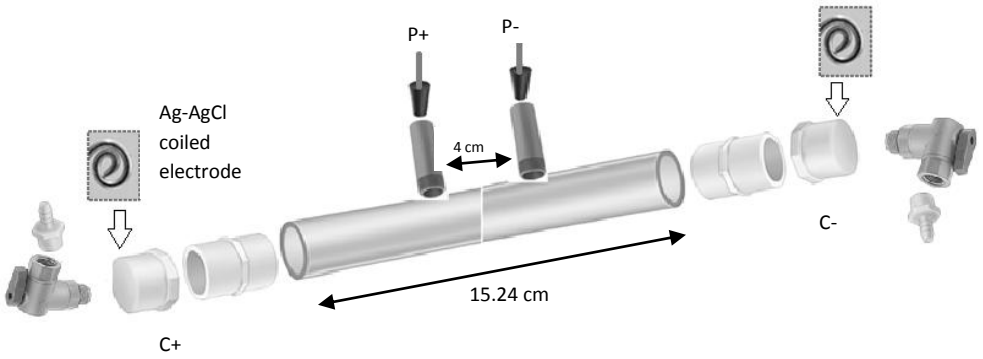

Figure 3. Schematic of the column used in this experiment. The construction of all eight columns was identical.

Oil was added to the sediment mixture following standard laboratory procedures, including stirring/overturning, until a consistent medium was observed (Heenan et al., 2013). Column preparation included the adhesion of a two layer oil resistant mesh at each end of the column to prevent the movement of solids, but allow the flow of fluids – including oil. Supporting fluids used in each column can be found in Table 1 below.

Table 1 Inflow solutions per column

Column	Active or Control	Inflow Solution	Notes
1	Active	25% strength Bushnell Haas Broth and 0.01 M NaCl	
2	Active	25% strength Bushnell Haas Broth and 0.01 M NaCl	
3	Active	25% strength Bushnell Haas Broth	
5	Active	25% strength Bushnell Haas Broth and 0.03 M NaCl	
6	Active	25% strength Bushnell Haas Broth and 0.03 M NaCl	
4	Control	25% strength Bushnell Haas Broth	No GTI sediments
7	Control	25% strength Bushnell Haas Broth and 0.1 mM $HgCl_2$	
8	Control	25% strength Bushnell Haas Broth and 0.1 mM $HgCl_2$	

The purpose of the control columns is to study the effect of only flow on the SIP signal. The inflow solution of $HgCl_2$ amended 25% strength Bushnell Haas Broth was designed to act as a microbial killer. The salt concentrations (Table 1) were chosen for the active columns in order to create solution conductivities higher than those found in previous studies, going up to brackish water conductivities. A diffuser was placed in each of the inflow solutions for the duration of the experiment to create aerobic conditions by providing aeration of the fluids.

Electrical Measurements

The instrument used in this experiment is the portable spectral induced polarization (PSIP) manufactured by Ontash & Ermac (O&E). Electrical current was injected into the two Ag-AgCl electrode coils located on the end caps of each column (Figure 3). The resulting voltage response was recorded via the potential electrodes located in the center of each column. Magnitude and phase were measured over a wide frequency range (10000 - 0.01 Hz) and then various parameters, such as resistivity and real and imaginary

conductivity were calculated (See Appendix II for this data per column). Electrical measurements on each column were taken twice each week for 20 weeks.

Geometric Factor

Prior to column packing with sediment/sand, fluid tests were conducted on each of the columns. The purpose of these tests was to obtain the exact geometric factor of each column in order to accurately calculate sample resistivity. The geometric factor represents the volume between the potential electrodes. From the phase and magnitude values obtained from the electrical measurements, the real conductivity was calculated from equations 5 through 8 as seen in Appendix I. Plotting fluid conductivity versus measured conductance and taking the inverse of the slope (Figure 4) gives the geometric factor of each column. Procedures and results of the fluid tests can be seen in Appendix II.

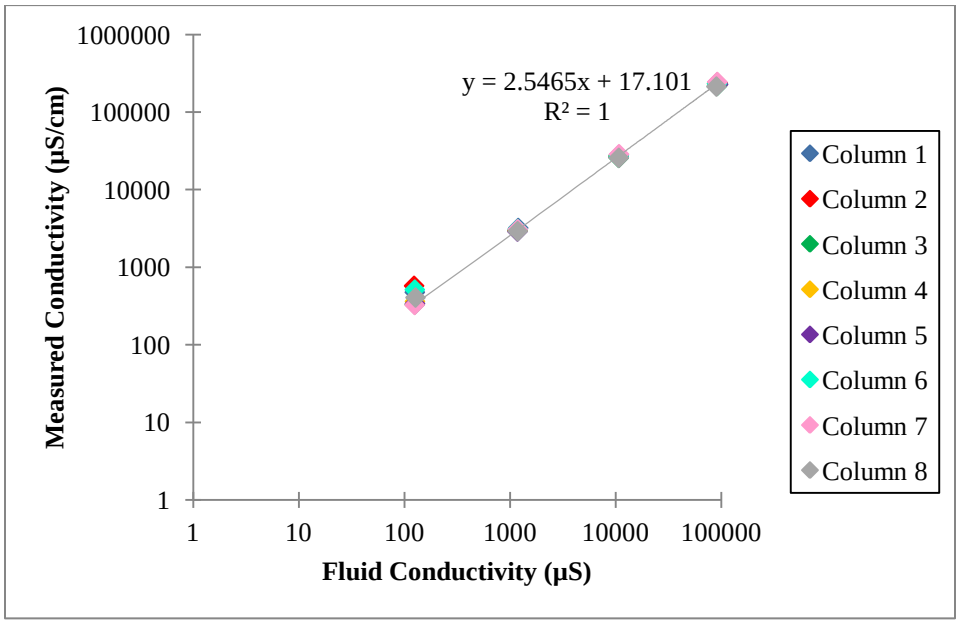

Figure 4. Plot of measured conductance vs. fluid conductivity of each column at 1 Hz for each fluid. The geometric factor is calculated by taking the inverse of the slope. This procedure is illustrated for Column 6. The equation of the line for all four points is calculated and then taking the inverse of the slope would give the geometric factor for Column 6. Columns 1, 2, 3, 5, and 6 are the active columns; Columns 4, 7, and 8 are the control columns.

Microcosm Study

Prior to the start of this experiment, microbial growth within the Louisiana sediment was verified with microcosm set-ups in order to ensure that degradation could take place via the indigenous microorganisms. Autoclaved flasks and petri dishes were prepared with a Bushnell Haas saturating solution and then small amounts of oil and the microbial sediment were added. The observed oil emulsion/clouding was interpreted as microbial activity from the only microbial source, the added sediment (Bunge and Lechner, 2009).

Most Probable Number Method

Verification of microbial activity and increases in population numbers was performed utilizing the most probable number (MPN) method (Gómez-Ullate et al., 2008). MPN estimates the number of bacteria by cultivating a sample and growing the microorganisms within a selected medium. The technique is based on statistical methods and serial dilutions of the sample. Population numbers are estimated from positive growth across the serial dilution and using mathematical tables that extrapolate numbers in the original sample. Changing the carbon source allows for differentiation between different types of bacteria, such as hydrocarbon degraders and heterotrophs (Gómez-Ullate et al., 2008). The disadvantage of this method is that it will only indicate numbers of bacteria capable of growing on the medium, not which strains are active in degrading the oil. Additionally, only bacterial that are capable of growth within the medium are counted while other strains may be present within the sample.

The procedures involved taking three outflow samples from each column and preparing three separate serial dilutions of each sample in order to improve accuracy of the interpolation of the number of microorganisms in the original sample. Samples were

inoculated in a 25% strength Bushnell Haas Broth solution. The specific procedures involved adding 200 µL of the outflow sample into the first well of each of the three rows of the microtiter plate, adding 180 µL of pure Bushnell Haas broth into the subsequent 11 wells of each row, transferring 20 µL from the first well into the second well, and repeating this dilution eleven times to achieve a final dilution factor of 10^{-11}. In order to distinguish between hydrocarbon degraders and acetate degraders (that could be used as an indication of heterotrophs present in the columns), 2 µL crude oil or 2 µL sodium acetate was added respectively into each well as a carbon source. Plates were incubated at 25 ^{o}C for 14 days for hydrocarbon degraders and 7 days for acetate degraders. As specified in previous studies, bacterial growth was indicated by oil emulsion for the hydrocarbon degraders and cloudiness for the acetate degraders (Gómez-Ullate et al., 2008). The number of positive wells was identified per dilution, the three consecutive sets of wells that showed "dilution to extinction" were determined, and a 3 MPN calculator was utilized to compute the number of organisms present in the original sample.

The use of sodium acetate as a carbon source was devised by Trabulsi and Ewing, (1962) in order to distinguish between different bacterial strains (Costin, 1965). In a study by Costin (1965), sodium acetate agar medium was used to distinguish between Shigella and Escherichia. The medium was prepared with 0.2 g sodium acetate per 100 mL of distilled water (Costin, 1965). Results of this study indicated that acetate utilization was useful for the differentiation between members of the different strains (Costin, 1965).

Fluid Geochemistry

Some restrictions on microbial oil degradation include pH and salinity, as well as nutrient availability, accessibility of the carbon source, and oxygen availability assuming aerobic degradation (Personna et al., 2014). The pH and salinity of the column outflow are monitored throughout this study in order to identify optimal conditions and any variations (Löffler et. al., 2006). Prior to and after each electrical measurement, fluid samples were taken directly from the column outflow. Samples were analyzed for conductivity, temperature, and pH, and once a week a fluid sample was taken from each column outflow, stored in an amber colored glass vial to prevent photooxidation, and immediately refrigerated for further analysis. In order to verify consistency, pH and salinity were measured each time new inflow solutions were prepared.

Gas Chromatography

Gas Chromatography/Mass Spectrometry (GC/MS) analysis was performed on column outflow samples, as well as a sample of crude oil and uncontaminated inflow samples in order to determine changes in the oil GC signature. Samples were chosen from replicate columns at the beginning and end of the experiment, as well as the day that corresponded with the peak conductivity change. See Appendix I for the protocol used in extracting hydrocarbons from column outflow samples.

RESULTS

Geophysical Data

Figures 5 and 6 below show that over the course of the 143 day experiment, increases in imaginary conductivity at the peak frequency were observed for some of the active columns. The peak frequency remained at ~0.1 Hz for the duration of the experiment.

The conductivity in the control columns remains steady over the course of the experiment. Columns 5 and 6 showed an increase in imaginary conductivity that reached a peak at day 41 (Figure 5); these columns show the most pronounced increase in imaginary conductivity (Figures 5, 7). Real conductivity results show that all columns behave similarly throughout the course of the experiment, regardless of microbial processes (Figures 6, 8). Column 4 has a distinctive response consistent with the fact that it did not receive any Louisiana beach sediment; Column 4 acted as an additional abiotic control column. See Appendix II for real and imaginary conductivity results at 0.1, 1, and 10 Hz.

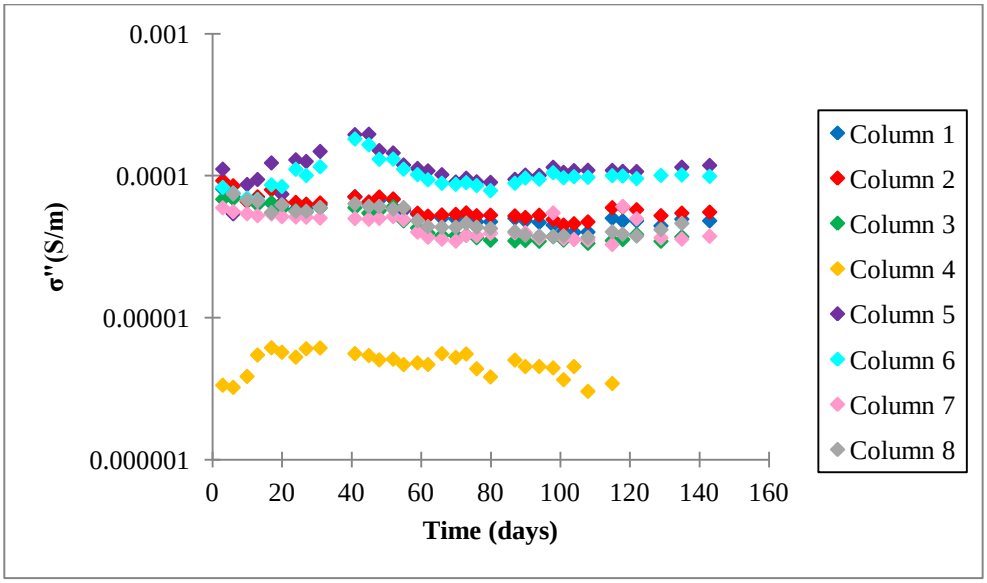

Figure 5. Imaginary conductivity at the peak frequency (~0.1 Hz) for each column. Columns 5 and 6 show an increase in imaginary conductivity to a peak at day 41 whereas the control columns show no appreciable change in conductivity. Columns 1, 2, 3, 5, and 6 are the active columns; Columns 4, 7, and 8 are the control columns.

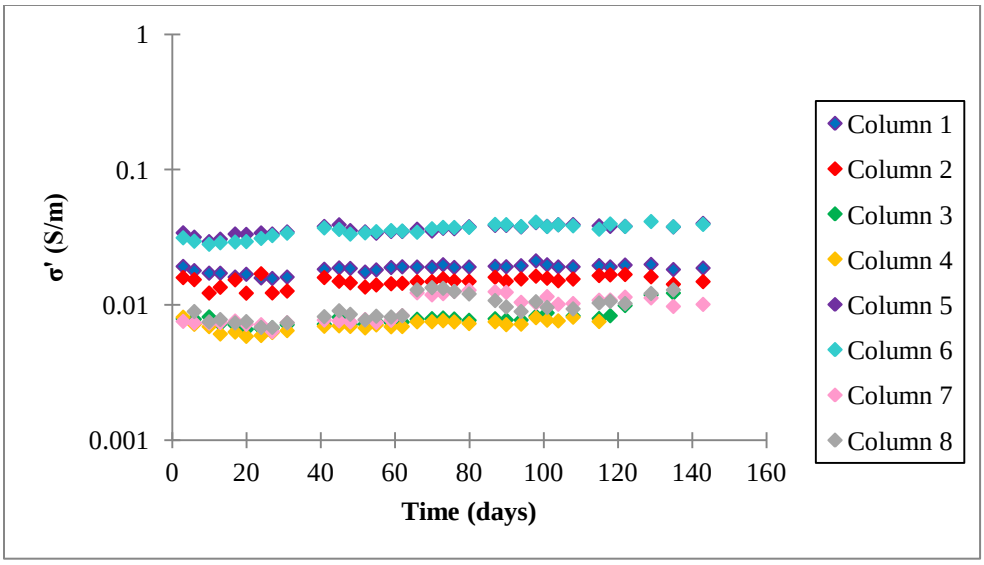

Figure 6. Real Conductivity at the peak frequency (~0.1 Hz). Both the active and control columns show no appreciable change in conductivity. Columns 1, 2, 3, 5, and 6 are the Active Columns; Columns 4, 7, and 8 are the Control Columns.

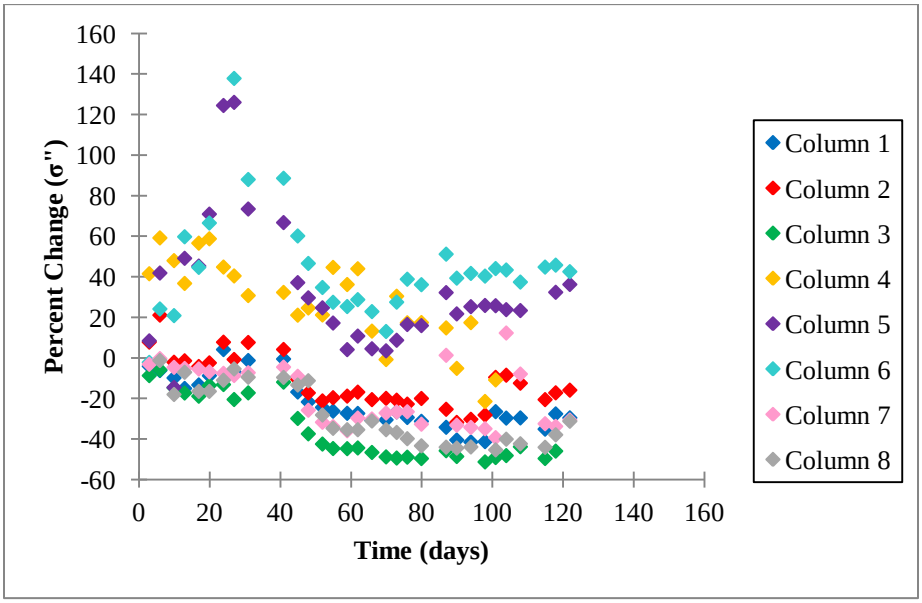

Figure 7. Percent change in imaginary conductivity for each column throughout the duration of the experiment. Columns 5 and 6 showed the largest change in imaginary conductivity up to a peak at approximately day 30 after which it decreases before leveling off for the duration of the experiment. The percent change in imaginary conductivity for Columns 1, 2, 3, 7, and 8 increases until approximately day 40 after which it levels off , whereas for Column 4 it decreases throughout the duration of the experiment. Columns 1, 2, 3, 5, and 6 are the Active Columns; Columns 4, 7, and 8 are the Control Columns.

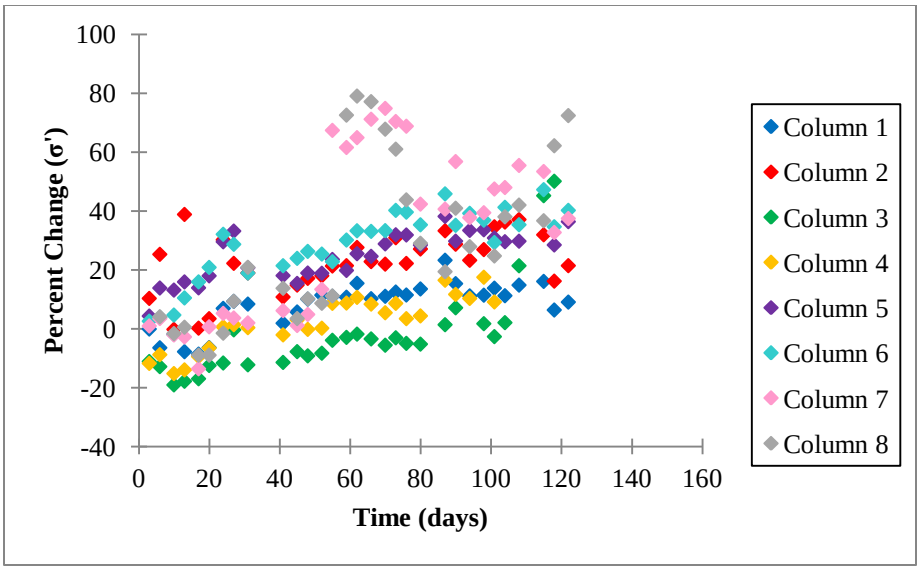

Figure 8. Percent change in real conductivity for each column throughout the duration of the experiment. Neither the active nor the control columns show any appreciable change in real conductivity throughout the course of the experiment. Columns 1, 3, and 4 remain stable while Columns 7 and 8 are stable until approximately day 40 after which the data becomes erratic. Columns 2, 5, and 6 do seem to increase but only after day 40. Columns 1, 2, 3, 5, and 6 are the Active Columns; Columns 4, 7, and 8 are the Control Columns.

Fluid Geochemistry

Analysis of the outflow fluid geochemistry from each of the columns indicates that both the control and active columns follow similar trends in fluid conductivity and pH (Figures 9 and 10). Column 7 had no outflow fluid geochemistry analyzed after day 87 due to a clog in the column that caused outflow to leave the column through the potential electrode holders as opposed to the outflow valve. This clog was likely the result of crude oil accumulation in or near the outflow port as changing the outflow valve and tubing had no effect. As seen in Figure 9, pH varied from approximately 6.5 to 9, though after around day 60, the pH normalized and only varied from 6.7 to 7.1 for each of the columns.

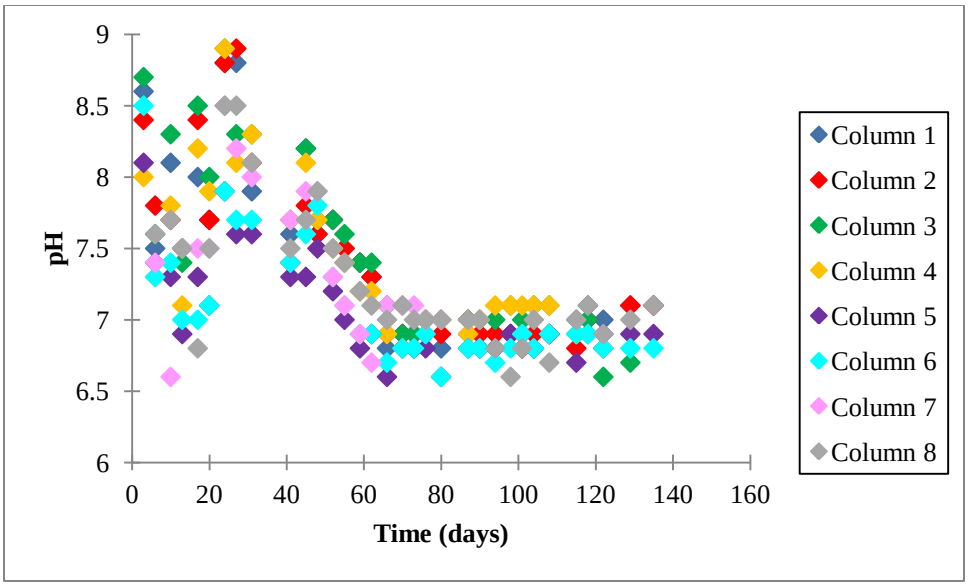

Figure 9. pH variation in column outflow solutions over the course of the experiment. Both the active and control columns followed similar trends in pH; pH varied from approximately 6.5 to 9, though after around day 60, the pH normalized and only varied from 6.7 to 7.1 for each of the columns. Columns 1, 2, 3, 5, and 6 are the Active Columns; Columns 4, 7, and 8 are the Control Columns. See Table A1 in Appendix II for actual pH values from each column by day.

Outflow fluid conductivity did not vary greatly from the fluid conductivities of the inflow solutions. Fluid conductivities of the inflow solutions for the pure 25% strength Bushnell Haas broth and control (0.1 mM $HgCl_2$ and 25% strength Bushnell Haas broth) were approximately 1 mS/cm; the 0.01 M NaCl and 25% strength Bushnell Haas broth solution typically measured fluid conductivities of 2 mS/cm; and the 0.03 M NaCl and 25% strength Bushnell Haas broth solution typically measured fluid conductivities of 3.5 mS/cm. Outflow fluid conductivities varied between approximately 900 µS/cm to 1.3 mS/cm for Columns 3, 4, 7, and 8; 1.9-2.5 mS/cm for Columns 1 and 2; and 3.5-4.5 mS/cm for Columns 5 and 6 (Figure 10). However, days 66 and 70 saw a large increase in fluid conductivity in the control columns and these were taken as outliers; this is likely the result of contamination as it coincides with a decrease in pH.

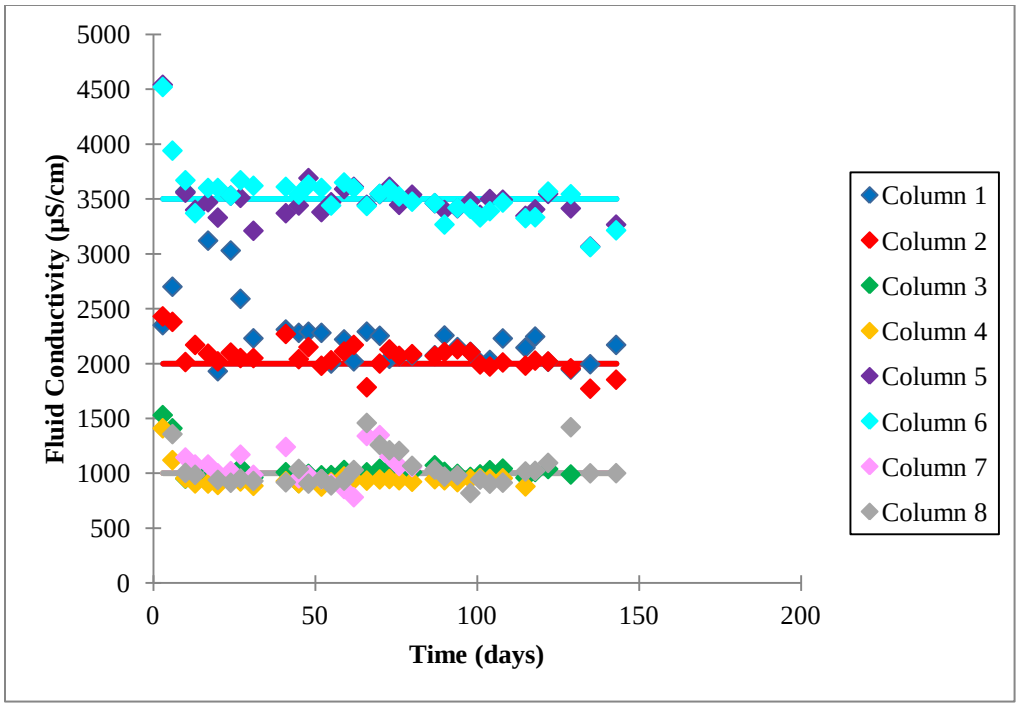

Figure 10. Fluid conductivity variation in column outflow solutions over the course of the experiment. The solid lines show the inflow conductivity of each column. Columns 1, 2, 3, 5, and 6 are the active columns; Columns 4, 7, and 8 are the control columns.

Bacterial Counts

The MPN method was performed twice. The first attempt did not yield any measureable results due to a large dilution of the outflow that prevented any microbial growth. However, when repeated a second time, results of the MPN count indicated a greater amount of oil degraders than acetate degraders present in each of the columns. The amount of oil degraders were much higher in the active columns versus the controls, with the highest amounts found in Columns 3, 5, and 6. Even though an inflow solution was used that was made to act as a microbial killer in the control columns, the presence of both oil degraders and acetate degraders (though at significantly reduced numbers, as seen in Table 2) were observed, which can be attributed to the fact that either the concentration of mercuric chloride was not high enough to in fact kill all the microbes

present or contamination occurred during MPN counting. These samples were taken on Day 122 and therefore Column 7 is not included in the analysis due to a lack of outflow from the column as mentioned above.

Table 2. Results of MPN Method for each column

Column	# Oil Degraders	# Acetate Degraders
1	4.65×10^3	11.5
2	5.50×10^4	11.5
3	2.15×10^8	120
4	1.05×10^5	11.5
5	7.50×10^9	46.5
6	3.65×10^6	11.5
8	2.15×10^2	11.5

Gas Chromatography

The GC results support the occurrence of oil degradation processes in the active columns. GC analysis was performed on two active columns, Columns 1 and 6, and one control column, Column 8. On day 27 (Figure 11a), Column 8 had two unique peaks and Column 1 had one unique peak, which had a poor match to oleic acid, an 18C fatty acid. On day 41 (Figure 11b), at the time of the SIP peak (Figures 5 and 6) the outflow of the control column has significantly more peaks compared to the active columns. Since the only difference between the two columns is microbial activity it is safe to assume that oil biodegradation is occurring in the active column. Interestingly, on day 115 (Figure 11c) the outflow difference is very small between control and active columns. At this time it is believed that the microbial activity had significantly declined in the active columns. This is confirmed by the geophysical data which showed a consistent response in imaginary conductivity after approximately day 100. This observation suggests that other oil degradation processes can also occur but with significant delay compared to

biodegradation. Figure 11c also indicates that the abundance of oil components is higher in Column 1 than in Column 8, indicating that biodegradation is occurring in the control column as well as the active columns; this is likely due to either contamination or a concentration of mercuric chloride in the inflow solutions of insufficient strength as previously mentioned.

a)

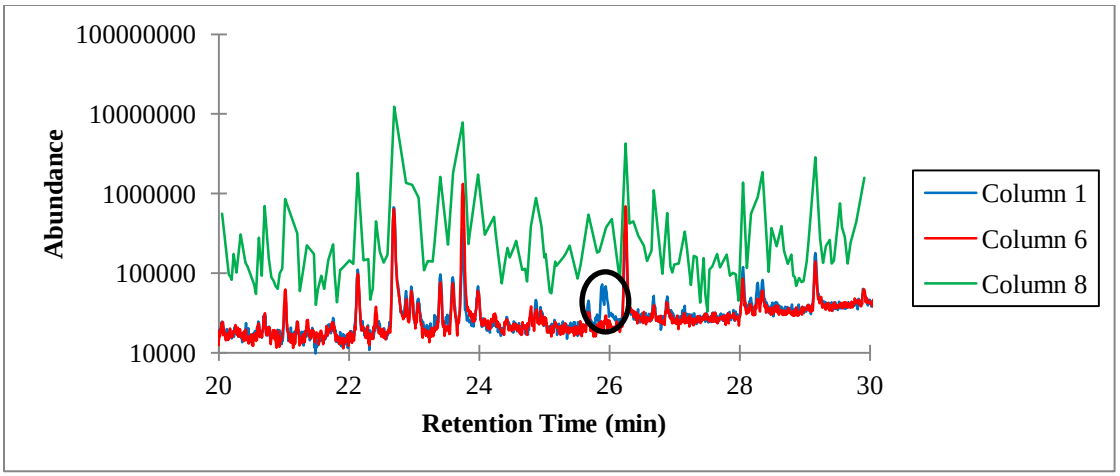

b)

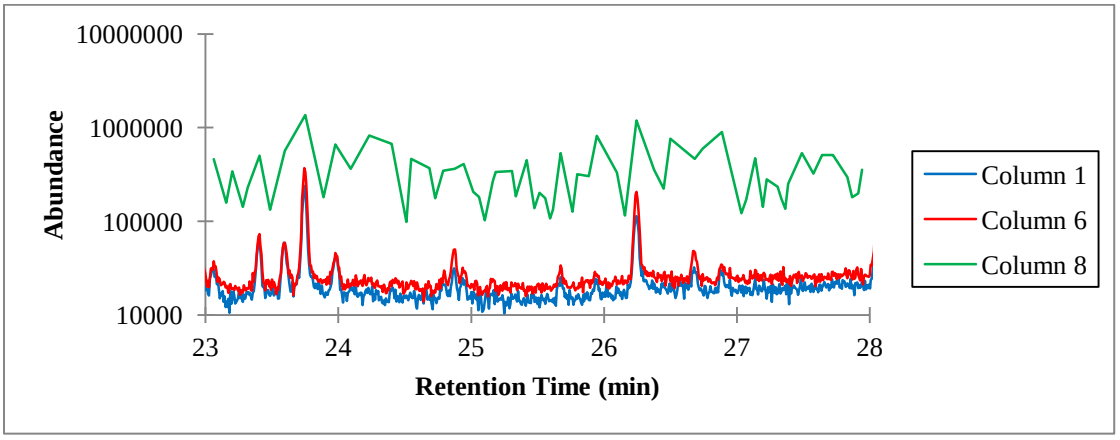

c)

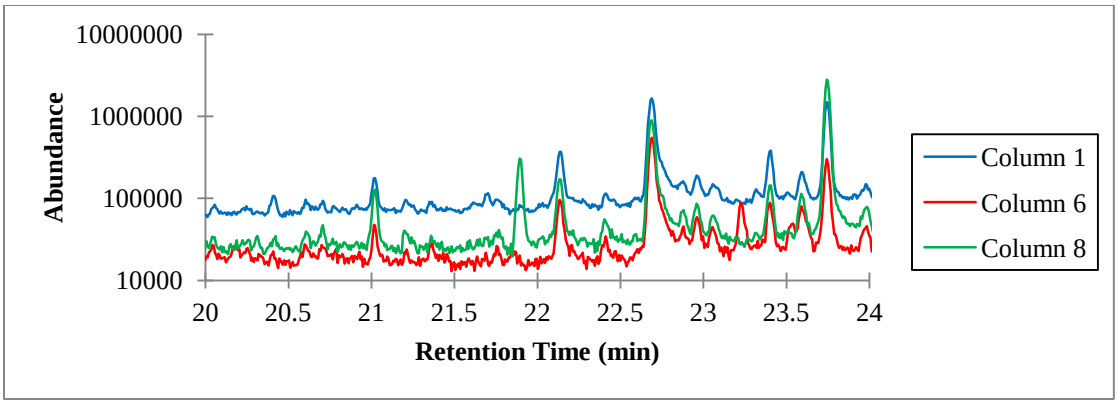

Figure 11. Chromatograms from a) day 27 comparing the active versus control columns; circled is a peak corresponding to a C18 fatty acid; b) day 41 active versus control columns showing the appearance of additional peaks in the control column; c) day 115 active and control columns showing a similar GC fingerprint. Columns 1 and 6 are active columns; Column 8 is a control column.

DISCUSSION

The main objective was to test whether SIP can detect oil biodegradation under high conductivity environments. Active degradation of the oil contamination was observed in some of the columns. GC/MS measurements from the outflow samples confirm the change of the oil fingerprint over time in the columns. The changes observed were most pronounced and faster in Columns 5 and 6, the columns saturated with the fluid with salinity closest to the natural conditions of the sediments. Oil degradation supporting evidence comes from:

- the presence of fatty acids, a common product of alkane degradation, and
- the chromatogram change; for the first 115 days of the experiment, the GC results show less peaks and a decrease in abundance in the active columns compared to

the control columns, suggesting active degradation of the substrate (oil contaminant in our cases).

Finally, after 115 days of operation the active columns appear to have a similar GC fingerprint to the control columns, suggesting the attainment of similar conditions. It is evident that the oil is degrading in the columns, with the processes occurring faster in the active versus the controls.

All columns were very similar, with identical operation. The flow regime was identical in all 8 columns. All supporting fluids contained the same nutrients and for all columns the carbon source was the contaminant oil. As shown previously, the oil degraded faster in the active columns, especially the ones with supporting fluids having fluid conductivity similar to the ones where the field sediments were collected. The only logical explanation is that the faster oil degradation is attributed to the presence of microbes capable of degrading the oil. Indeed, MPN counts did show that hydrocarbon degraders were most abundant in Columns 5 and 6 (Table 2). Indigenous microbes to Grand Terre Island capable of biodegradation of hydrocarbons were confirmed via 16S rRNA polymerase chain reaction (PCR) amplification (Heenan et al., 2015).

The SIP monitoring shows the highest change in imaginary conductivity within the same pair of columns (5 and 6). The response peaks occurred at ~ day 41 (Figure 5), the same day for which the GC fingerprint of these columns is significantly different than the response from the control columns (Figure 11b). This is also consistent with the highest cell population of hydrocarbon degraders in the same columns.

The observed geophysical response is consistent with previous research showing that sediments contaminated with hydrocarbons, undergoing biodegradation, show a higher

bulk conductivity over time (Allen et al., 2007; Atekwana and Slater 2009). The source of the conductivity change has been attributed to microbial action, and in some cases redox processes, that ultimately produce CO_2 (as well as other biogenic gases) and organic acids. These acids lead to the weathering of minerals within the sediment, releasing additional ions, and further raising the conductivity of the medium (Atekwana and Slater, 2009). This process is probably not the dominant one in our system; both the control and active columns show the same pH trend, therefore microbial activity is not controlling pH.

Recent field data (Heenan et al., 2015) showed an increase in conductivity as oil biodegrades in brackish environments. This is consistent with our experimental results. As shown by Allen et al. (2007) higher bulk conductivity corresponds to areas of increased populations of oil degrading bacterial strains (Allen et al., 2007). During microbial respiration, terminal electron acceptors are utilized to break down organic carbon in the production of energy. Depending on the strain of bacteria and the oxic conditions of the environment, electron acceptors are used according to their placement on the redox ladder, from O_2 to NO_3^- to Fe^{3+} to Mn^{4+} to SO_4^{2-}, and finally to CO_2 during methanogenesis (Langmuir, 1997; Eby, 2003). By-products of these redox reactions cause changes to the pore fluid chemistry; this increase in ions changes the fluid conductivity. Some of the changes observed in this experiment can be attributed to changes in fluid conductivity; increases in real conductivity were observed in Columns 5 and 6 (Figure 6).

The larger, and more interesting geophysical signal increase was observed in the imaginary component of conductivity (Figure 5). Columns 5 and 6 showed the largest

increase in imaginary conductivity to a peak and day 41, after which the imaginary conductivity decreased before leveling off for the remainder of the experiment. This increase in imaginary conductivity is quantified through analysis of the percent change (Figure 7). The control columns showed no appreciable change in imaginary conductivity, while Columns 1, 2, and 3 show slight decreases in imaginary conductivity. These results clearly suggest that SIP is sensitive to oil degradation processes in high conductivity environments. The increase in imaginary conductivity in Columns 5 and 6 indicates microbial activity as the oil degradation process whereas the other columns are likely experiencing degradation due to fluid flow or contamination (as in the case of the control columns).

Although the experiment was not designed to explore the signal sources, the results can provide some information on contributing mechanisms. The pH response indicates microbial growth; pH values were high at the beginning of the experiment due to slow biodegradation of alkanes and then returned to near the neutral range after degradation processes had slowed. Changes in fluid conductivity and mineral weathering may have played a role in the observed SIP response. The GC analysis showed that the oil is actively degrading over the course of the experiment, suggesting changes in oil properties that can be a change to the wetting state of the oil; oil saturation and wetting have been show to affect SIP measurements (Schmutz, et al., 2010). Based on the data collected and analyzed so far, the observed changes to the oil properties are attributed to biodegradation, which affects the wetting state and leads to the SIP signals. Since this is a complex process further investigation is required to fully determine the source of the observed SIP signals.

By the conclusion of the experiment all columns showed similar SIP behavior. Due to the different magnitudes of fluid conductivity the results are not equal, but rather display a consistence response, without the appearance of any additional peaks. The decline in the geophysical data for Columns 5 and 6 after day 41 supports active degradation processes as the driver of the SIP signals; at this stage degradation processes possibly started to decrease, a timeframe consistent with previous research (Davis et al., 2010; Abdel Aal and Atekwana 2014).

The major limitations of this study involve the MPN method and GC/MS analysis due to experimental design. The MPN method should have been repeated multiple times throughout the course of the experiment in order to show microbial growth; however, the procedure was only performed once on day 122 (at the end of the experiment). Additionally, the procedures used could have introduced some contamination as the dilutions were not performed in a sterile fume hood, and this could account for the microbial growth seen in the control columns. Lastly, the inoculation was performed with a 25% strength Bushnell Haas Broth solution, yet the columns all used different inflow solutions of varying sodium chloride concentration for the active columns and mercuric chloride for the control columns (Table 1). To get an accurate representation of how the microbes would grow in the columns, the mediums used in the plates should have mirrored the inflow solutions used in the respective columns.

The second major limitation involves the limited chemical analysis performed to date. In order to quantify the actual oil component concentration to determine the change over time in the active versus control columns, the peaks present in each of the chromatograms should be identified. Additionally, a hopane normalization (Venosa et al., 1996) could be

done in order to distinguish oil biodegradation from any abiotic removal. This method assumes that hopane is a nonbiodegradable constituent of oil and that physical washout is dominant, while dissolution and volatilization are negligible (Venosa et al., 1996). The rate of biodegradation is assumed to be first order: $\frac{A}{H} = \frac{A_0}{H_0} e^{-kt}$ where $\frac{A}{H}$ is the hopane normalized concentration of the analyte and $\frac{A_0}{H_0}$ is the value at time 0 (Venosa et al., 1996). Hopane half life can then be calculated from the overall first-order curve. This represents the physical loss of crude oil due to wave and tidal action and tidal inundation (Venosa et al., 1996). However, as this study was instead focused on SIP, more time was spent on the analysis of the geophysical data.

CONCLUSIONS

Previous studies have shown that SIP can non-invasively monitor the biogeochemical changes occurring during microbial oil degradation; the current study took this idea one step further to successfully show that SIP can be used to distinguish these changes in brackish environments. Conductivities in this experiment varied between approximately 1 – 4 mS/cm, ranging from previous experiments with fresh water environments and the indigenous conditions at GTI. Results indicate that SIP measurements taken under high conductivity conditions are influenced by microbial oil degradation, indicating that SIP is a useful tool to non-invasively monitor natural attenuation within brackish environments.

Increases in real and imaginary conductivity, as well as an increase in the phase response at the peak frequency were observed for some of the active columns, whereas the control columns showed no such changes. This data, combined with the results of the GC/MS showing fewer peaks in the active columns versus the control columns, as well as

the appearance of metabolites, indicates that microbial oil degradation is occurring and that SIP is sensitive to these changes under higher conductivity conditions.

The implications of this study are that SIP can potentially be utilized in a wider range of environments and will further limit costly and time consuming fluid sampling and analysis. While SIP is sensitive to these geophysical changes, like other geophysical methods, SIP is indirect, so interpretation of results should be taken with caution.

REFERENCES

Abdel Aal, G. Z., E. A. Atekwana, L. D. Slater, and E. A. Atekwana, 2004, Effects of microbial processes on electrolytic and interfacial electrical properties of unconsolidated sediments: Geophysical Research Letters, 31.

Abdel Aal, G. Z., L. D. Slater, E. A. Atekwana, 2006, Induced-polarization measurements on unconsolidated sediments from a site of active hydrocarbon biodegradation: Geophysics, 71, no. 2, H13-H24.

Abdel Aal, G. Z. and E. A. Atekwana, 2014, Spectral induced polarization (SIP) response of biodegraded oil in porous media: Geophysical Journal International, 196, 804-817.

Allen, J. P., E. A. Atekwana, J. W. Duris, D. D. Werkema, and S. Rossback, 2007, The microbial community structure in petroleum-contaminated sediments corresponds to geophysical signatures: Applied and Environmental Microbiology, 73, no. 9, 2860-2870.

Archie, G. E., 1942, The electrical resistivity log as an aid in determining some reservoir characteristics: Transactions of the American Institute of Mining, Metallurgical, and Petroleum Engineers, 146, 54-62.

Atekwana, E. A., W. A. Sauck, and D. D. Werkema, Jr., 2000, Investigations of geoelectrical signatures at a hydrocarbon contaminated site: Journal of Applied Geophysics, 44, 167-180.

Atekwana, E. A., E. A. Atekwana, D. D. Werkema Jr., J. P. Allen, L. A. Smart, J. W. Duris, D. P. Cassidy, W. A. Sauck and S. Rossback, 2004, Evidence for microbial enhanced electrical conductivity in hydrocarbon-contaminated sediments: Geophysical Research Letters, 31, L23603.

Atekwana, E. A. and L. D. Slater, 2009, Biogeophysics: A New Frontier in Earth Science Research: Reviews of Geophysics, 47, RG4004.

Atlas, R. and J. Bragg, 2009, Bioremediation of marine oil spills: when and when not – the Exxon Valdez experience: Microbial Biotechnology, 2, 213-221.

Bekins, B. A., I. M. Cozzarelli, E. M. Godsy, E. Warren, H. I. Essaid, and M. E. Tuccillo, 2001, Progression of natural attenuation processes at a crude oil spill site: Il. Controls on spatial distribution of microbial populations: Journal of Contaminant Hydrology, 53, 387-406.

Binley, A. and A. Kemna, 2005, DC resistivity and induced polarization methods, in: Rubin, Y., Hubbard, S. S. (Eds), Hydrogeophysics. Springer-Verlag.

Bunge, M. and U. Lechner, 2009, Anaerobic reductive dehalogenation of polychlorinated dioxins: Applied Microbiology and Biotechnology, 84, 429-444.

Costin, I. D., 1965, Utilization of Sodium Acetate by Shigella and Escherichia: Journal of General Microbiology, 41, 23-27.

Davis, C. A., E. Atekwana, E. Atekwana, L. D. Slater, S. Rossbach, and M. R. Mormile, 2006, Microbial growth and biofilm formation in geologic media is detected with complex conductivity measurements: Geophysical Research Letters, 33, L18403.

Eby, G. N. Principles of Environmental Geochemistry. 1st ed. Boston: Cengage Learning, 2003.

Environmental Protection Agency, Method 3510C: Separatory Funnel Liquid-Liquid Extraction.

Environmental Protection Agency, Method 8270D: Semivolatile Organic Compounds by Gas Chromatography/Mass Spectrometry (GC/MS).

Gómez-Ullate, E., J. R. Bayon, D. Castro, and S. J. Coupe, 2008, Efficiency of MPN method to indicate hydrocarbon biodegradation processes within permeable pavements: 11th International Conference on Urban Drainage, Edinburgh, Scotland, UK.

Heenan, J., A. Porter, D. Ntarlagiannis, L. Y. Young, D. D. Werkema, and L. D. Slater, 2013, Sensitivity of the spectral induced polarization method to microbial enhanced oil recovery processes: Geophysics, 78, no. 5, E261-E269.

Heenan, J., L. D. Slater, D. Ntarlagiannis, E. A. Atekwana, B. Z. Fathepure, S. Dalvi, C. Ross, D. D. Werkema, and E. A. Atekwana, 2015, Electrical resistivity imaging for long-term autonomous monitoring of hydrocarbon degradation: Lessons from the Deepwater Horizon oil spill: Geophysics, 80, no. 1, B1-B11.

Heitzer, A. and G. S. Sayler, 1993, Monitoring the efficacy of bioremediation: Trends in Biotechnology, 11, 334-343.

Kemna, A., A. Binley, G. Cassiani, E. Niederleithinger, A. Revil, L. Slater, K. H. Williams, A. Flores Orozco, Franz-Hubert Haegel, A. Hördt, S. Kruschwitz, V. Leroux, K. Titov and E. Zimmermann, 2012, An overview of the spectral induced polarization method for near-surface applications: Near Surface Geophysics, 10, 453-468.

Knight, R., L. J. Pyrak-Nolte, L. Slater, E. Atekwana, A. Endres, J. Geller, D. Lesmes, S. Nakagawa, A. Revil, M. M. Sharma and C. Straley, 2010, Geophysics at the interface: response of geophysical properties to solid-fluid, fluid-fluid, and solid-solid interfaces: Reviews of Geophysics, 48, RG4002.

Kostka, J. E., O. Prakash, W. A. Overhold, S. J. Green, G. Freyer, A. Canion, J. Delgardio, N. Norton, T. C. Hazen, and M. Huettel, 2011, Hydrocarbon-Degrading Bacteria and the Bacterial Community Response in Gulf of Mexico Beach Sands Impacted by the Deepwater Horizon Oil Spill: Applied and Environmental Microbiology, 77, no. 22, 7962-7974.

Krumins, V., Joong-Wook Park, Eun-Kyeu Son, L. A. Rodenburg, L. J. Kerkhof, M. M. Häggblom, D. E. Fennell, 2009, PCB dechlorination enhancement in Anacostia River sediment microcosms: Water Research, 43, 4549-4558.

Langmuir, D. Aqueous Environmental Geochemistry. 1st ed. Upper Saddle River: Prentice Hall, 1997.

Lesmes, D. P. and F. D. Morgan, 2001, Dielectric spectroscopy of sedimentary rocks: Journal of Geophysical Research, 106, B7, 13329-13346.

Liu, Z., J. Liu, Q. Zhu, and W. Wu, 2012, The weathering of oil after the Deepwater Horizon oil spill: insights from the chemical composition of the oil from the sea surface, salt marshes and sediments: Environmental Research Letters, 7, 1-14.

Löffler, F. E. and E. A. Edwards, 2006, Harnessing microbial activities for environmental cleanup: Current Opinion in Biotechnology, 17, 274-284.

Madsen, E. L., 1991, Determining in situ biodegradation: Environmental Science and Technology, 25, no. 10, 1662-1673.

Madsen, E. L., 1998, Epistemology of Environmental Microbiology: Environmental Science and Technology, 32, no. 4, 429-439.

Mwakanyamale K., L. Slater, A. Binley, D. Ntarlagiannis, 2012, Lithologic imaging using complex conductivity: Lessons learned from the Hanford 300 Area: Geophysics, 77, no. 6, E397-E409.

Ntarlagiannis, D., K. H. Williams, L. Slater, and S. Hubbard, 2005, Low-frequency

electrical response to microbial induced sulfide precipitation: Journal of Geophysical Research, 110.

Ntarlagiannis, D., N. Yee, and L. Slater, 2005, On the low-frequency electrical polarization of bacterial cells in sands: Geophysical Research Letters, 32, no. 24, 2-5.

Ntarlagiannis, D., 2006, Investigating Geophysical Signatures of Microbial Cells, Processes, and Degradation: Implications for the Geophysical Monitoring of Microbial Activity and Degradation in the Subsurface: PhD Dissertation, Rutgers University.

Ntarlagiannis, D. and A. Ferguson, 2009, SIP response of artificial biofilms: Geophysics, 74, no. 1, A1-A5.

Ntarlagiannis, D., R. Doherty and K. H. Williams, 2010, Spectral induced polarization signatures of abiotic FeS precipitation: Geophysics, 75, no. 4, F127-F133.

Olson, J. J., G. L. Mills, B. E. Herbert, and P. J. Morris, 1999, Biodegradation rates of separated diesel components: Environmental Toxicology and Chemistry, 18, 2448-2453.

Personna, Y. R., L. Slater, D. Ntarlagiannis, D. Werkema, and Z. Szabo, 2013, Electrical signatures of ethanol-liquid mixtures: Implications for monitoring biofuels migration in the subsurface: Journal of Contaminant Hydrology, 144, 99-107.

Personna, Y. R., L. Slater, D. Ntarlagiannis, D. Werkema, and Z. Szabo, 2013, Complex resistivity signatures of ethanol in sand-clay mixtures: Journal of Contaminant Hydrology, 149, 76-87.

Personna Y. R., T. King, M. C. Boufadel, S. Zhang, A. Kustka, 2014, Assessing weathered Endicott oil biodegradation in brackish water: Marine Pollution Bulletin, 86, 102-110.

Phelps, C. D., J. Battistelli, L. Y. Young, 2002, Metabolic biomarkers for monitoring anaerobic naphthalene biodegradation in situ: Environmental Microbiology, 9, 532-537.

Pritchard, P. H. and C. F. Costa, 1991, EPA's Alaska oil spill bioremediation project: Environmental Science and Technology, 25, 372-379.

Revil, A., E. Atekwana, C. Zhang, A. Jardani, and S. Smith, 2012, A new model for the spectral induced polarization signature of bacterial growth in porous media: Water Resources Research, 48, W09545.

Rufe, R. VADM, RADM C. Moore, D. Behler, J. Cunningham, L. Dietrick, A. Joves, D. Moore, B. Parker, G. Pollock, R. Shaneyfelt, J. Tarpley, J. Ayers, B. Johnson, B.

House, 2011, BP Deepwater Horizon Oil Spill Incident Specific Preparedness Review.

Schmutz, M., A. Revil, P. Vaudelet, M. Batzle, P. Femenía Viñao and D. D. Werkema, 2010, Influence of oil saturation upon spectral induced polarization of oil-bearing sands: Geophysical Journal International, 183, 211-224.

Schmutz, M., A. Blondel, and A. Revil, 2012, Saturation dependence of the quadrature conductivity of oil-bearing sands: Geophysical Research Letters, 39.

Slater, L. and E. Atekwana, 2013, Geophysical Signatures of Subsurface Microbial Processes: EOS, Transactions American Geophysical Union, 94, no. 8, 77-84.

Werkema Jr., D. D., E. A. Atekwana, A. L. Endres, W. A. Sauck, and D. P. Cassidy, 2003, Investigating the geoelectrical response of hydrocarbon contamination undergoing biodegradation: Geophysical Research Letters, 30, no. 12.

Vanhala, H. and H. Soininen, 1995, Laboratory technique for measurement of spectral induced polarization response of soil samples: Geophysical Prospecting, 43, 655-676.

Venosa, A. D., M. T. Suidan, B. A. Wrenn, K. L. Strohmmeier, J. R. Haines, B. L. Eberhart, D. King, and E. Holder, 1996, Bioremediation of an experimental oil spill on the shoreline of Delaware Bay: Environmental Science and Technology, 30, 1764-1775.

APPENDIX I

Low frequency electrical properties of porous media

Conductivity is a measure of the ability of a material to conduct electrical current, while IP measures the strength of electric charge storage in the electrical double layer (EDL) (Mwakanyamale et al., 2012). The conduction and polarization properties of materials can be represented by complex conductivity (σ*):

$$\sigma^* = \sigma' + i\sigma'' \quad (1)$$

where $i = \sqrt{-1}$ (Mwakanyamale et al., 2012). Real conductivity (σ') represents the in-phase conduction term (describes conduction loss in the system), whereas the imaginary conductivity (σ") represents the out of phase energy storage (describes the polarization that occurs at the interfaces) (Ntarlagiannis et al., 2005b; Ntarlagiannis, 2006). The

magnitude of the imaginary conductivity is a function of surface area, charge density, and the mobility of the ions (Lesmes and Morgan, 2001).

For non-metallic systems, electric charge is transmitted via electrolytic conduction and surface conduction (Mwakanyamale et al., 2012). Electrolytic conduction occurs via ions in the fluid in the interconnected pore space and surface conduction involves the EDL at the mineral interface. Electrolytic conduction is a factor of water saturation, porosity, and ionic concentration. Surface conduction is a factor of specific surface area and grain and pore size (Mwakanyamale et al., 2012). Real and imaginary conductivity are related to electrolytic (σ_{ele}) and surface conduction (σ_{surf}) as follows:

$$\sigma' = \sigma_{ele} + \sigma^*_{surf} \tag{2}$$

$$\sigma'' = \sigma''_{surf} \tag{3}$$

The conductivity response of minerals and soils is controlled by water content, the conductivity of the saturating solution, and the sample lithology. The conductivity of aqueous solutions generally increases with the concentration, mobility, and electronic charge of the ions in the solution, as well as the temperature of the solution (Binley and Kemna, 2005).

Electrolytic conductivity can be expressed using Archie's Law (1942):

$$\sigma_{el} = \sigma_w \Phi^m S^n = \left(\frac{1}{F}\right)\sigma_w \tag{4}$$

where σ_w is the solution conductivity, Φ is the porosity, S is the saturation, F is the formation factor (related to the physical properties of the medium), m is the cementation factor, and n is the saturation exponent (Archie, 1942). Archie's law effectively predicts the electrical conductivity response of a saturated medium and assumes that all electrical

conduction in saturated soil results from the migration of ions in the bulk solution (Binley and Kemna, 2005).

The IP response is affected by lithology, pore fluid chemistry, and water content (Binley and Kenmna, 2005). The response is the result of polarization, a diffusion of ions in the EDL of interconnected pore space after application of current (Lesmes and Morgan, 2001). The imaginary component is controlled by electrochemical polarization mechanisms resulting in current displacement and the real component is controlled by electrolytic conduction in the bulk solution. The current displacement is caused by two polarization mechanisms: blockage of ions by clay minerals at pore throats and the accumulation of counter-ions migrating along grain/pore surfaces (Mwakanyamale et al., 2012). Electrical measurements can be interpreted in terms of physical and chemical properties of the medium (Binley and Kemna, 2005).

In a typical IP configuration, two electrodes act as a current source and sink and two electrodes measure the potential difference (voltage). The two current electrodes create an electrical circuit and the measurement of the potential difference (voltage) allows for determination of apparent resistivity (Binley and Kemna, 2005). This apparent resistivity is actually a measure of impedance via the magnitude and phase response. When current is applied at different frequencies, the result is a spectrum of impedance and this is referred to as SIP (Binley and Kemna, 2005).

For SIP measurements, magnitude and the phase angle of the column are measured throughout a frequency range. Magnitude $|\sigma|$ and phase (φ) are related to real and imaginary conductivity as follows:

$$|\sigma| = \sqrt{\sigma'^2 + \sigma''^2} \quad (5)$$

$$\varphi = \tan^{-1}\frac{\sigma'}{\sigma''} \quad (6)$$

where:

$$\sigma'' \left(S/m\right) = \left[\left(1/\rho\right) \times \sin(\varphi^0)\right] \quad (7)$$

$$\sigma' \left(S/m\right) = \left[\left(1/\rho\right) \times \cos(\varphi^0)\right] \quad (8)$$

(Mwakanyamale et al., 2012).

The shape of the spectra provides information on the driving forces that control the polarization (Schön, 1993; Ntarlagiannis et al., 2005b). All spectral data (phase, real and imaginary conductivity) should be plotted versus frequency over time for additional analysis (in addition to the changes in signal magnitude).

Gas Chromatography

The below protocol was used in extracting hydrocarbons from column outflow samples for Gas Chromatography/Mass Spectrometry (GC/MS) analysis.

1. Samples were centrifuged at 3,000 rpm in a benchtop centrifuge for 5 minutes in order to remove any large particulate material.
2. 5 ml of the supernatant was then transferred to a new vial.
3. A surrogate was added to the sample in order to determine extraction efficiency. The surrogate used in this instance was naphthalene-d8 (deuterated). 50 ul of a stock of naphthalene-d8 (0.272 mg/ml stock concentration) in dichloromethane was added to the sample to yield ~100 nmoles
4. Samples were acidified with HCl to a pH of <2. This was done to deprotonate any organic acids.

5. The samples were then extracted 3 times with 5 ml dichloromethane as follows: Extractions were done in a 40-ml glass EPA vial. The vials were vortexed briefly to mix the solvent and sample. Once the phases separated, the top aqueous phase was carefully transferred to a new vial and then mixed with a new volume of 5 ml solvent. This was repeated for a total of 3 solvent applications.
6. Extracts were pooled and visual verification of the removal of the aqueous phase was confirmed.
7. Extracts were then concentrate by evaporating the solvent under a stream of N_2 gas to ~ 1 ml and then stored at -20°C before drying.
8. The concentrated extract was passed through a drying column of anhydrous sodium sulfate to remove any residual water.
9. The extract was evaporated to completion and stored at -20°C until ready for analysis.
10. Prior to derivatization an internal standard, 4-fluoro-1-naphthoic acid, was added to measure the effectiveness of the derivatization step. 100 nm of 4-fluoro-1-naphthoic acid was added to each step, though no more than 100 ul of liquid was added to the dried sample. Volume was adjusted to 100 ul total with dichloromethane.
11. Samples were derivitized with 100 ul BTSFA (N,O-bis-(trimetylsilyl)trifluoroacetamide) and incubated at 60°C in a water bath for 10 minutes.
12. All liquid was transferred to a small glass insert that fits within a glass GC vial.
13. 2 ul was then injected into the GC/MS for analysis.

(Phelps et al., 2002; EPA).

APPENDIX II

Geometric Factor

The fluid tests were conducted with four different NaCl solutions (0.001 M NaCl, 0.01 M NaCl, 0.1 M NaCl, 1 M NaCl) and consisted of the following procedures: measurement of the conductivity of each solution, filling each column with solution, measuring the contact resistance of the current and potential electrodes, utilizing the PSIP for electrical measurements, and measuring contact resistances and conductivity again. Results of the fluid tests can be seen in Figure A-1.

a)

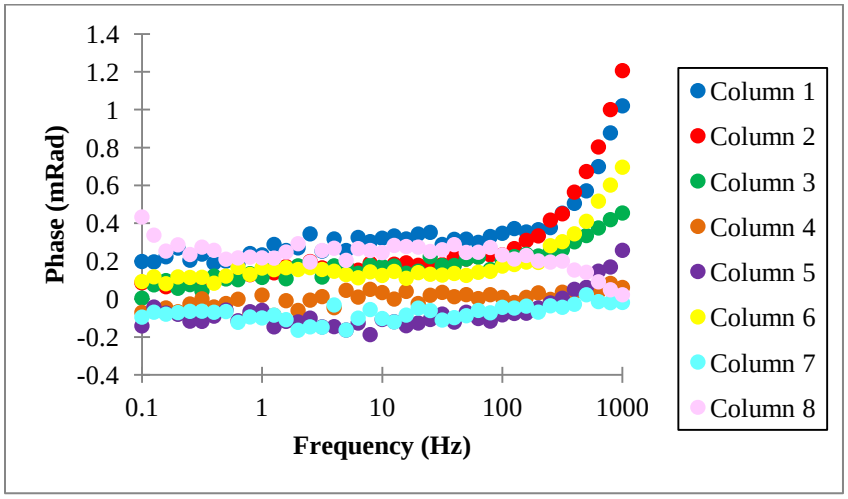

b)

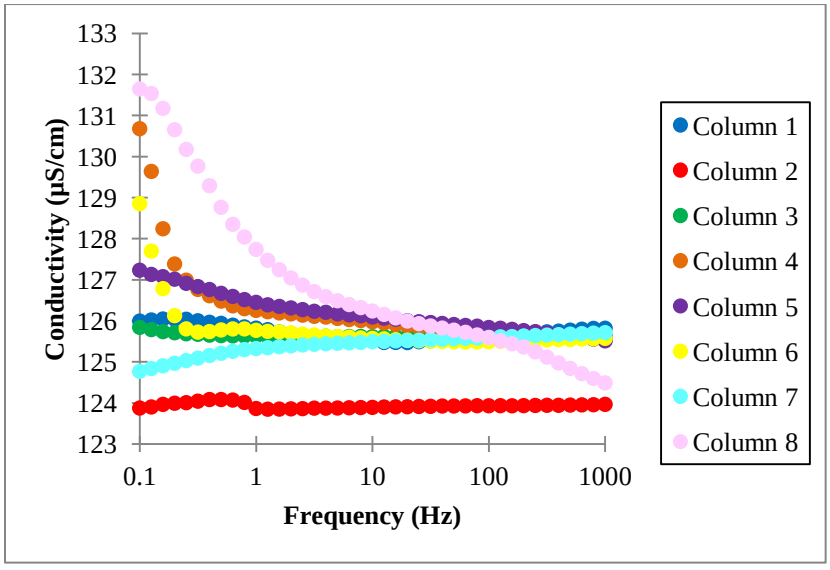

c)

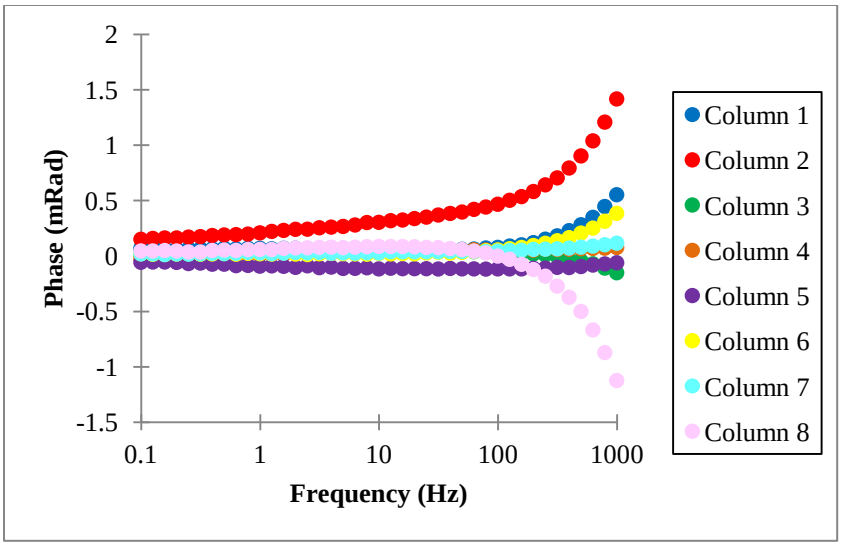
2
1.5
1
0.5
0
-0.5
-1
-1.5
Phase (mRad)
0.1
1
10
100
1000
Frequency (Hz)
Column 1
Column 2
Column 3
Column 4
Column 5
Column 6
Column 7
Column 8

d)

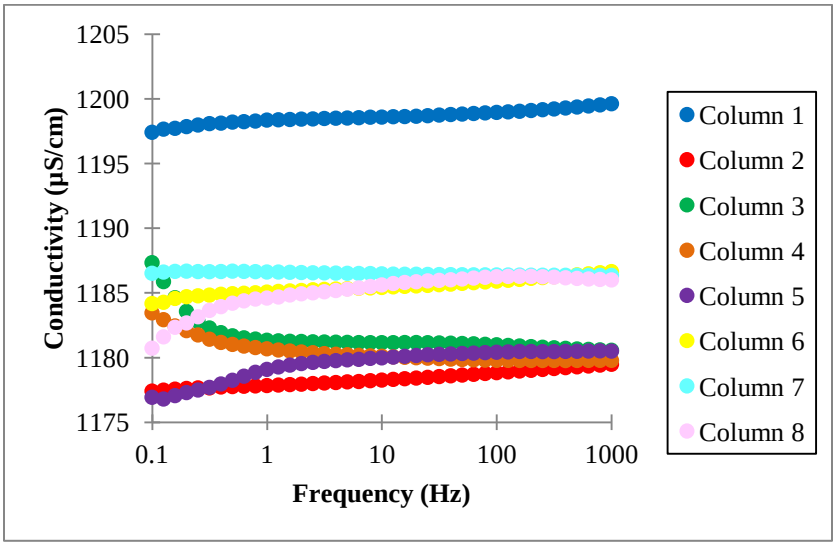
1205
1200
1195
1190
1185
1180
1175
Conductivity (µS/cm)
0.1
1
10
100
1000
Frequency (Hz)
Column 1
Column 2
Column 3
Column 4
Column 5
Column 6
Column 7
Column 8

e)

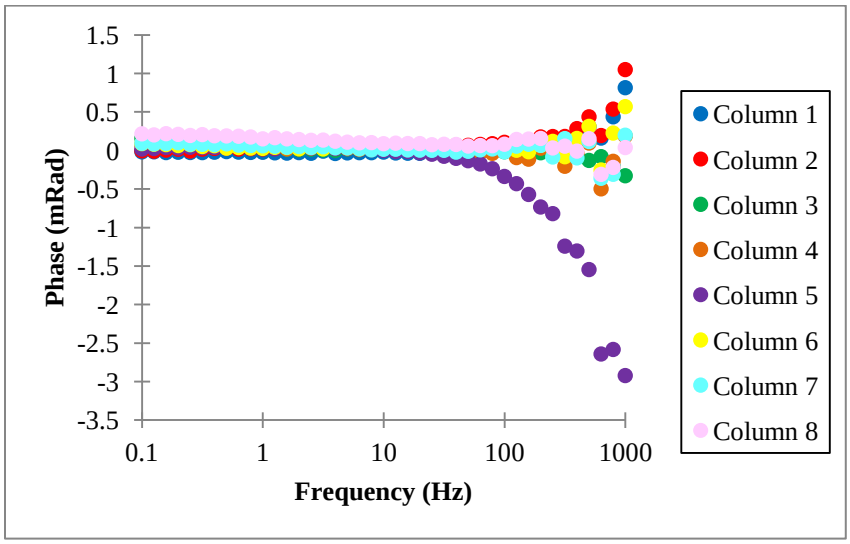
1.5
1
0.5
0
-0.5
-1
-1.5
-2
-2.5
-3
-3.5
Phase (mRad)
0.1
1
10
100
1000
Frequency (Hz)
Column 1
Column 2
Column 3
Column 4
Column 5
Column 6
Column 7
Column 8

f)

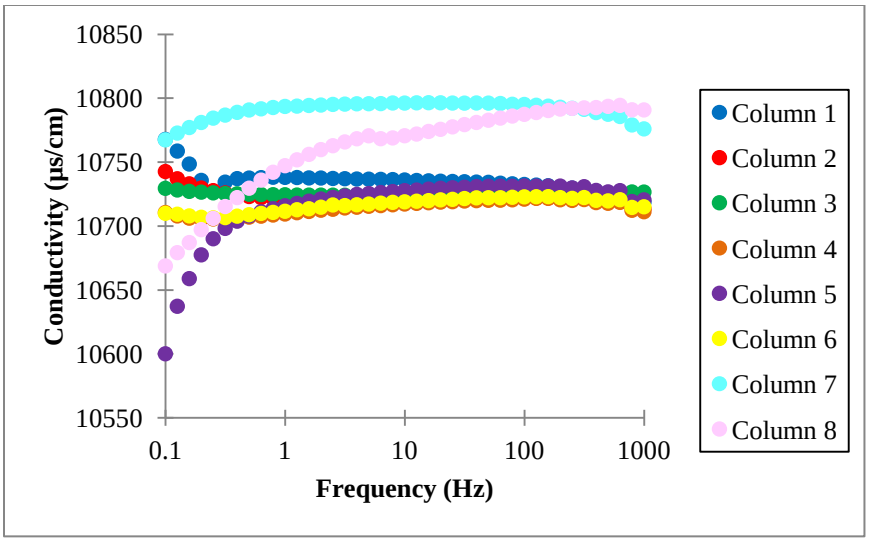
10850
10800
10750
10700
10650
10600
10550
Conductivity (µs/cm)
0.1
1
10
100
1000
Frequency (Hz)
Column 1
Column 2
Column 3
Column 4
Column 5
Column 6
Column 7
Column 8

g)

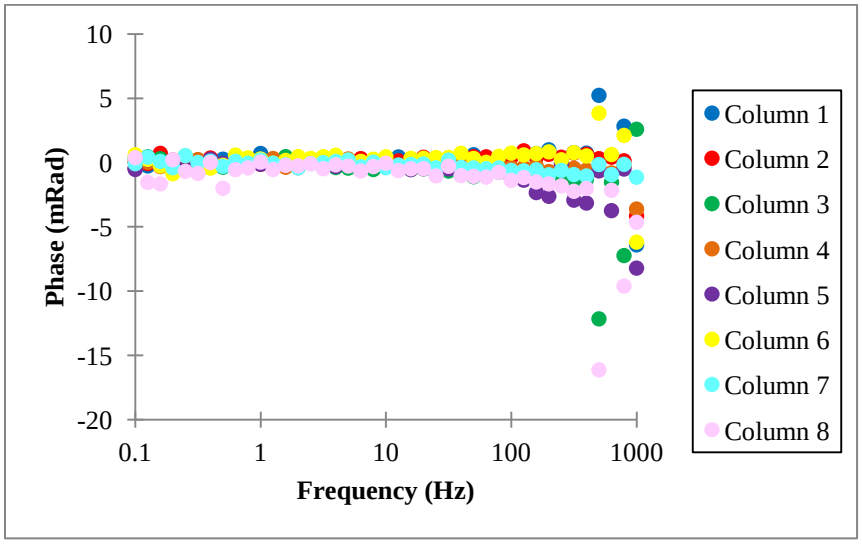
10
5
0
-5
-10
-15
-20
Phase (mRad)
0.1
1
10
100
1000
Frequency (Hz)
Column 1
Column 2
Column 3
Column 4
Column 5
Column 6
Column 7
Column 8

h)

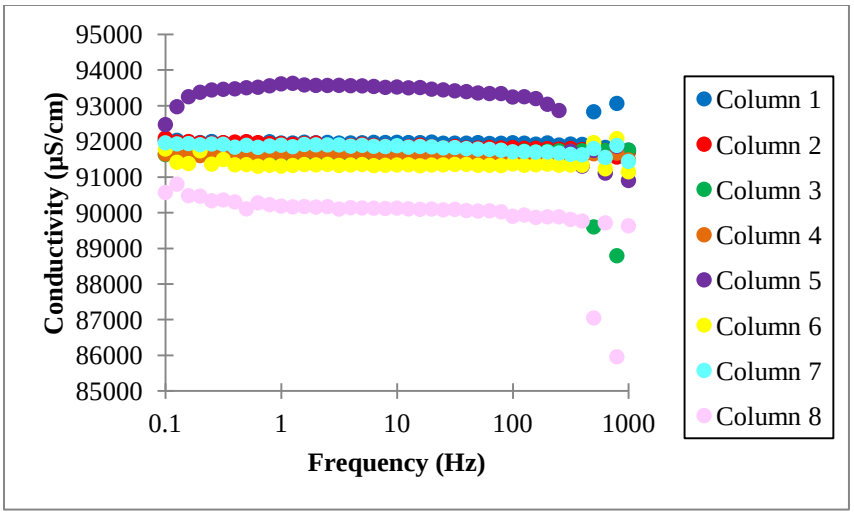

Figure A-1. Fluid conductivity and phase response of each column during fluid tests with a) and b) 0.001 M NaCl; c) and d) 0.01 M NaCl; e) and f) 0.1 M NaCl; g) and h) 1 M NaCl. Columns 1, 2, 3, 5, and 6 are the active columns; Columns 4, 7, and 8 are the control columns.

Electrical Measurement Results

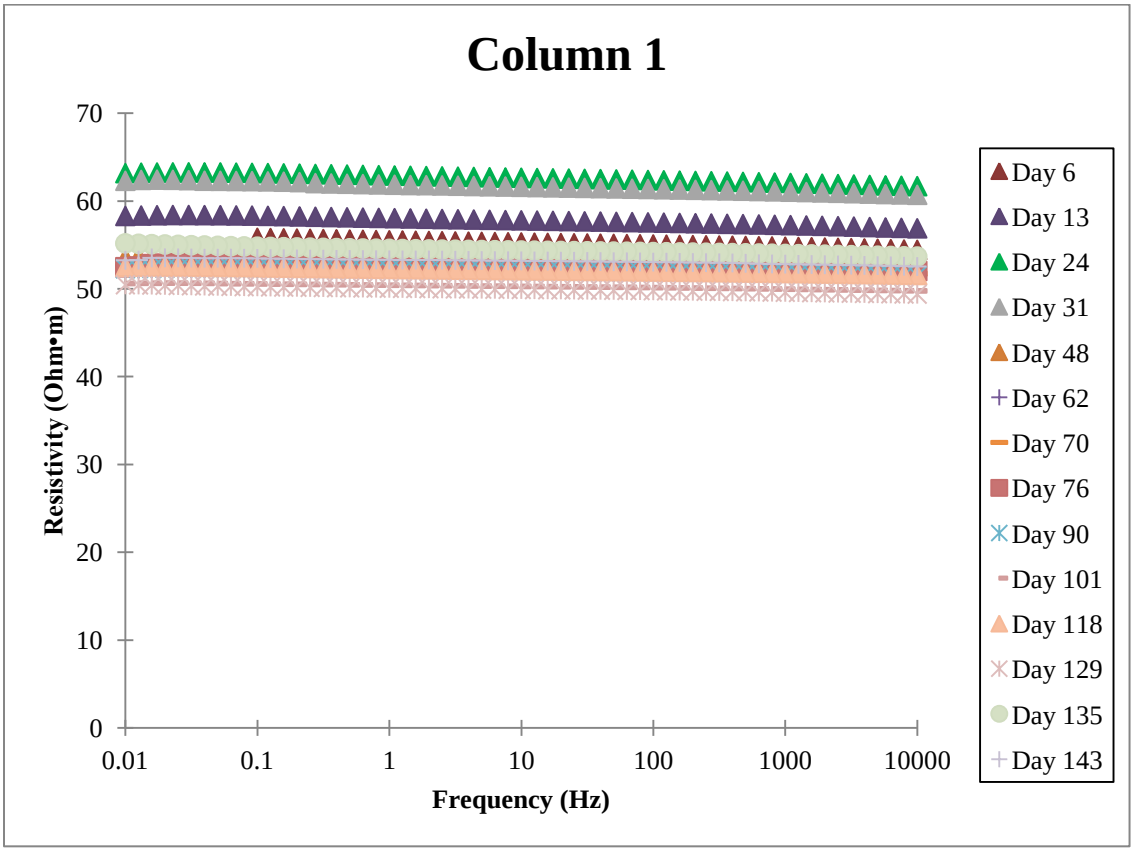

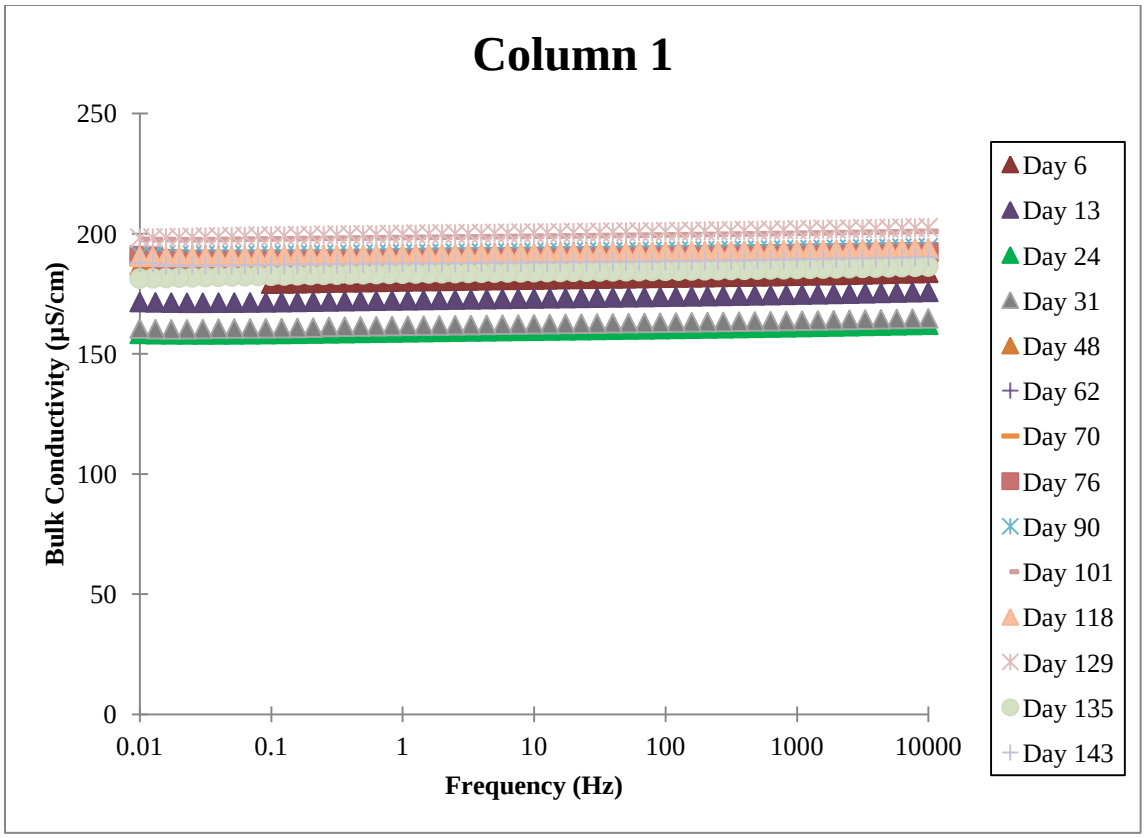
Column 1
Bulk Conductivity (µS/cm)
250
200
150
100
50
0
0.01
0.1
1
10
100
1000
10000
Frequency (Hz)
Day 6
Day 13
Day 24
Day 31
Day 48
Day 62
Day 70
Day 76
Day 90
Day 101
Day 118
Day 129
Day 135
Day 143

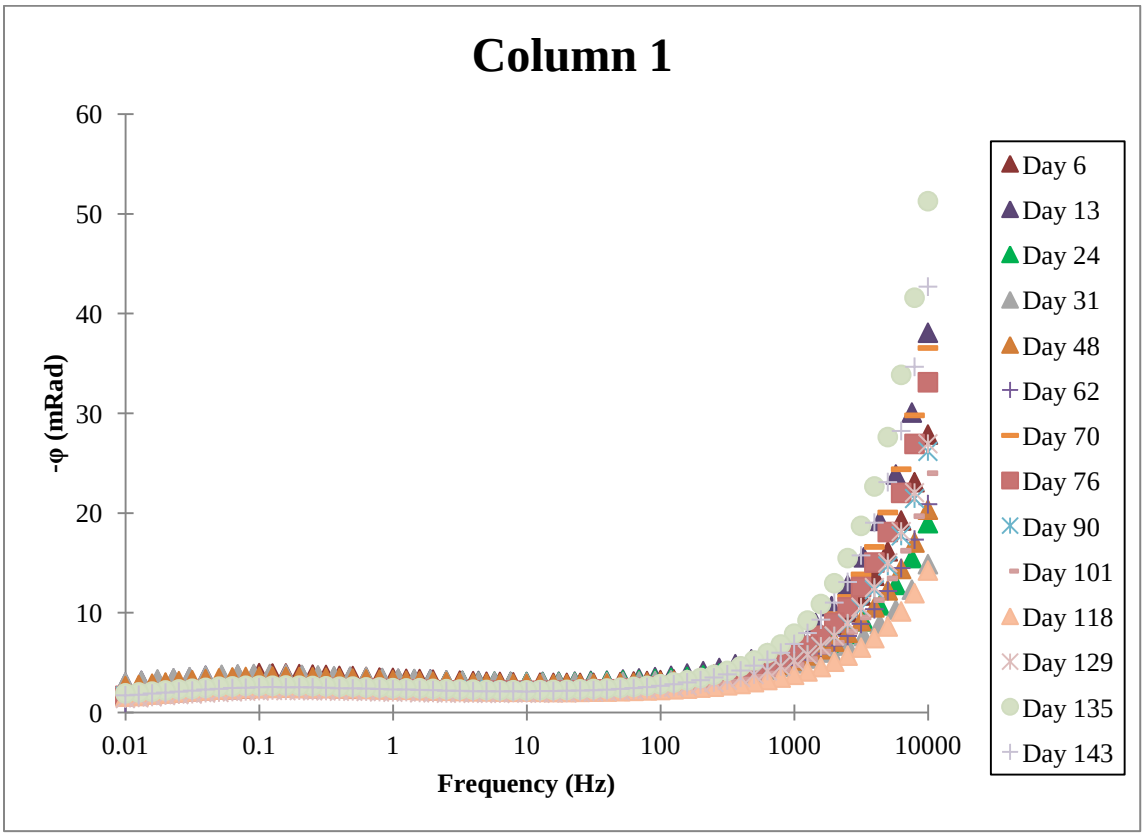
Column 1
-φ (mRad)
60
50
40
30
20
10
0
0.01
0.1
1
10
100
1000
10000
Frequency (Hz)
Day 6
Day 13
Day 24
Day 31
Day 48
Day 62
Day 70
Day 76
Day 90
Day 101
Day 118
Day 129
Day 135
Day 143

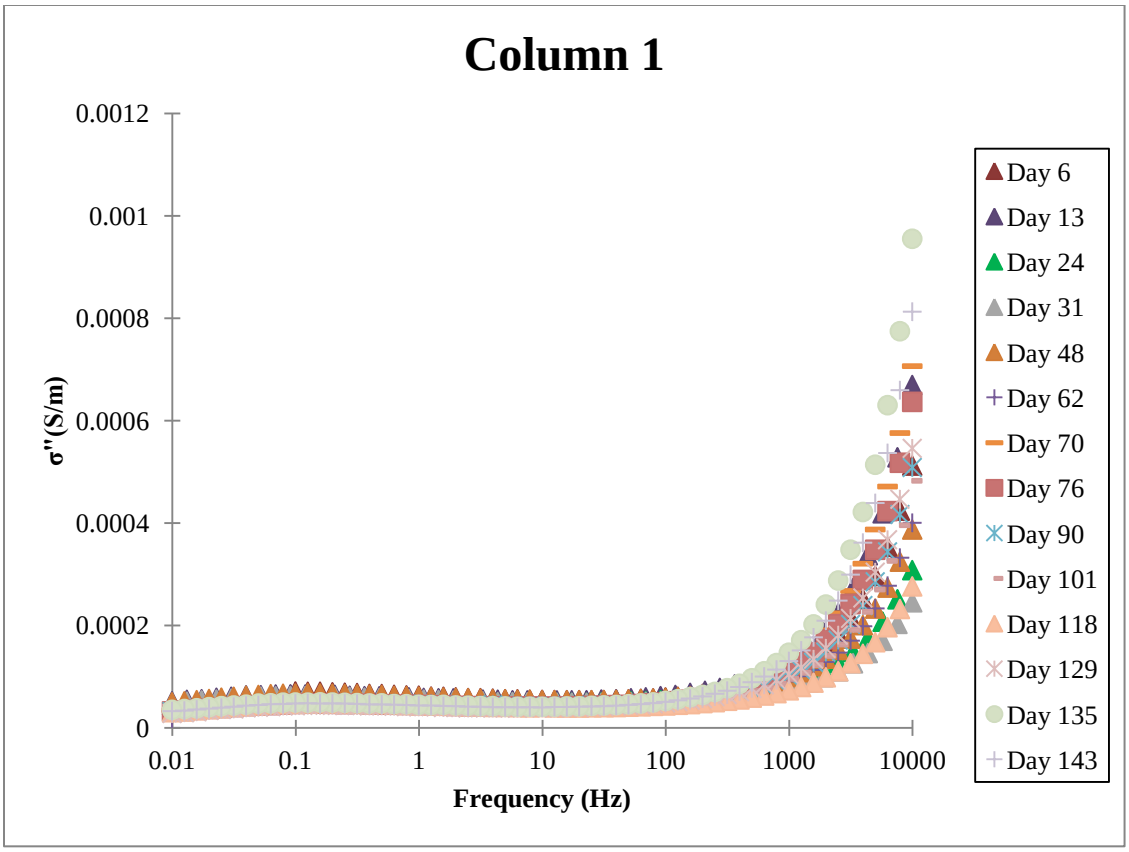
Column 1
0.0012
0.001
0.0008
0.0006
0.0004
0.0002
0
σ''(S/m)
0.01
0.1
1
10
100
1000
10000
Frequency (Hz)
Day 6
Day 13
Day 24
Day 31
Day 48
Day 62
Day 70
Day 76
Day 90
Day 101
Day 118
Day 129
Day 135
Day 143

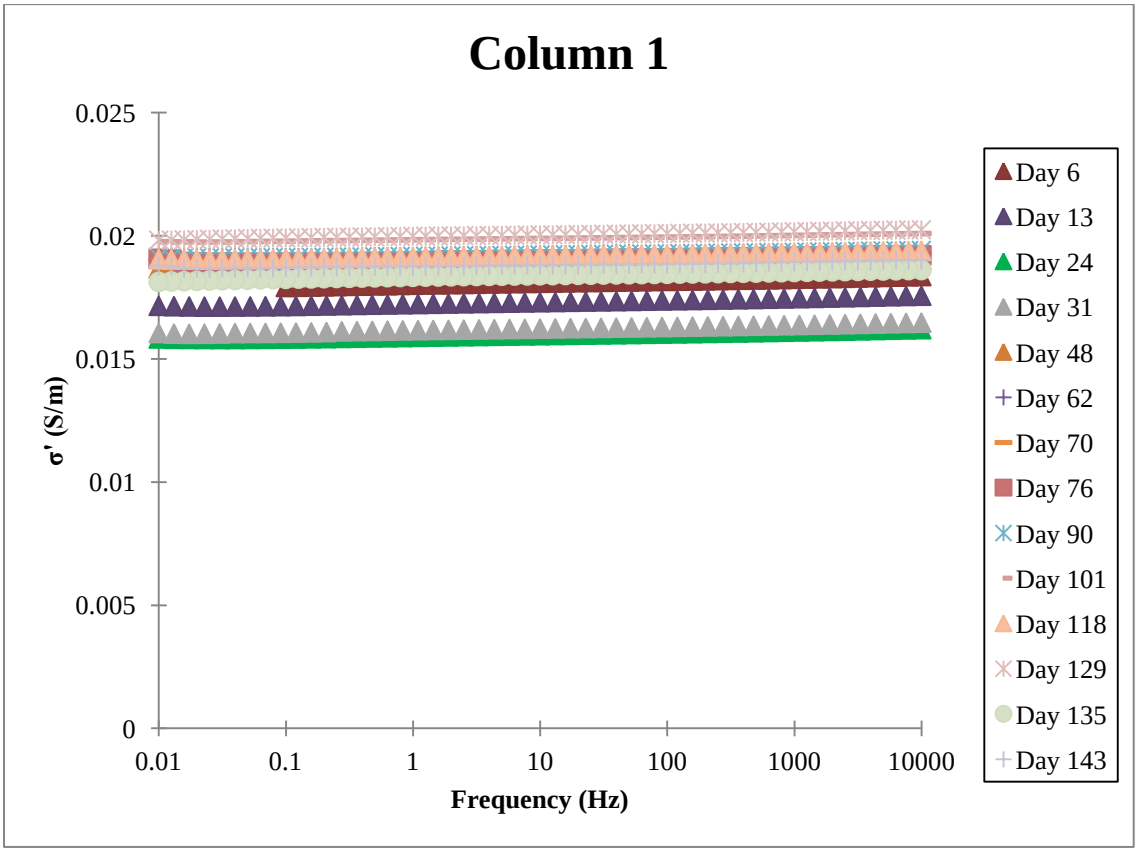
Column 1
0.025
0.02
0.015
0.01
0.005
0
σ' (S/m)
0.01
0.1
1
10
100
1000
10000
Frequency (Hz)
Day 6
Day 13
Day 24
Day 31
Day 48
Day 62
Day 70
Day 76
Day 90
Day 101
Day 118
Day 129
Day 135
Day 143

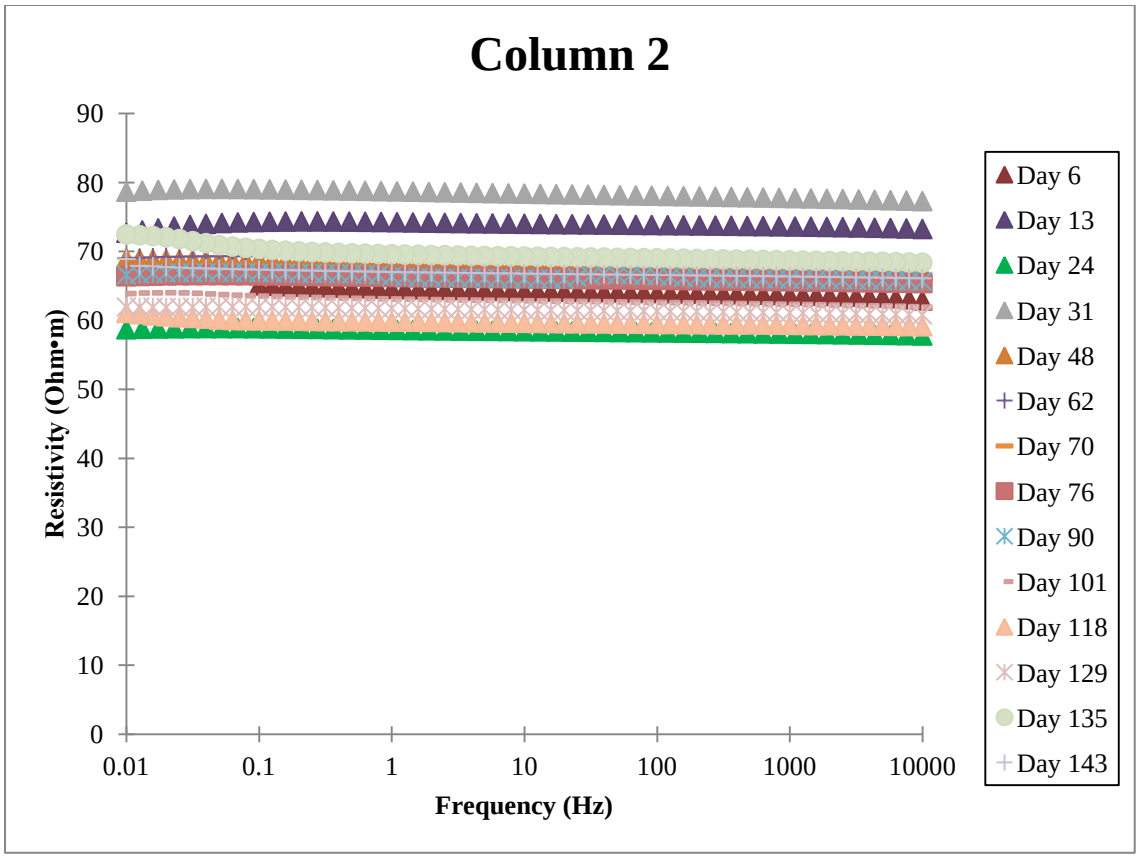
Column 2
Resistivity (Ohm*m)
90
80
70
60
50
40
30
20
10
0
0.01
0.1
1
10
100
1000
10000
Frequency (Hz)
Day 6
Day 13
Day 24
Day 31
Day 48
Day 62
Day 70
Day 76
Day 90
Day 101
Day 118
Day 129
Day 135
Day 143

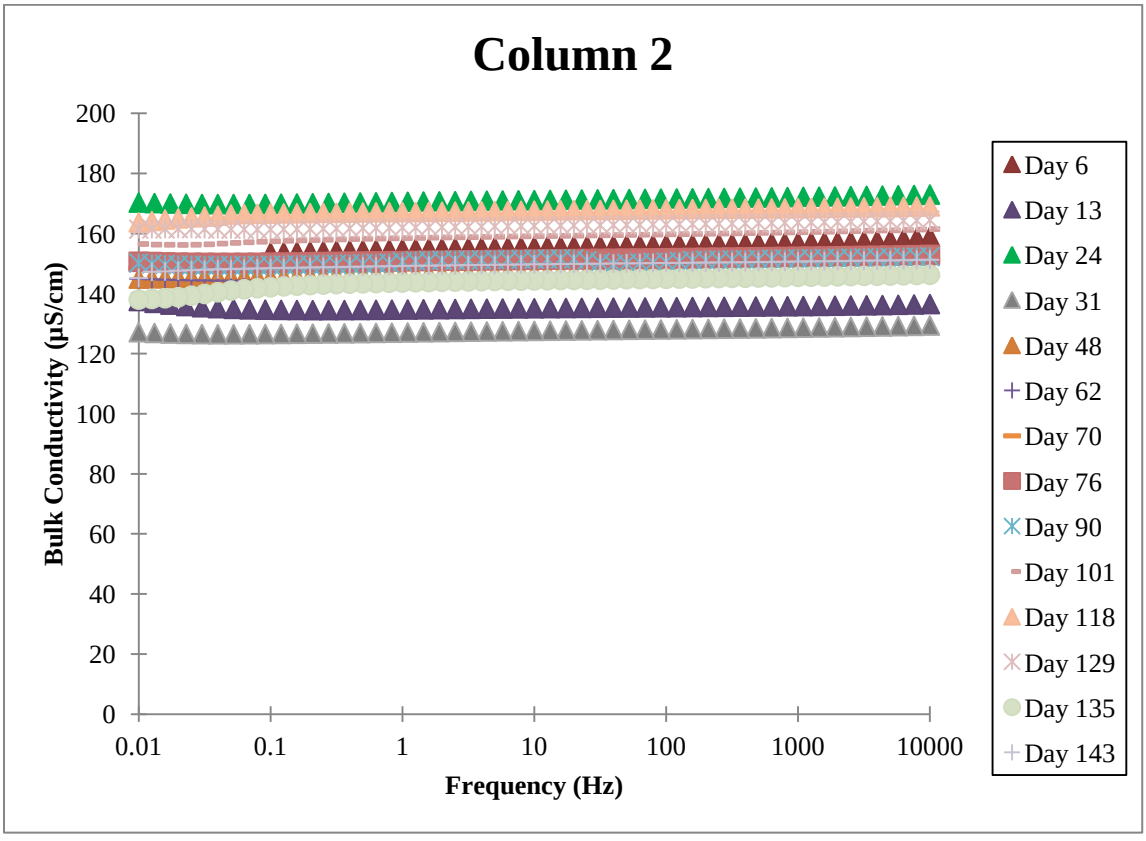
Column 2
Bulk Conductivity (µS/cm)
200
180
160
140
120
100
80
60
40
20
0
0.01
0.1
1
10
100
1000
10000
Frequency (Hz)
Day 6
Day 13
Day 24
Day 31
Day 48
Day 62
Day 70
Day 76
Day 90
Day 101
Day 118
Day 129
Day 135
Day 143

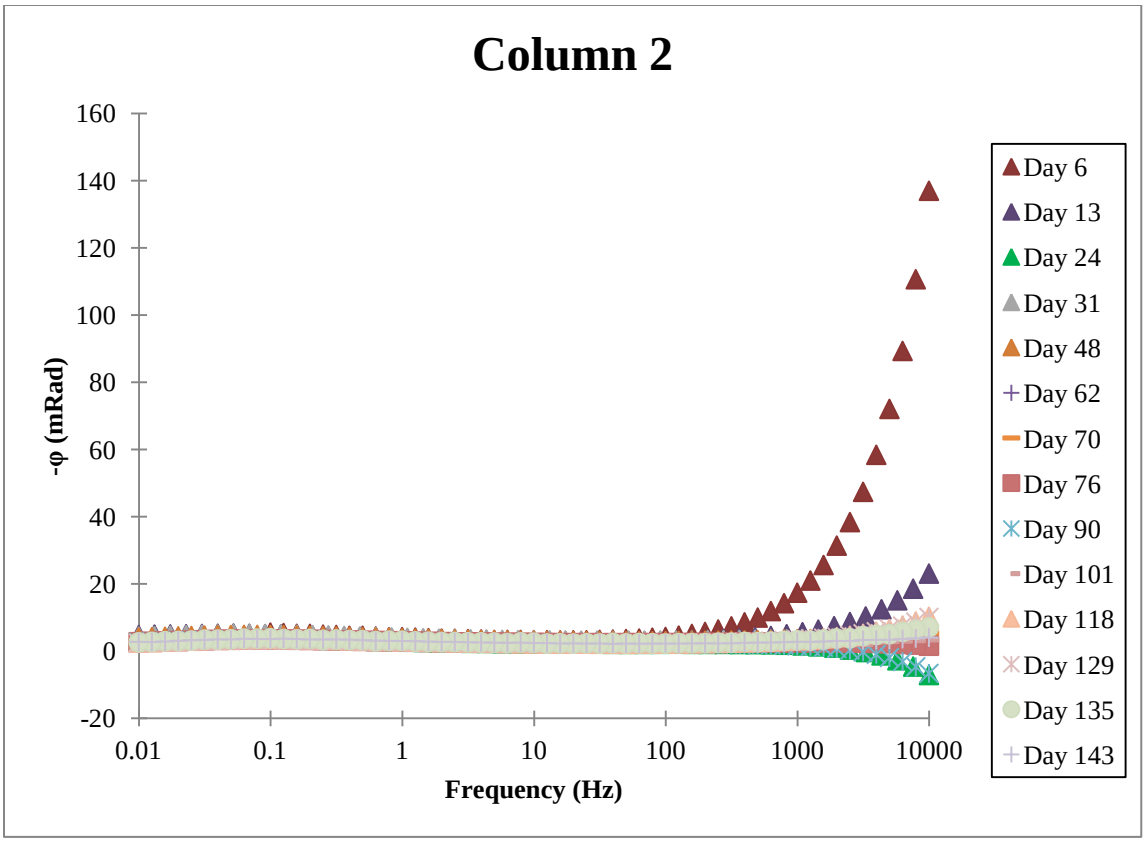
Column 2
160
140
120
100
80
60
40
20
0
-20
-φ (mRad)
0.01
0.1
1
10
100
1000
10000
Frequency (Hz)
Day 6
Day 13
Day 24
Day 31
Day 48
Day 62
Day 70
Day 76
Day 90
Day 101
Day 118
Day 129
Day 135
Day 143

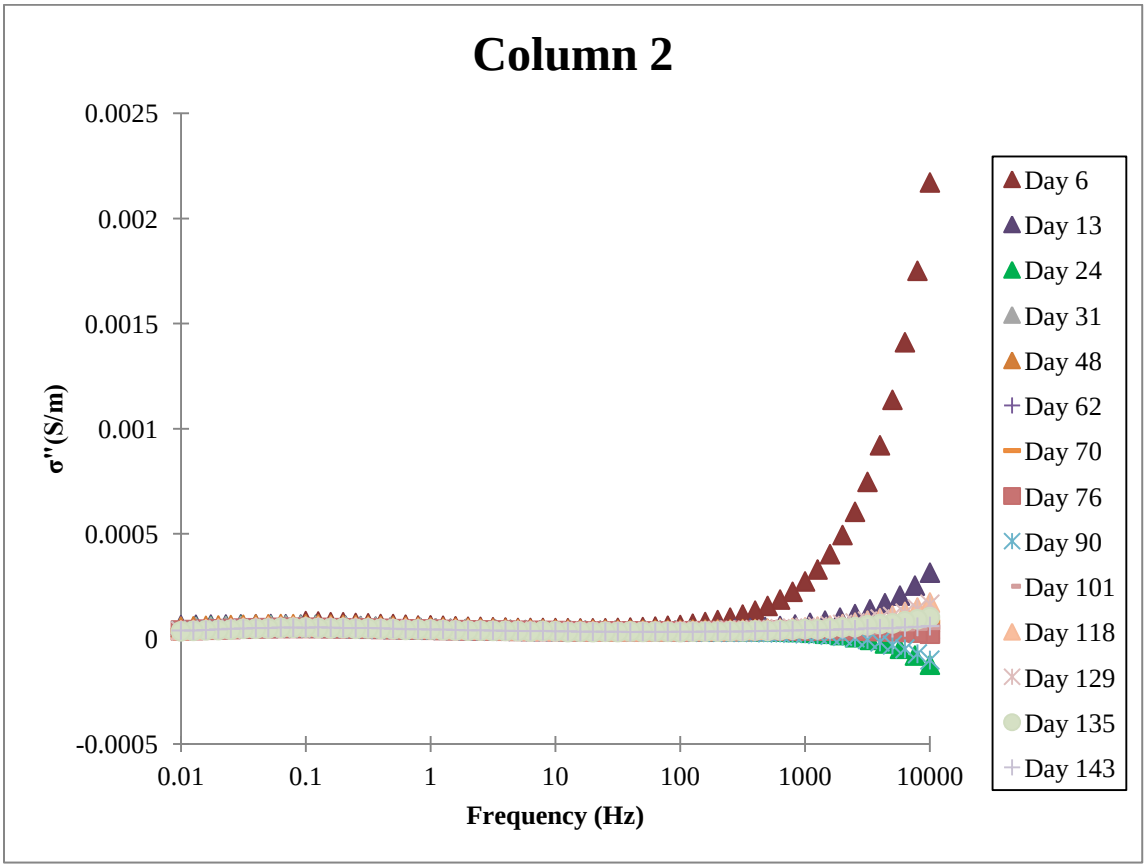
Column 2
0.0025
0.002
0.0015
0.001
0.0005
0
-0.0005
σ''(S/m)
0.01
0.1
1
10
100
1000
10000
Frequency (Hz)
Day 6
Day 13
Day 24
Day 31
Day 48
Day 62
Day 70
Day 76
Day 90
Day 101
Day 118
Day 129
Day 135
Day 143

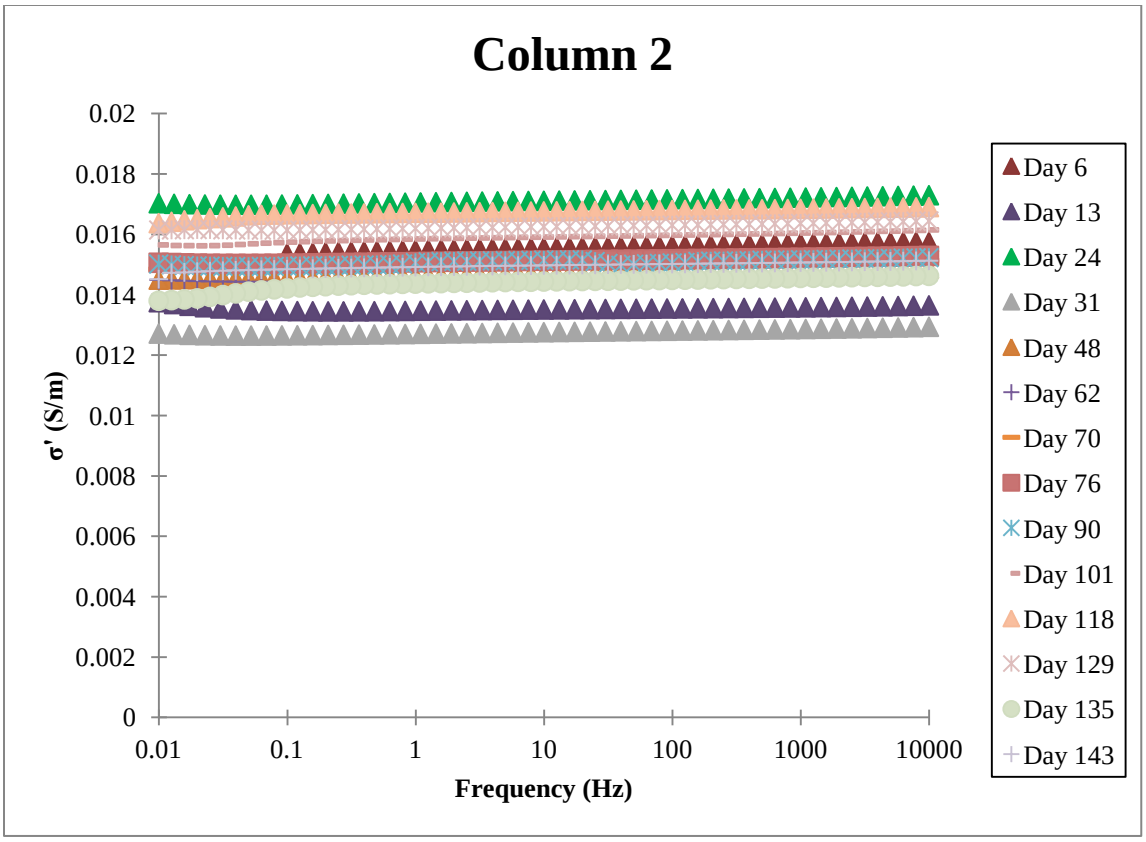
Column 2
0.02
0.018
0.016
0.014
0.012
0.01
0.008
0.006
0.004
0.002
0
σ' (S/m)
0.01
0.1
1
10
100
1000
10000
Frequency (Hz)
Day 6
Day 13
Day 24
Day 31
Day 48
Day 62
Day 70
Day 76
Day 90
Day 101
Day 118
Day 129
Day 135
Day 143

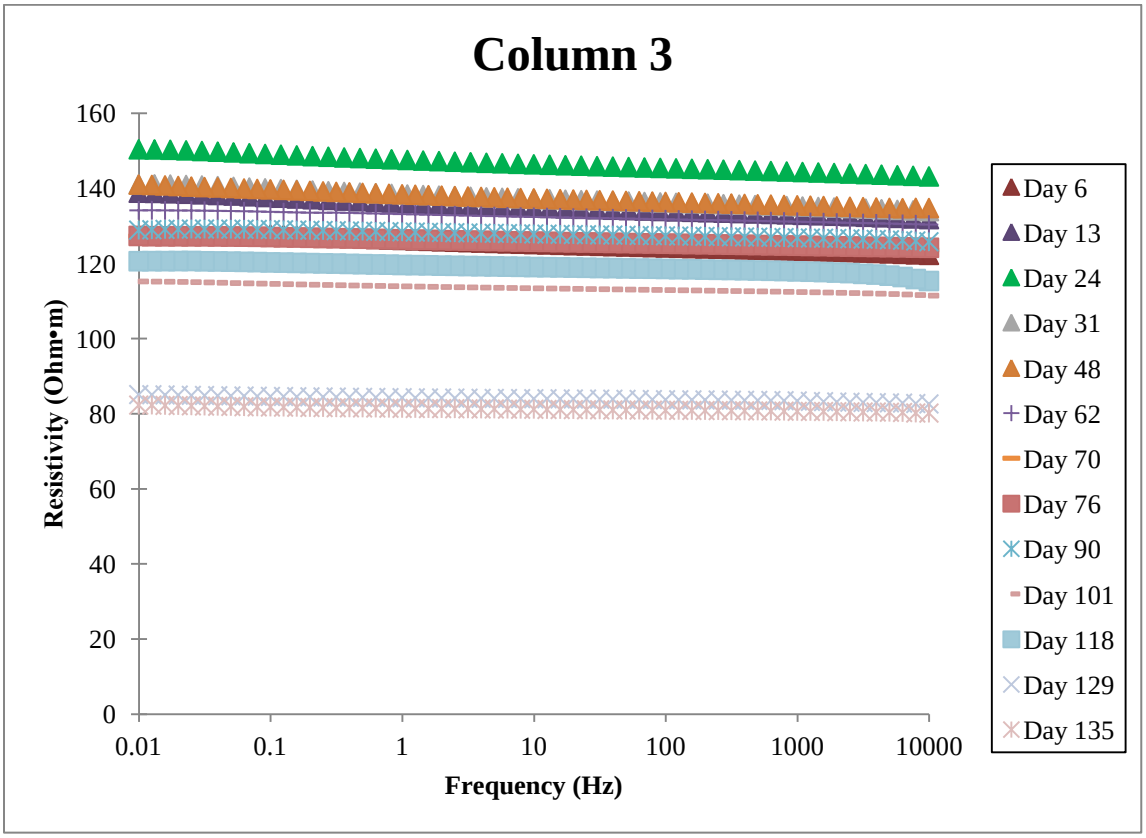
Column 3
160
140
120
100
80
60
40
20
0
Resistivity (Ohm•m)
0.01
0.1
1
10
100
1000
10000
Frequency (Hz)
Day 6
Day 13
Day 24
Day 31
Day 48
Day 62
Day 70
Day 76
Day 90
Day 101
Day 118
Day 129
Day 135

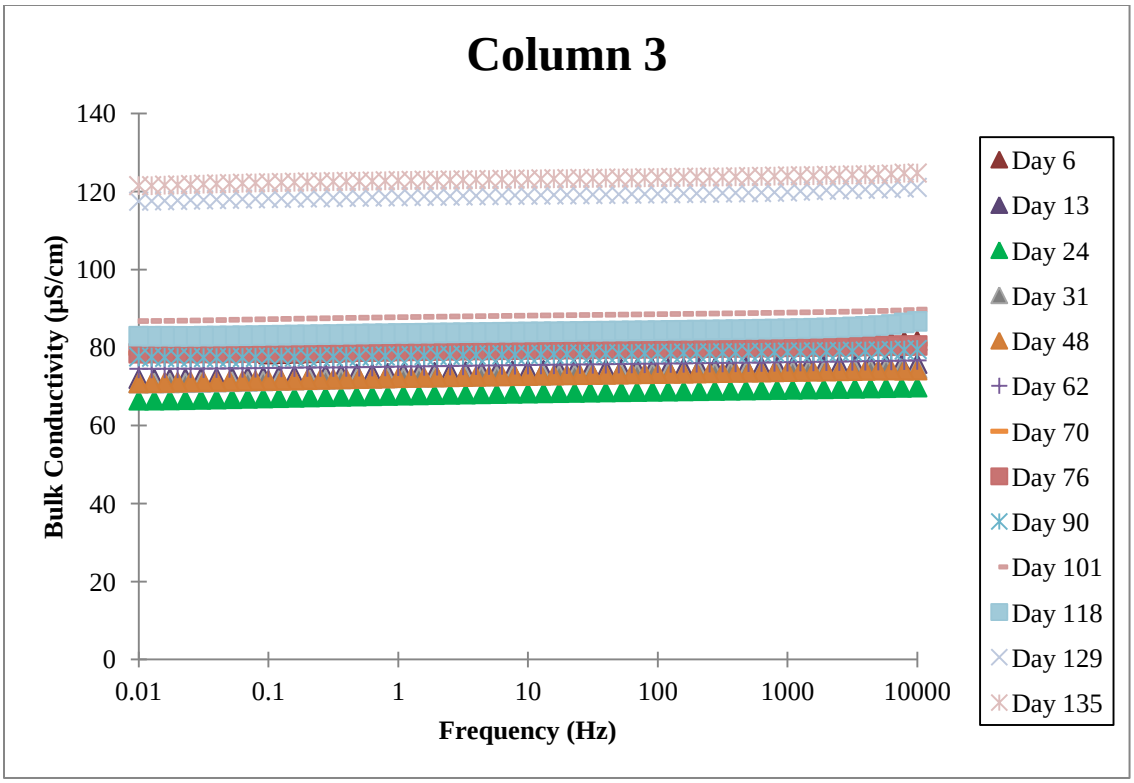
Column 3
Bulk Conductivity (µS/cm)
140
120
100
80
60
40
20
0
0.01
0.1
1
10
100
1000
10000
Frequency (Hz)
Day 6
Day 13
Day 24
Day 31
Day 48
Day 62
Day 70
Day 76
Day 90
Day 101
Day 118
Day 129
Day 135

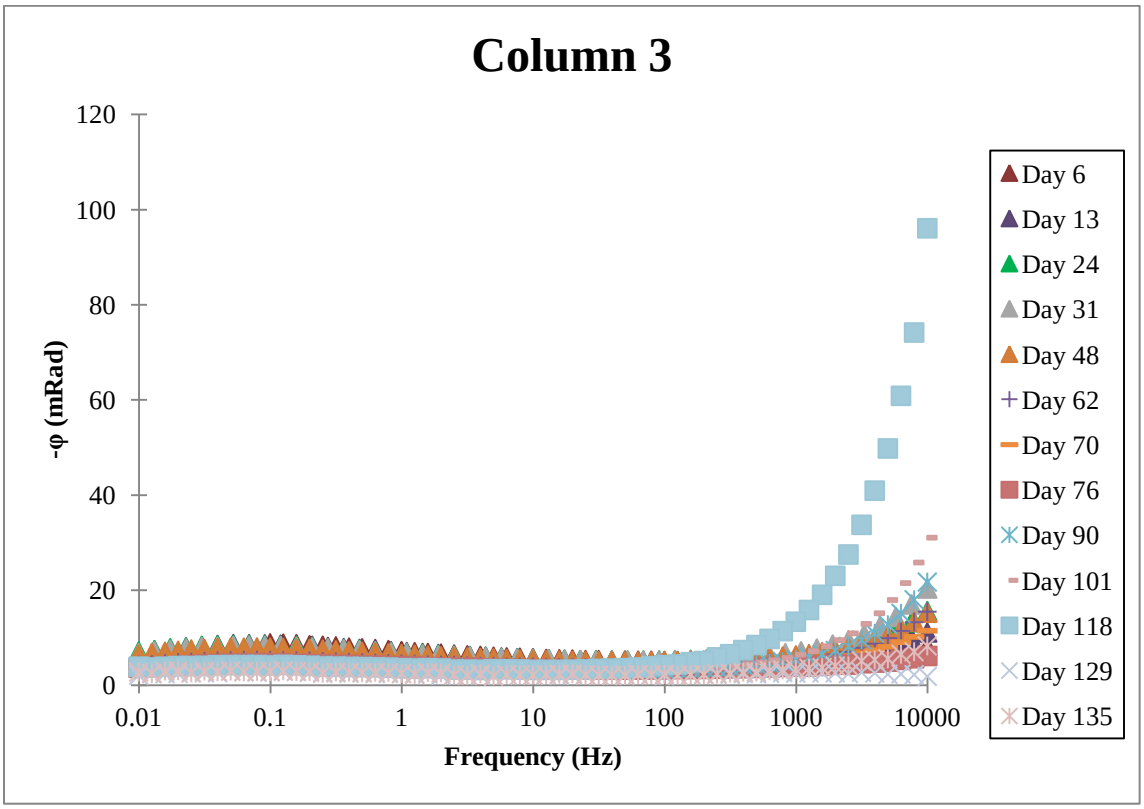
Column 3
-φ (mRad)
120
100
80
60
40
20
0
0.01
0.1
1
10
100
1000
10000
Frequency (Hz)
Day 6
Day 13
Day 24
Day 31
Day 48
Day 62
Day 70
Day 76
Day 90
Day 101
Day 118
Day 129
Day 135

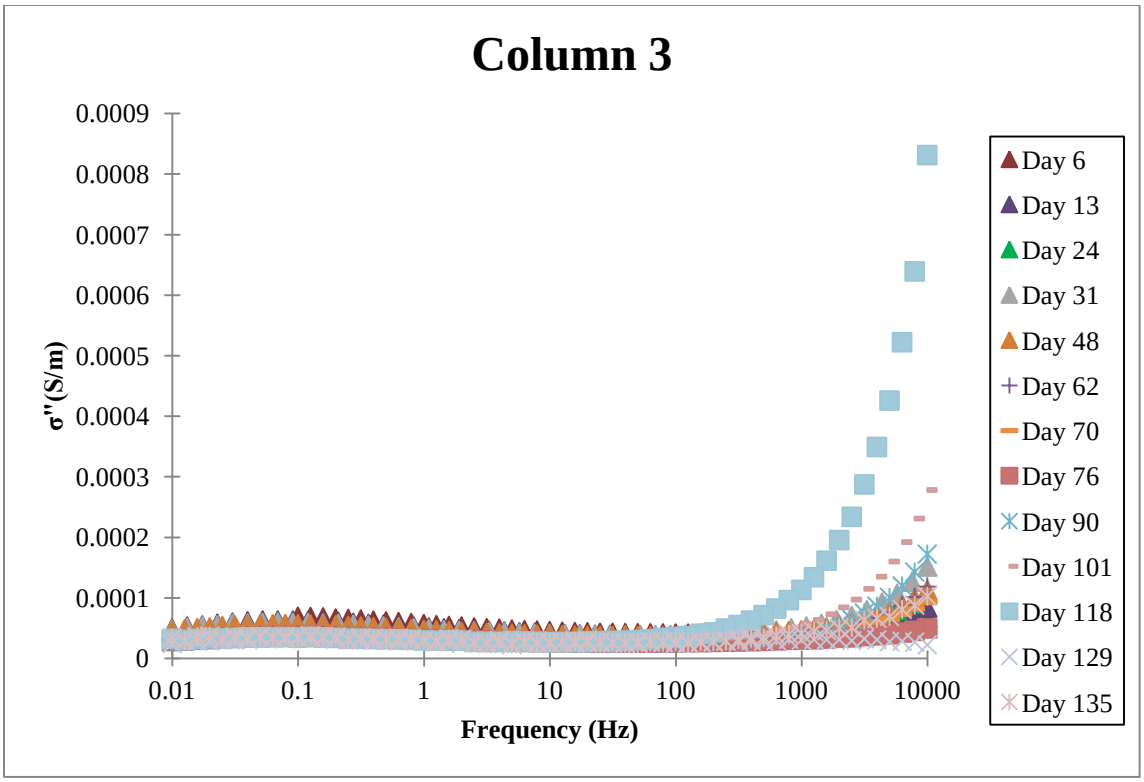
Column 3
0.0009
0.0008
0.0007
0.0006
0.0005
0.0004
0.0003
0.0002
0.0001
0
σ''(S/m)
0.01
0.1
1
10
100
1000
10000
Frequency (Hz)
Day 6
Day 13
Day 24
Day 31
Day 48
Day 62
Day 70
Day 76
Day 90
Day 101
Day 118
Day 129
Day 135

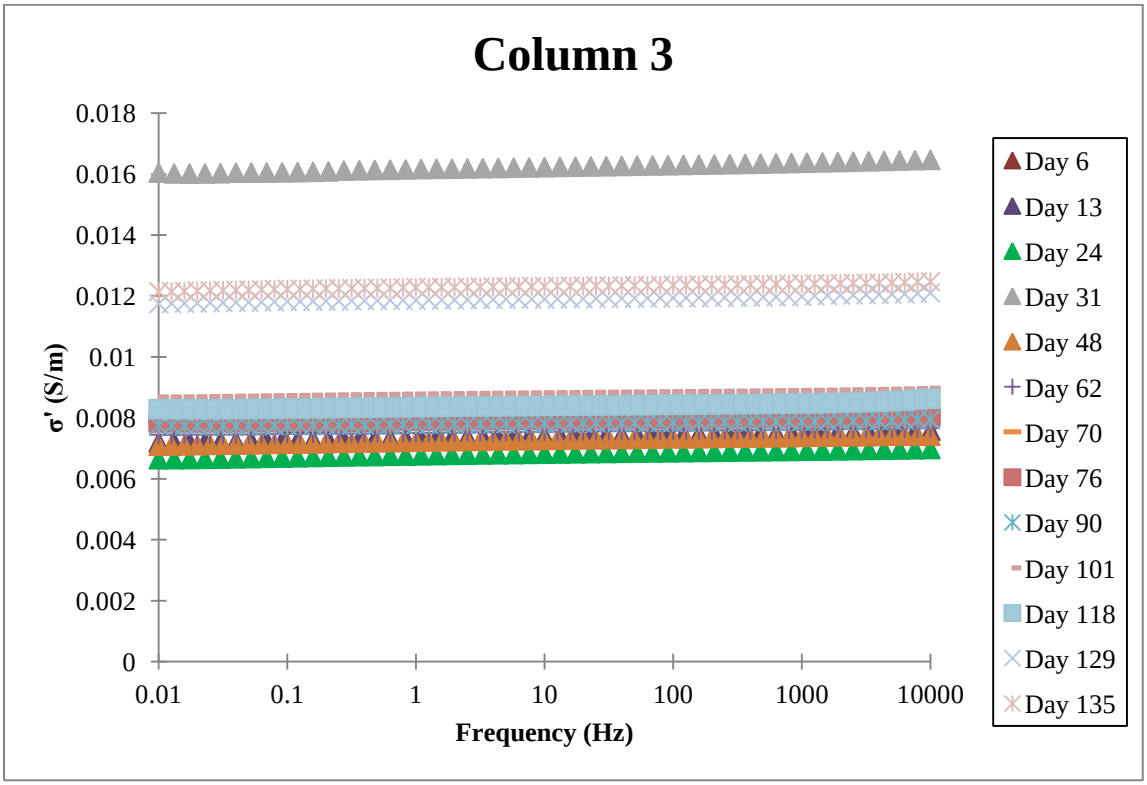
Column 3
0.018
0.016
0.014
0.012
0.01
0.008
0.006
0.004
0.002
0
σ' (S/m)
0.01
0.1
1
10
100
1000
10000
Frequency (Hz)
Day 6
Day 13
Day 24
Day 31
Day 48
Day 62
Day 70
Day 76
Day 90
Day 101
Day 118
Day 129
Day 135

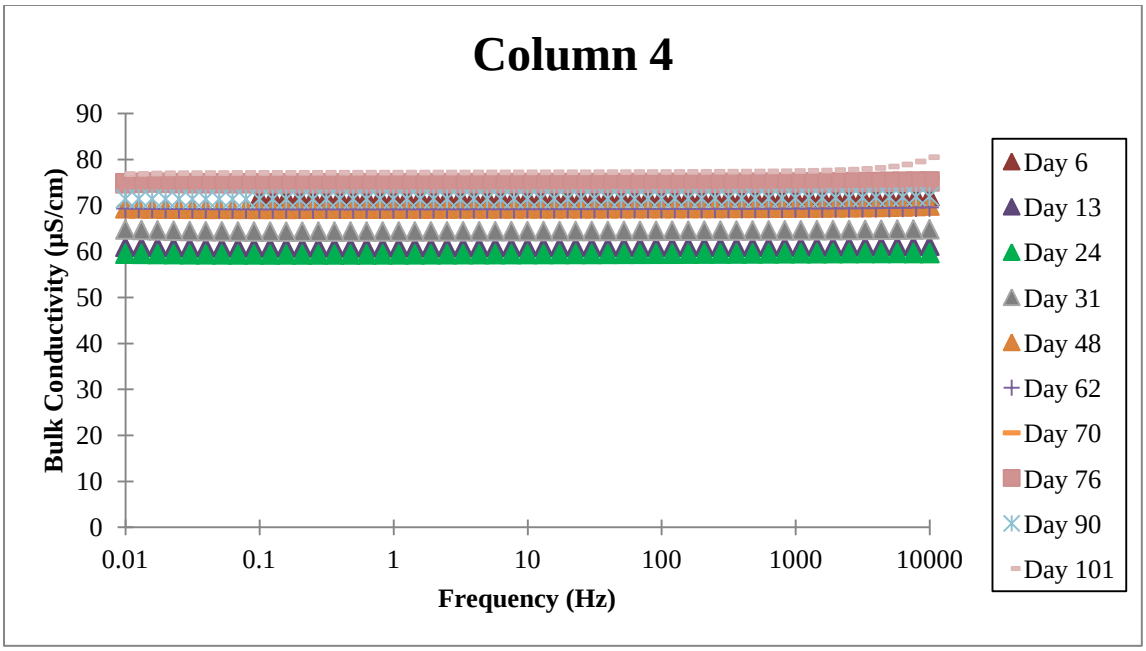
Column 4
Bulk Conductivity (µS/cm)
90
80
70
60
50
40
30
20
10
0
0.01
0.1
1
10
100
1000
10000
Frequency (Hz)
Day 6
Day 13
Day 24
Day 31
Day 48
Day 62
Day 70
Day 76
Day 90
Day 101

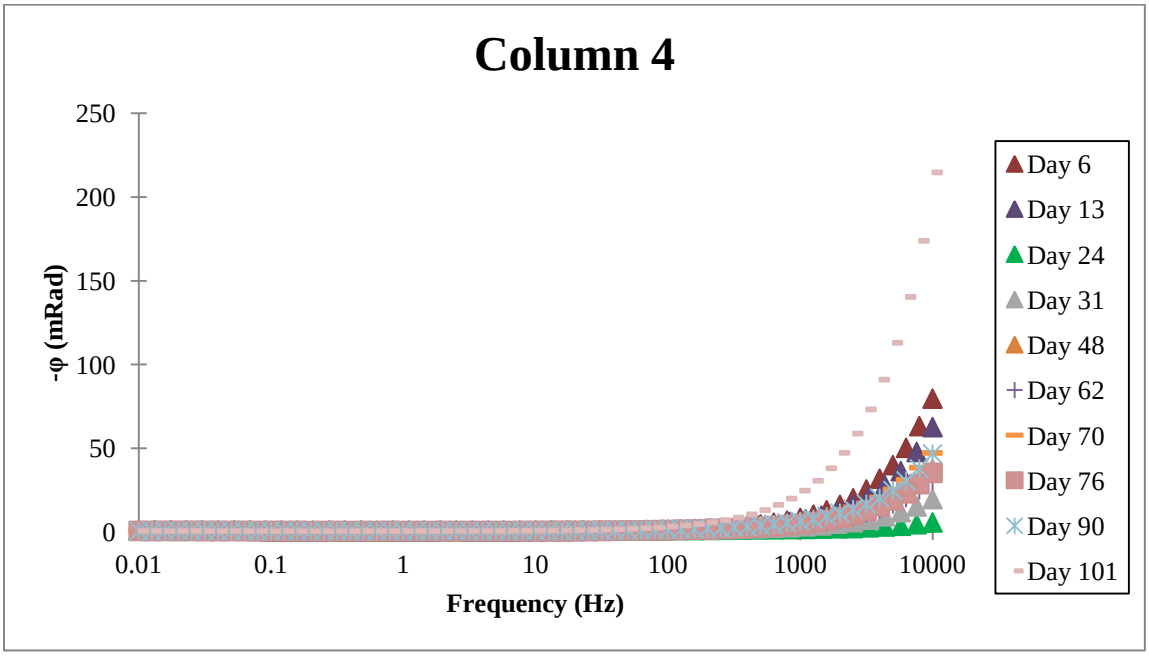
Column 4
-φ (mRad)
250
200
150
100
50
0
0.01
0.1
1
10
100
1000
10000
Frequency (Hz)
Day 6
Day 13
Day 24
Day 31
Day 48
Day 62
Day 70
Day 76
Day 90
Day 101

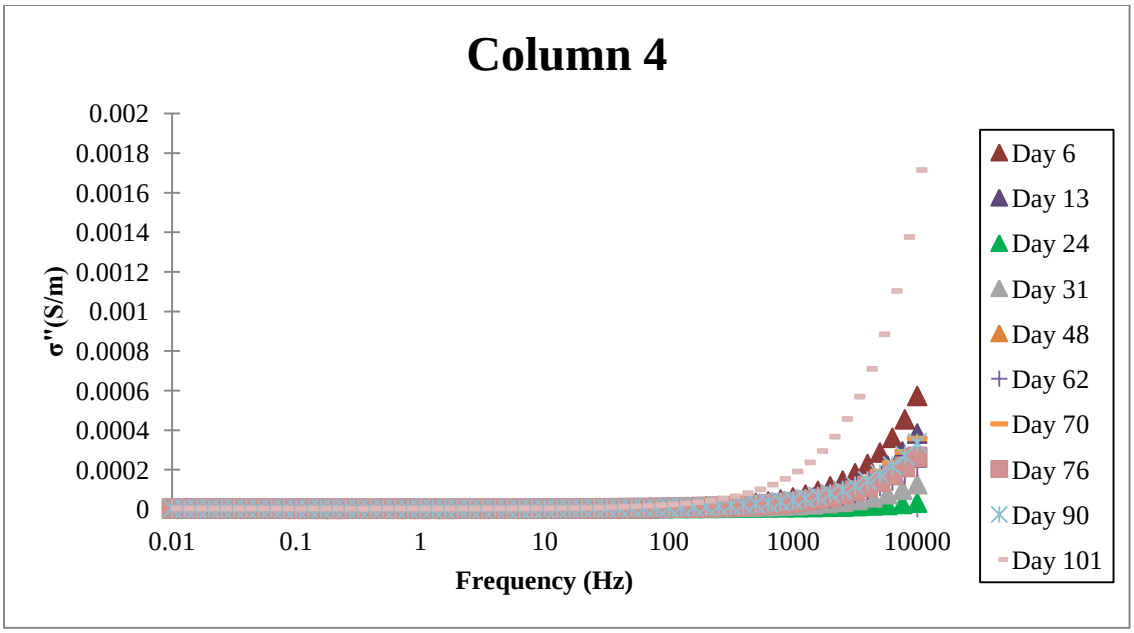
Column 4
σ''(S/m)
0.002
0.0018
0.0016
0.0014
0.0012
0.001
0.0008
0.0006
0.0004
0.0002
0
0.01
0.1
1
10
100
1000
10000
Frequency (Hz)
Day 6
Day 13
Day 24
Day 31
Day 48
Day 62
Day 70
Day 76
Day 90
Day 101

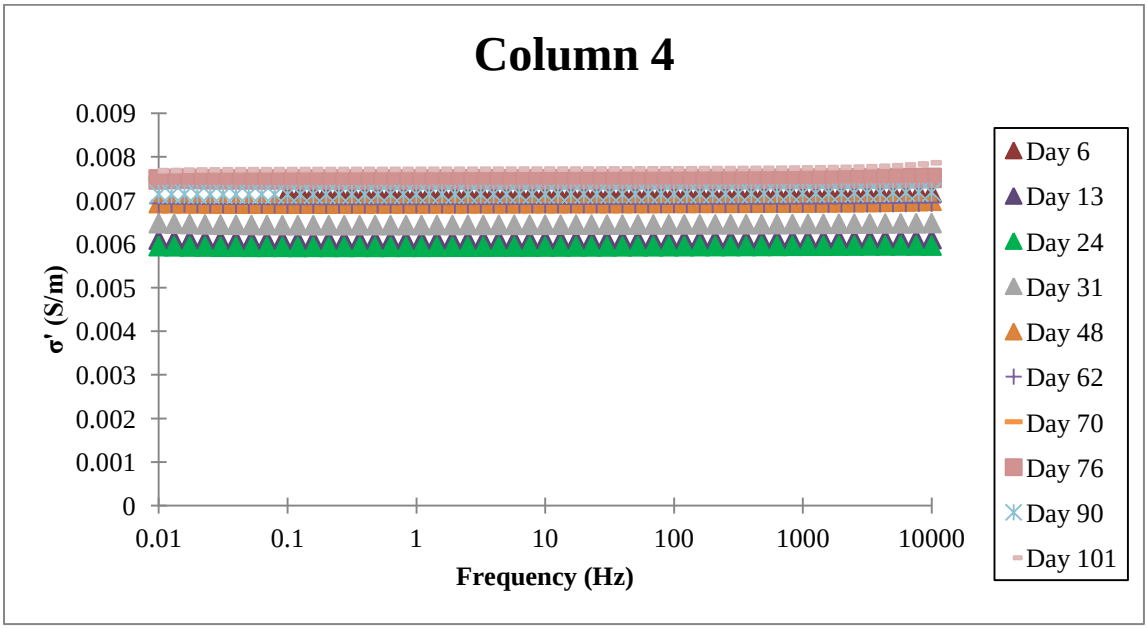
Column 4
σ' (S/m)
0.009
0.008
0.007
0.006
0.005
0.004
0.003
0.002
0.001
0
0.01
0.1
1
10
100
1000
10000
Frequency (Hz)
Day 6
Day 13
Day 24
Day 31
Day 48
Day 62
Day 70
Day 76
Day 90
Day 101

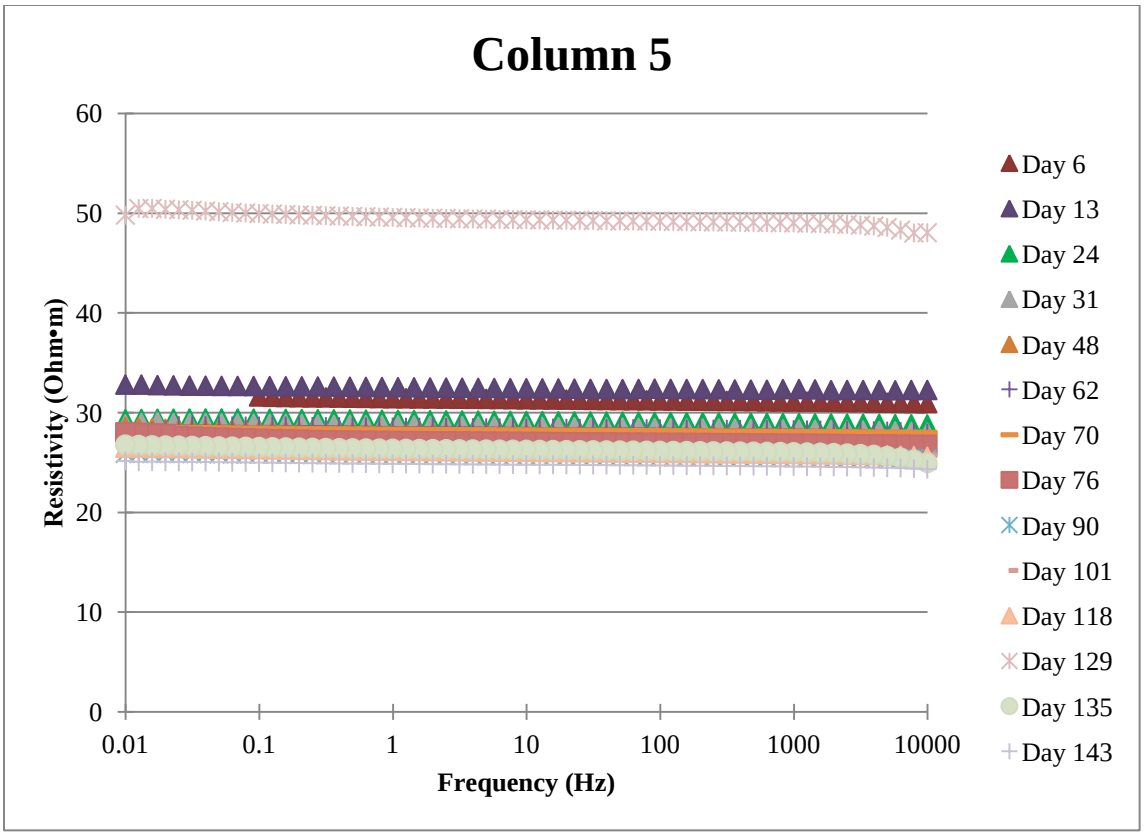
Column 5
Resistivity (Ohm•m)
60
50
40
30
20
10
0
0.01
0.1
1
10
100
1000
10000
Frequency (Hz)
Day 6
Day 13
Day 24
Day 31
Day 48
Day 62
Day 70
Day 76
Day 90
Day 101
Day 118
Day 129
Day 135
Day 143

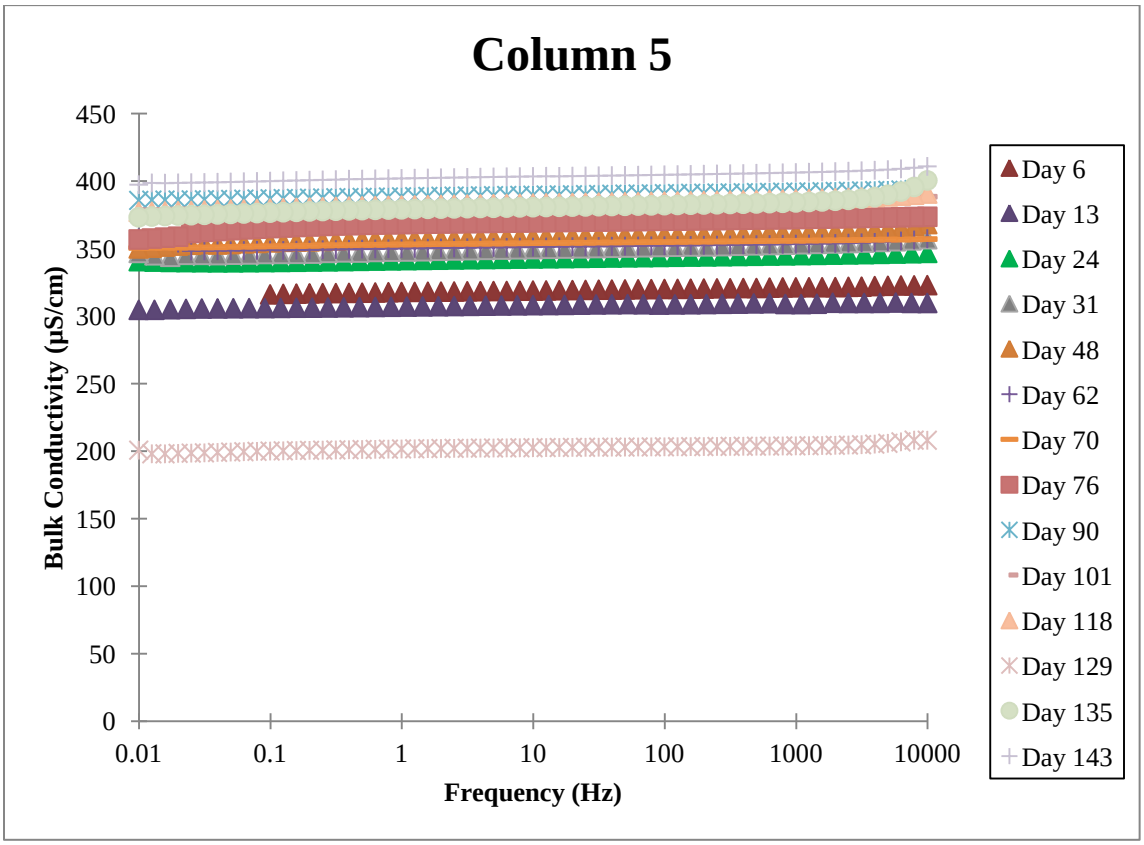
Column 5
Bulk Conductivity (µS/cm)
450
400
350
300
250
200
150
100
50
0
0.01
0.1
1
10
100
1000
10000
Frequency (Hz)
Day 6
Day 13
Day 24
Day 31
Day 48
Day 62
Day 70
Day 76
Day 90
Day 101
Day 118
Day 129
Day 135
Day 143

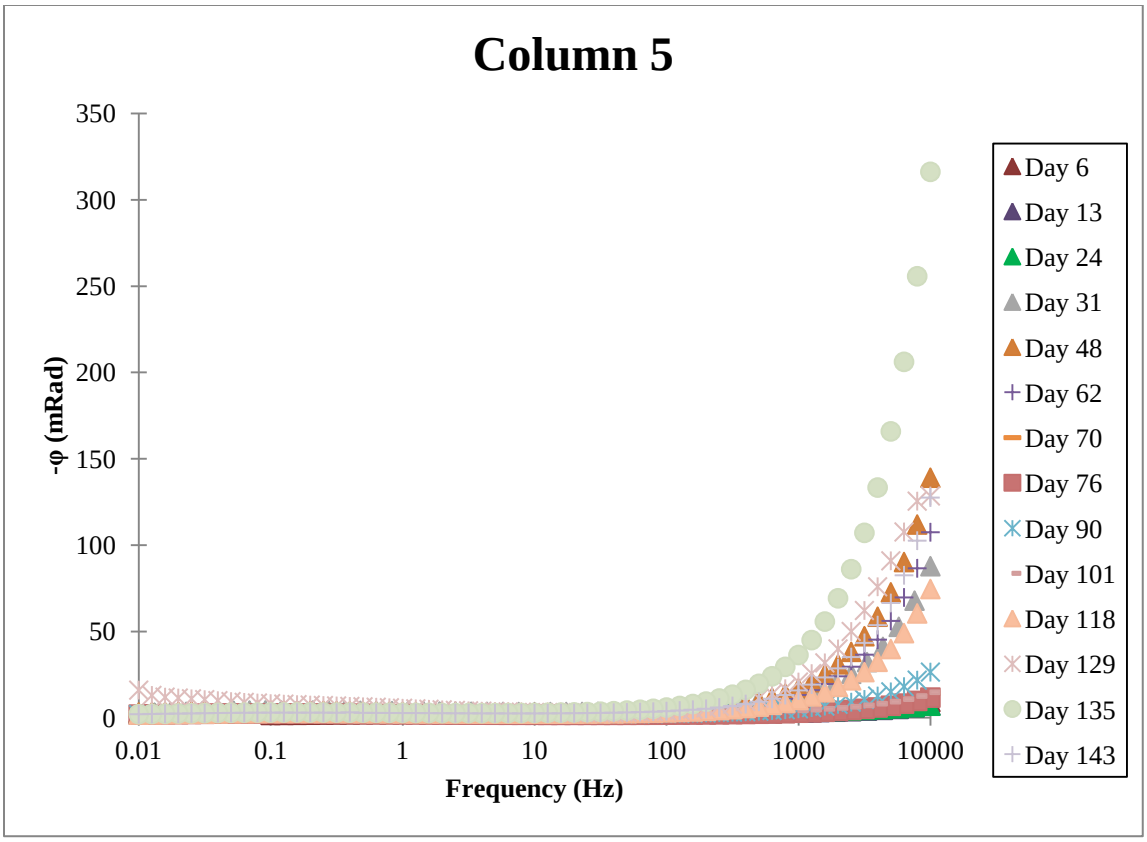
Column 5
350
300
250
200
150
100
50
0
-φ (mRad)
0.01
0.1
1
10
100
1000
10000
Frequency (Hz)
Day 6
Day 13
Day 24
Day 31
Day 48
Day 62
Day 70
Day 76
Day 90
Day 101
Day 118
Day 129
Day 135
Day 143

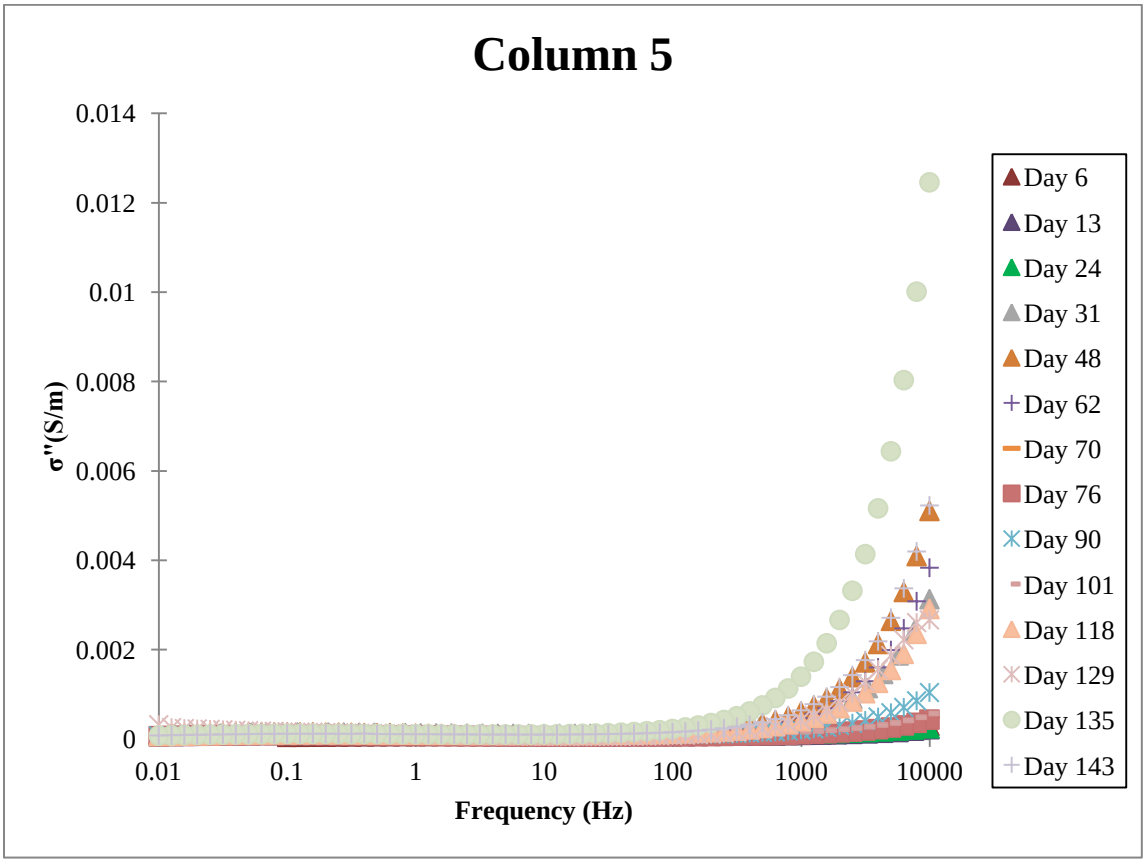
Column 5
0.014
0.012
0.01
0.008
0.006
0.004
0.002
0
σ''(S/m)
0.01
0.1
1
10
100
1000
10000
Frequency (Hz)
Day 6
Day 13
Day 24
Day 31
Day 48
Day 62
Day 70
Day 76
Day 90
Day 101
Day 118
Day 129
Day 135
Day 143

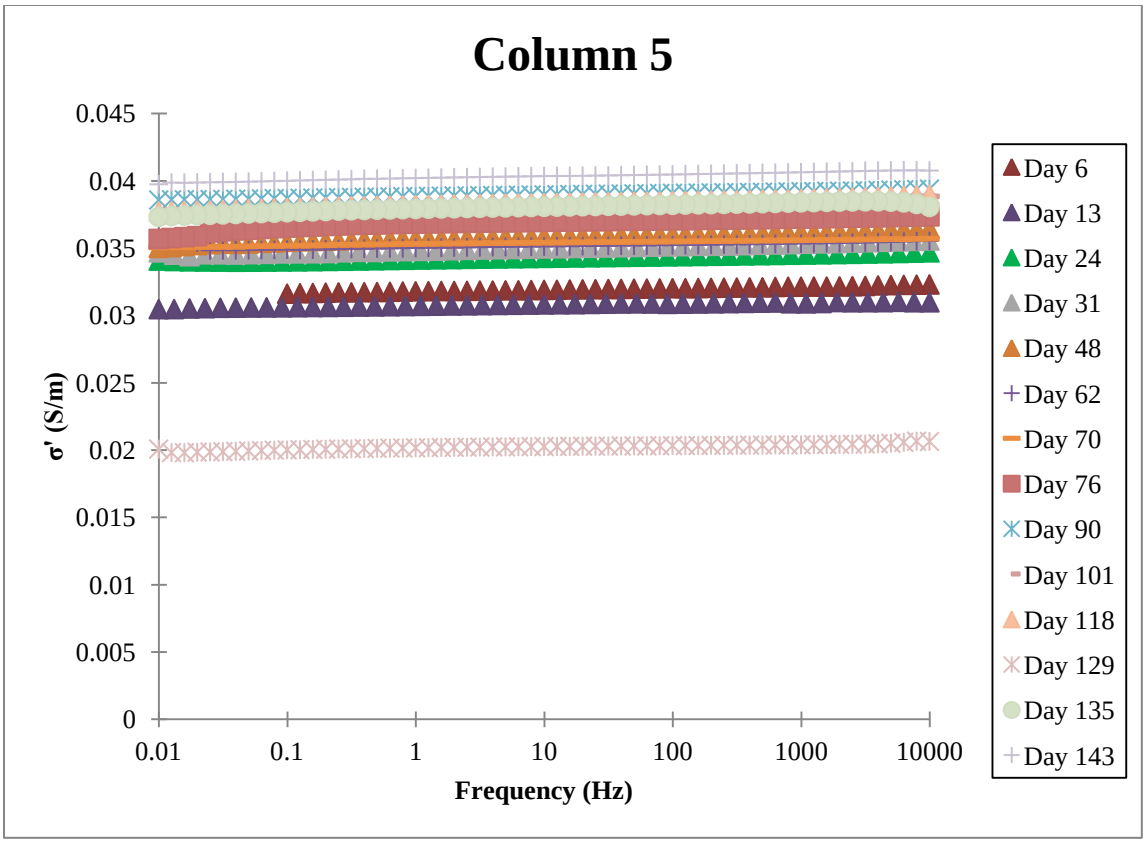
Column 5
0.045
0.04
0.035
0.03
0.025
0.02
0.015
0.01
0.005
0
σ' (S/m)
0.01
0.1
1
10
100
1000
10000
Frequency (Hz)
Day 6
Day 13
Day 24
Day 31
Day 48
Day 62
Day 70
Day 76
Day 90
Day 101
Day 118
Day 129
Day 135
Day 143

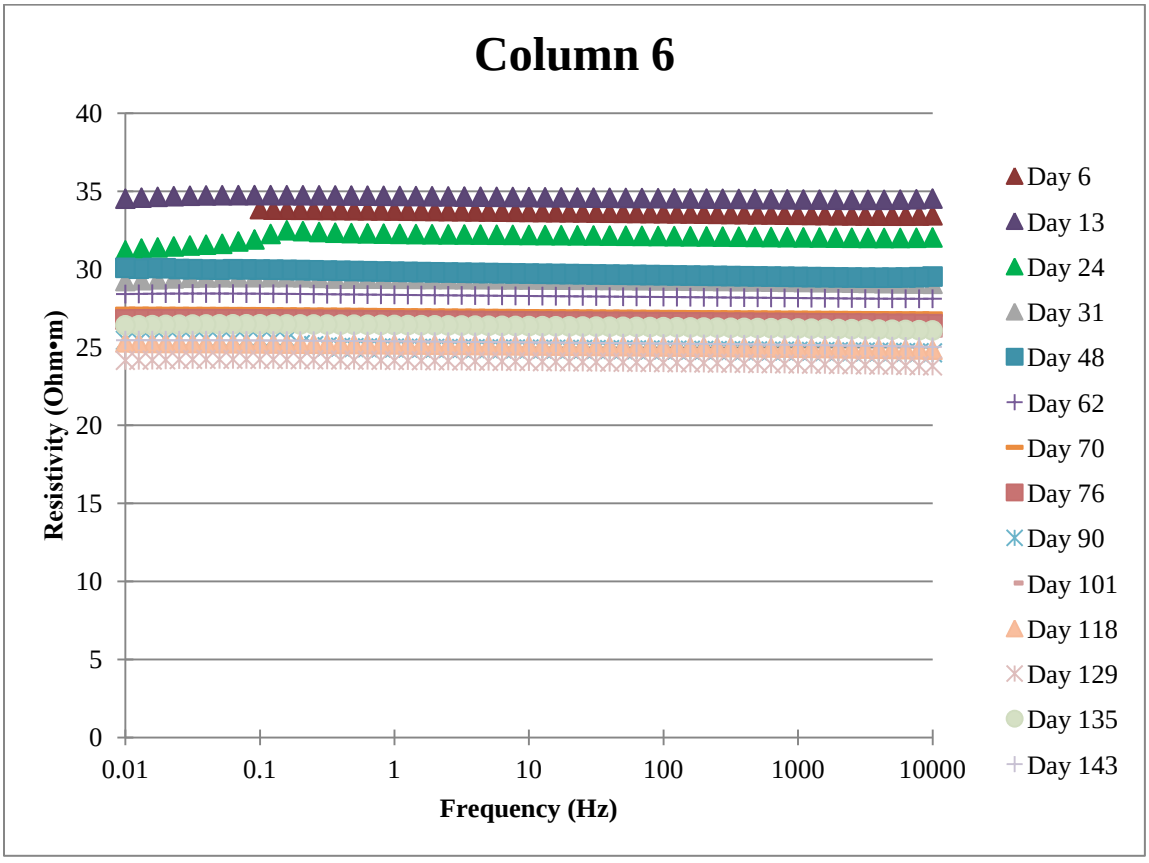
Column 6
40
35
30
25
20
15
10
5
0
Resistivity (Ohm•m)
0.01
0.1
1
10
100
1000
10000
Frequency (Hz)
Day 6
Day 13
Day 24
Day 31
Day 48
Day 62
Day 70
Day 76
Day 90
Day 101
Day 118
Day 129
Day 135
Day 143

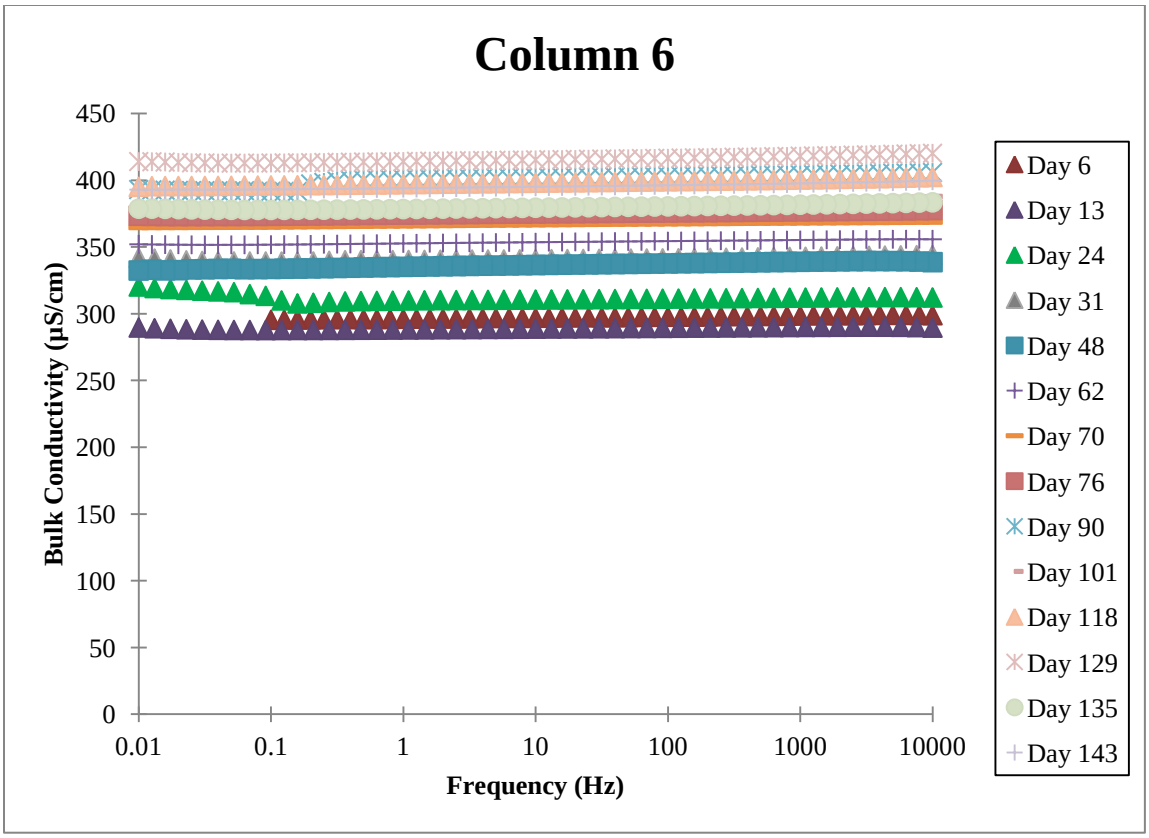
Column 6
Bulk Conductivity (µS/cm)
450
400
350
300
250
200
150
100
50
0
0.01
0.1
1
10
100
1000
10000
Frequency (Hz)
Day 6
Day 13
Day 24
Day 31
Day 48
Day 62
Day 70
Day 76
Day 90
Day 101
Day 118
Day 129
Day 135
Day 143

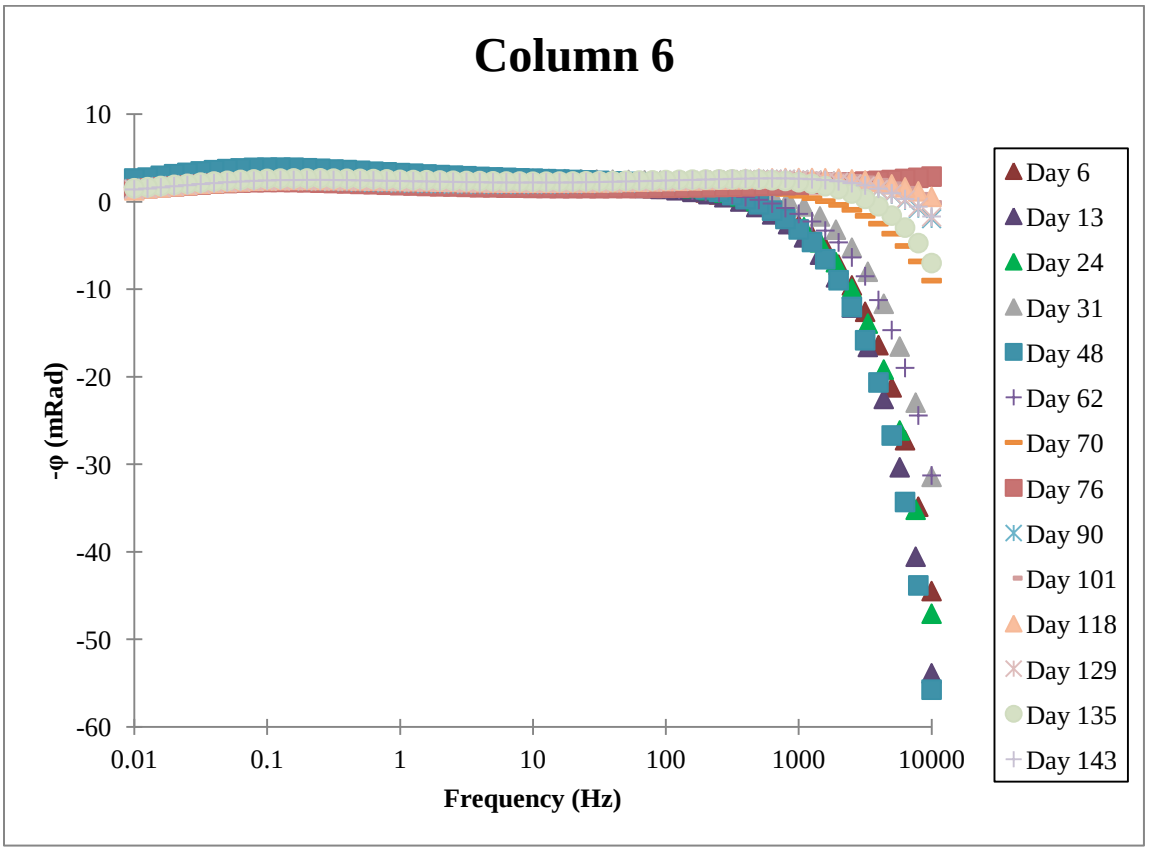
Column 6
-φ (mRad)
10
0
-10
-20
-30
-40
-50
-60
0.01
0.1
1
10
100
1000
10000
Frequency (Hz)
Day 6
Day 13
Day 24
Day 31
Day 48
Day 62
Day 70
Day 76
Day 90
Day 101
Day 118
Day 129
Day 135
Day 143

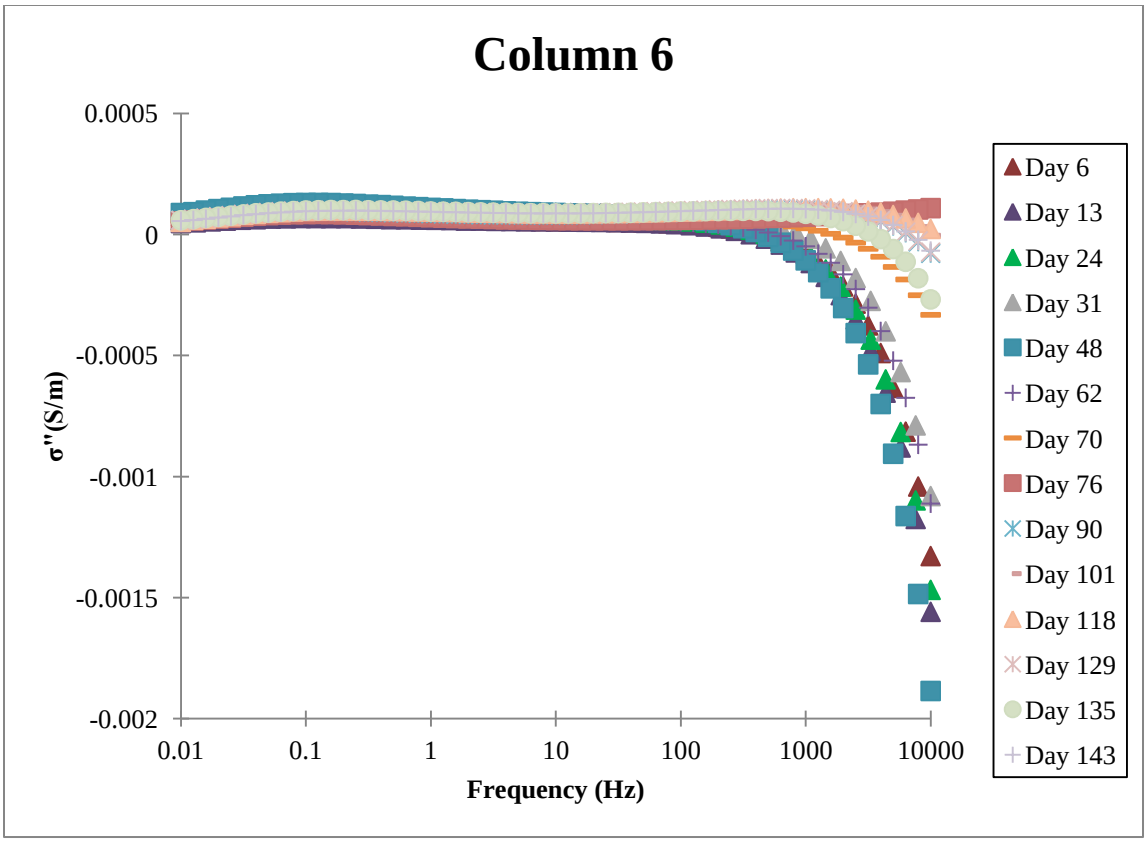
Column 6
0.0005
0
-0.0005
-0.001
-0.0015
-0.002
σ''(S/m)
0.01
0.1
1
10
100
1000
10000
Frequency (Hz)
Day 6
Day 13
Day 24
Day 31
Day 48
Day 62
Day 70
Day 76
Day 90
Day 101
Day 118
Day 129
Day 135
Day 143

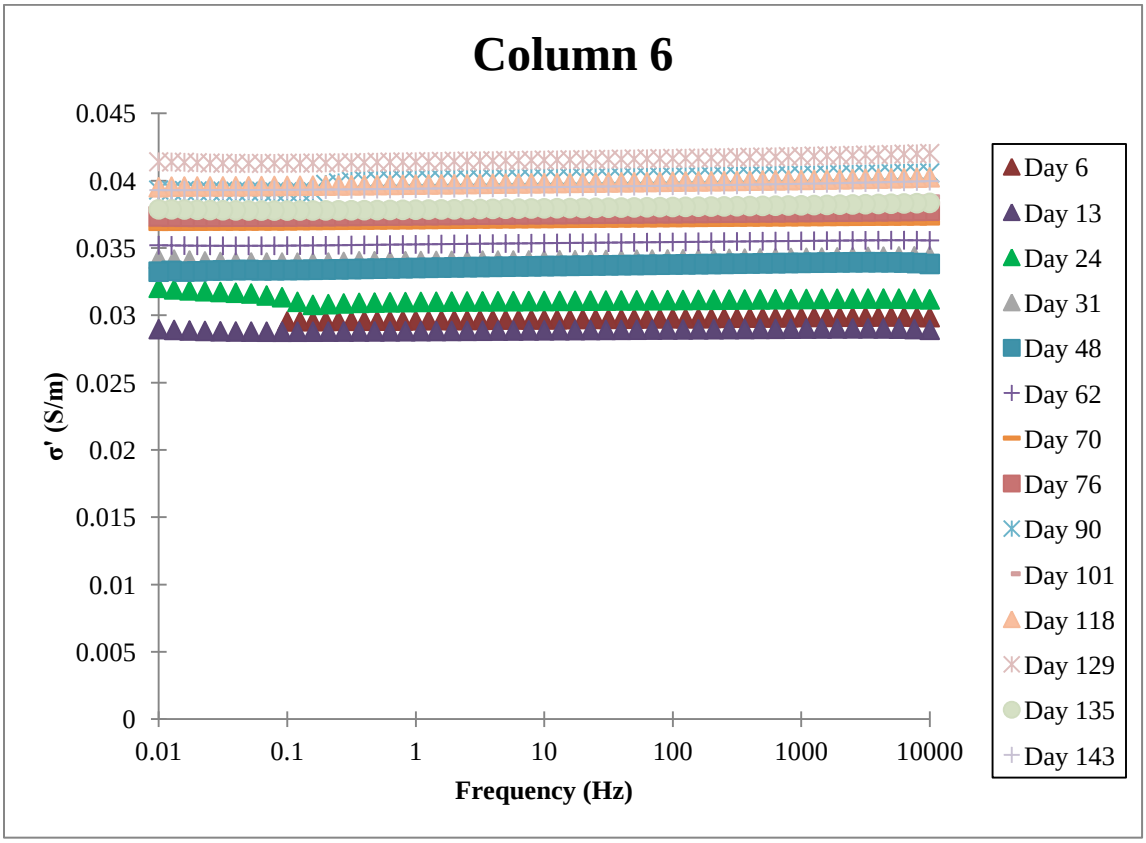
Column 6
0.045
0.04
0.035
0.03
0.025
0.02
0.015
0.01
0.005
0
σ' (S/m)
0.01
0.1
1
10
100
1000
10000
Frequency (Hz)
Day 6
Day 13
Day 24
Day 31
Day 48
Day 62
Day 70
Day 76
Day 90
Day 101
Day 118
Day 129
Day 135
Day 143

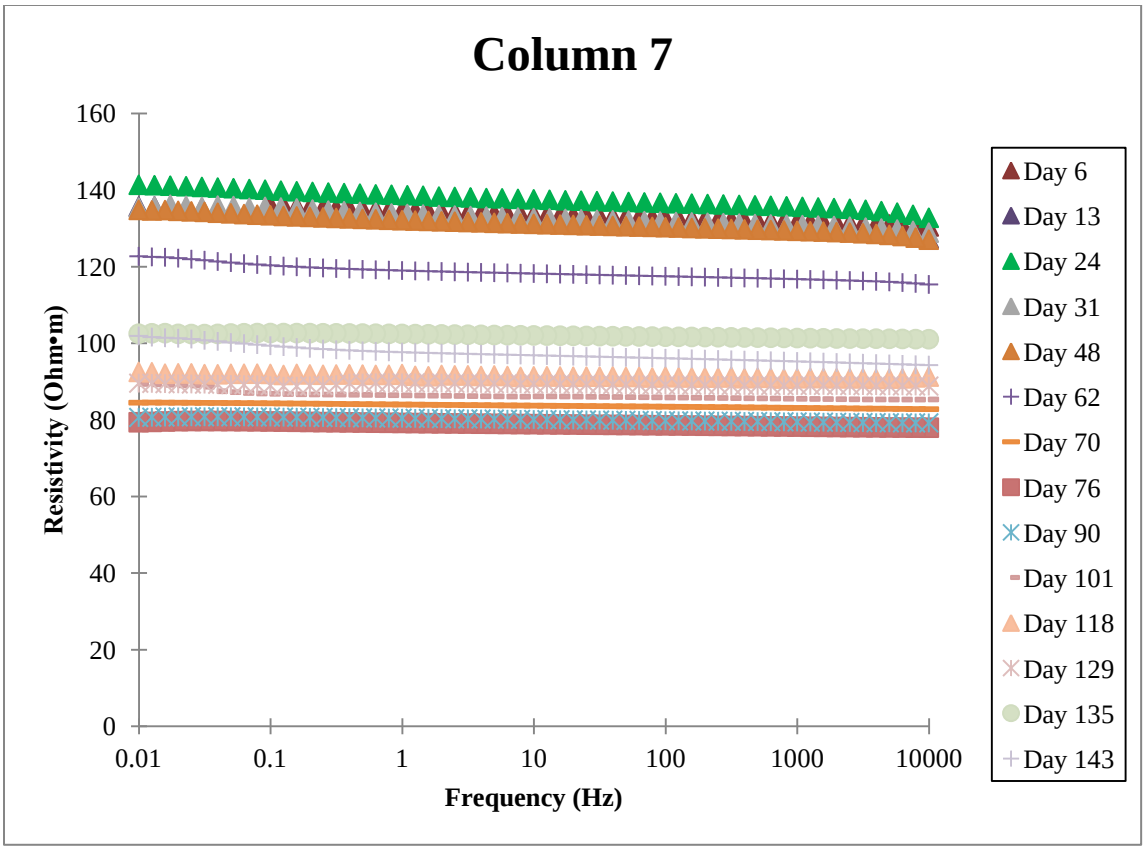
Column 7
Resistivity (Ohm•m)
160
140
120
100
80
60
40
20
0
0.01
0.1
1
10
100
1000
10000
Frequency (Hz)
Day 6
Day 13
Day 24
Day 31
Day 48
Day 62
Day 70
Day 76
Day 90
Day 101
Day 118
Day 129
Day 135
Day 143

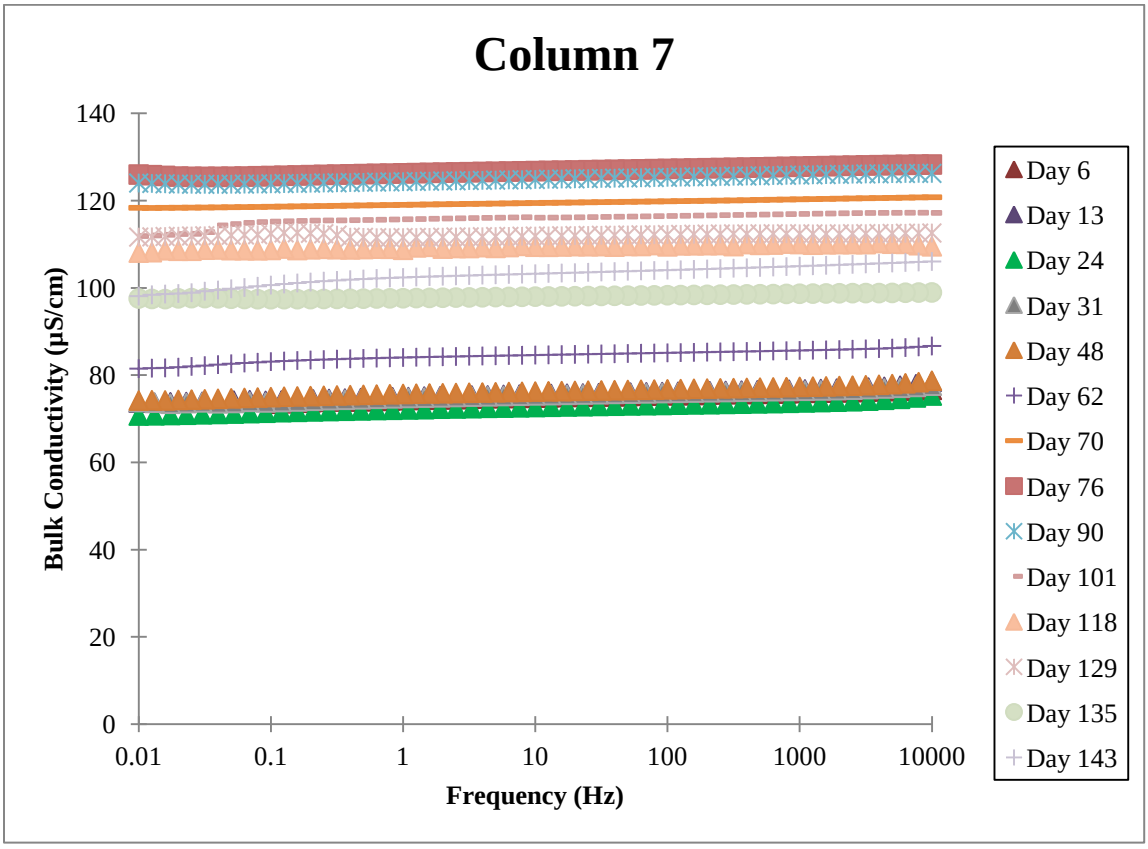
Column 7
Bulk Conductivity (µS/cm)
140
120
100
80
60
40
20
0
0.01
0.1
1
10
100
1000
10000
Frequency (Hz)
Day 6
Day 13
Day 24
Day 31
Day 48
Day 62
Day 70
Day 76
Day 90
Day 101
Day 118
Day 129
Day 135
Day 143

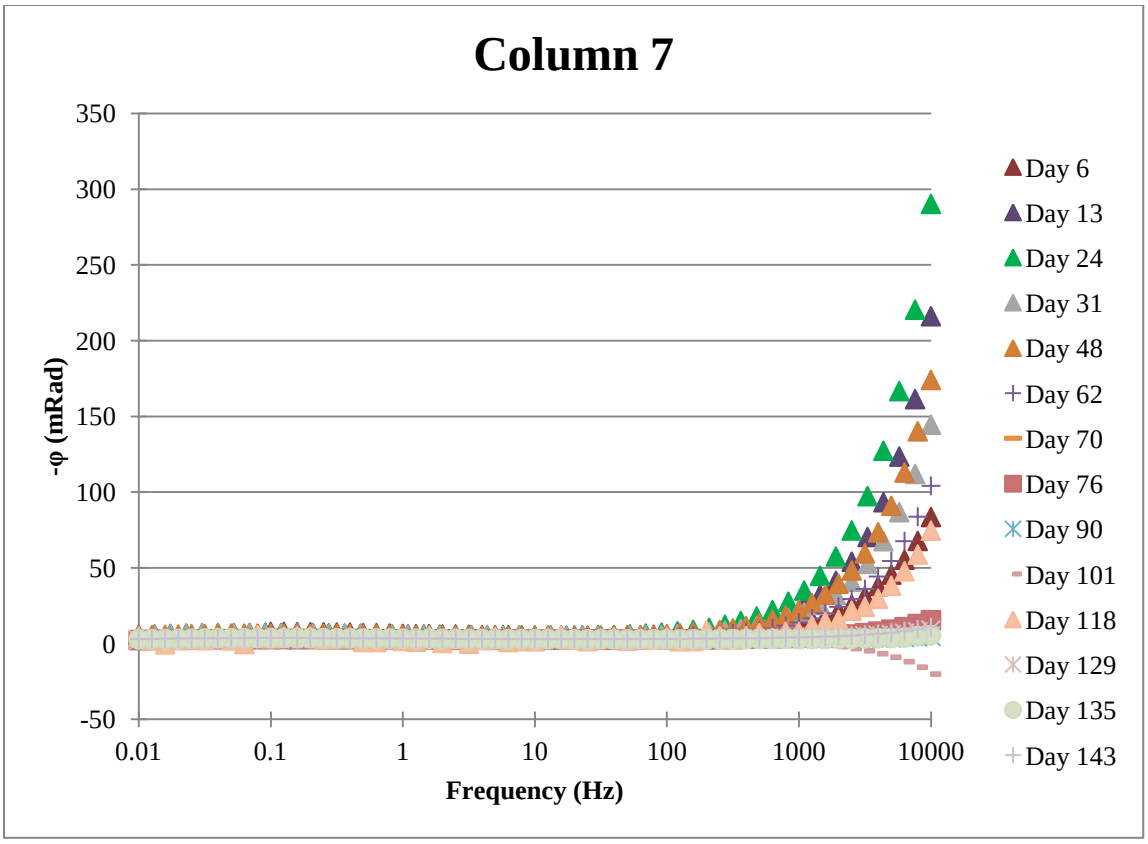
Column 7
350
300
250
200
150
100
50
0
-50
-φ (mRad)
0.01
0.1
1
10
100
1000
10000
Frequency (Hz)
Day 6
Day 13
Day 24
Day 31
Day 48
Day 62
Day 70
Day 76
Day 90
Day 101
Day 118
Day 129
Day 135
Day 143

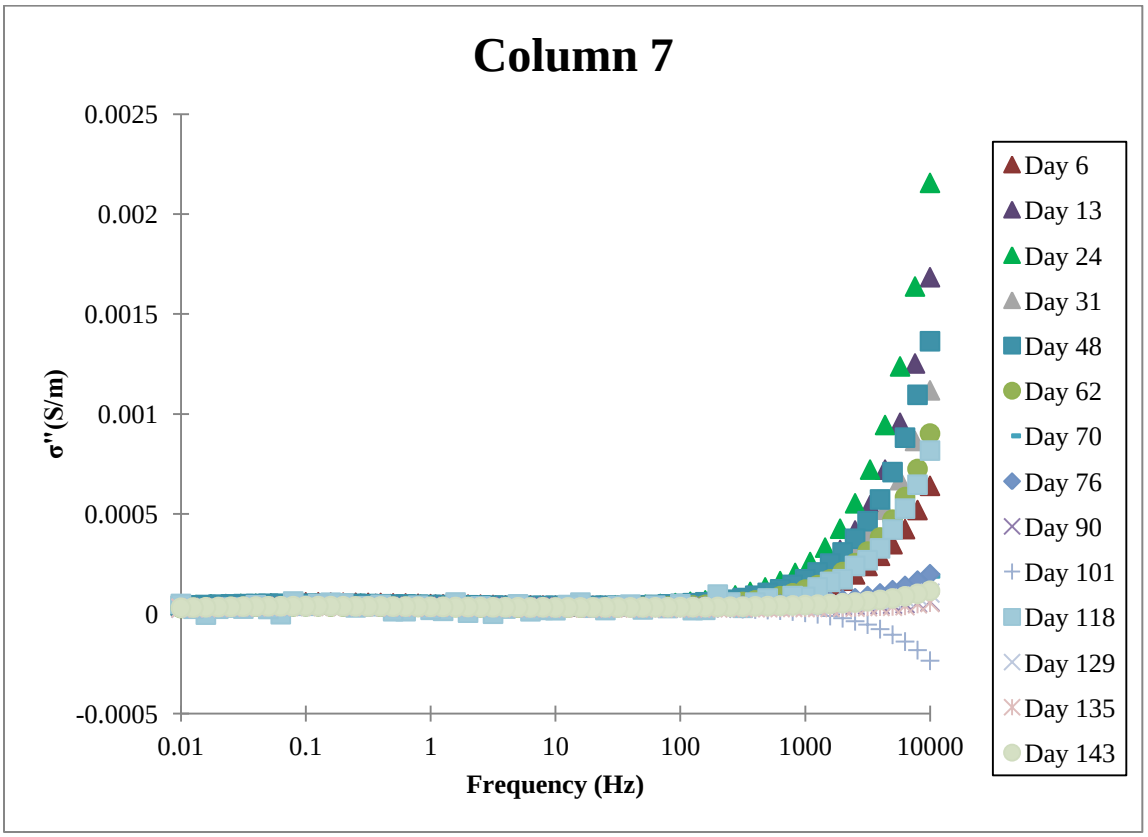
Column 7
0.0025
0.002
0.0015
0.001
0.0005
0
-0.0005
σ''(S/m)
0.01
0.1
1
10
100
1000
10000
Frequency (Hz)
Day 6
Day 13
Day 24
Day 31
Day 48
Day 62
Day 70
Day 76
Day 90
Day 101
Day 118
Day 129
Day 135
Day 143

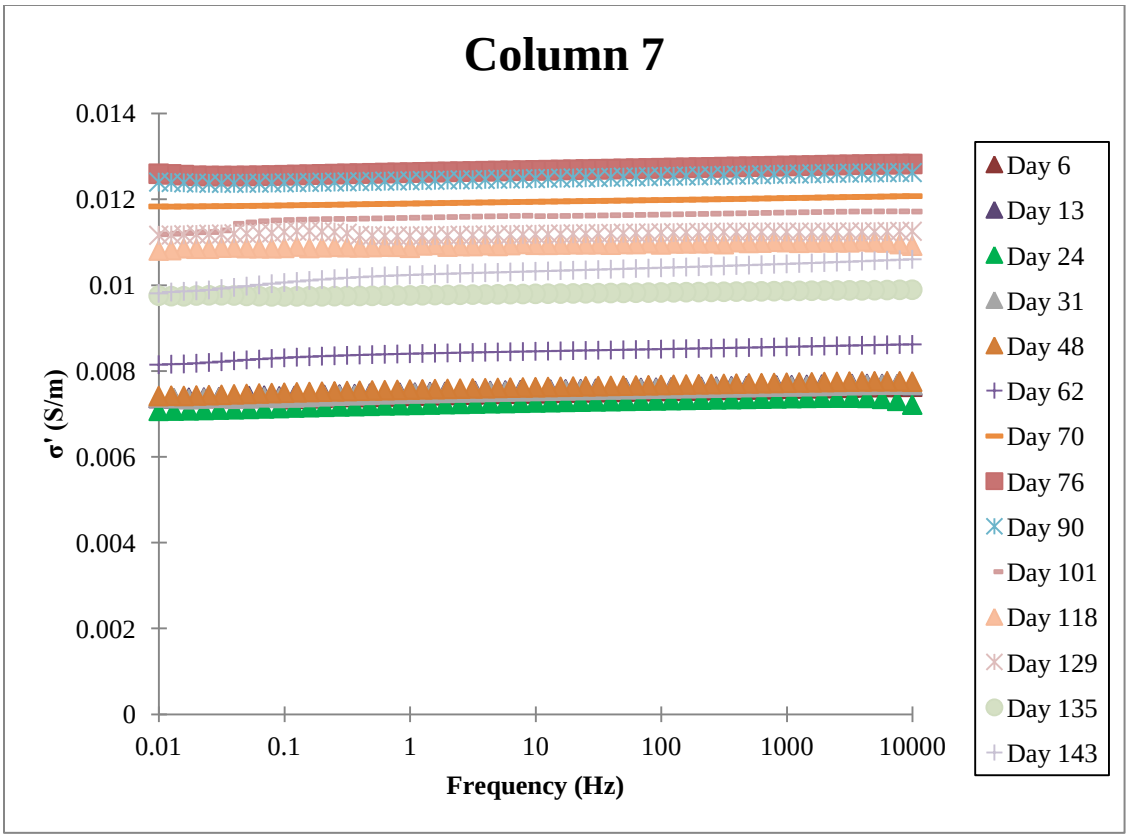
Column 7
0.014
0.012
0.01
0.008
0.006
0.004
0.002
0
σ' (S/m)
0.01
0.1
1
10
100
1000
10000
Frequency (Hz)
Day 6
Day 13
Day 24
Day 31
Day 48
Day 62
Day 70
Day 76
Day 90
Day 101
Day 118
Day 129
Day 135
Day 143

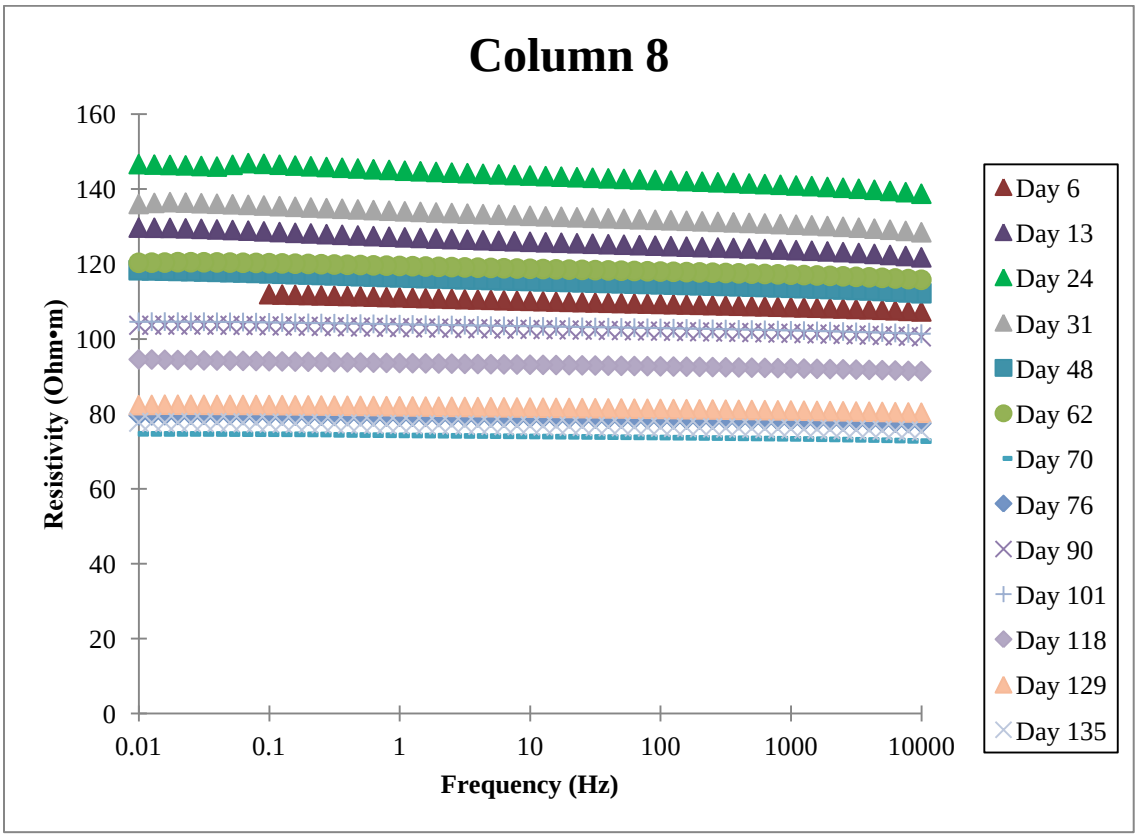
Column 8
160
140
120
100
80
60
40
20
0
Resistivity (Ohm•m)
0.01
0.1
1
10
100
1000
10000
Frequency (Hz)
Day 6
Day 13
Day 24
Day 31
Day 48
Day 62
Day 70
Day 76
Day 90
Day 101
Day 118
Day 129
Day 135

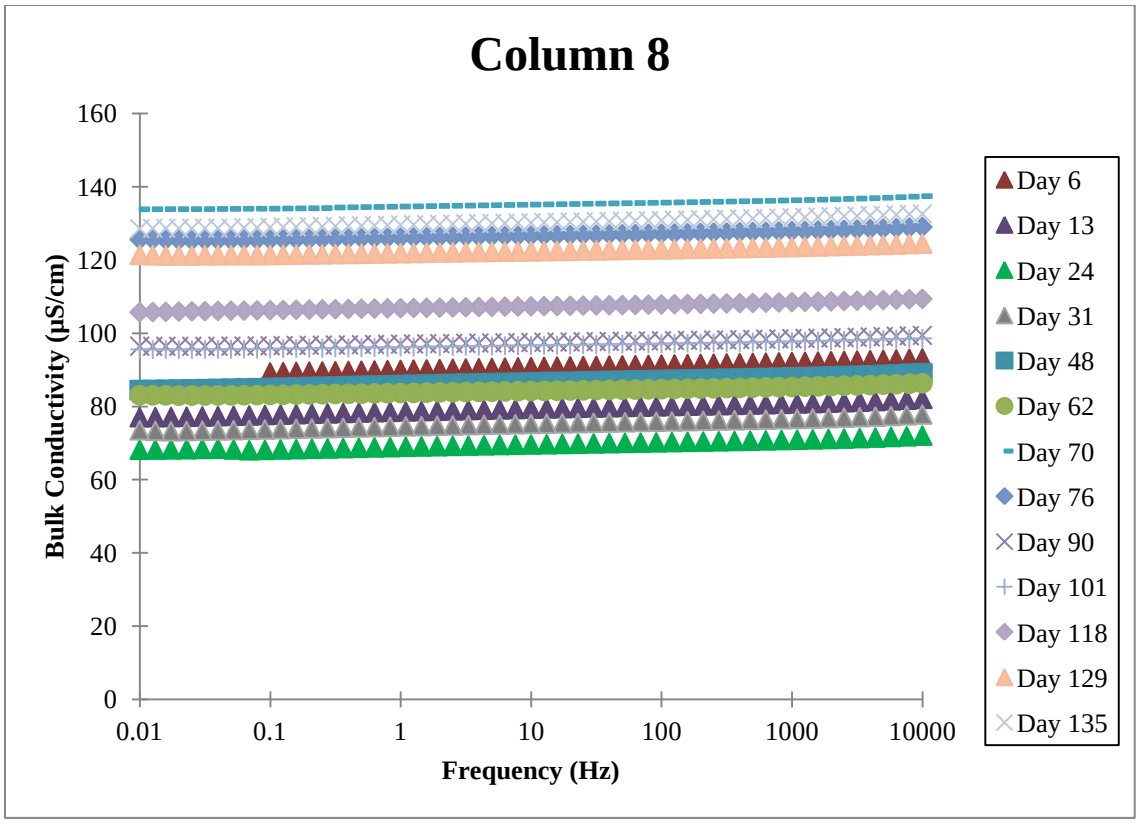
Column 8
Bulk Conductivity (µS/cm)
160
140
120
100
80
60
40
20
0
0.01
0.1
1
10
100
1000
10000
Frequency (Hz)
Day 6
Day 13
Day 24
Day 31
Day 48
Day 62
Day 70
Day 76
Day 90
Day 101
Day 118
Day 129
Day 135

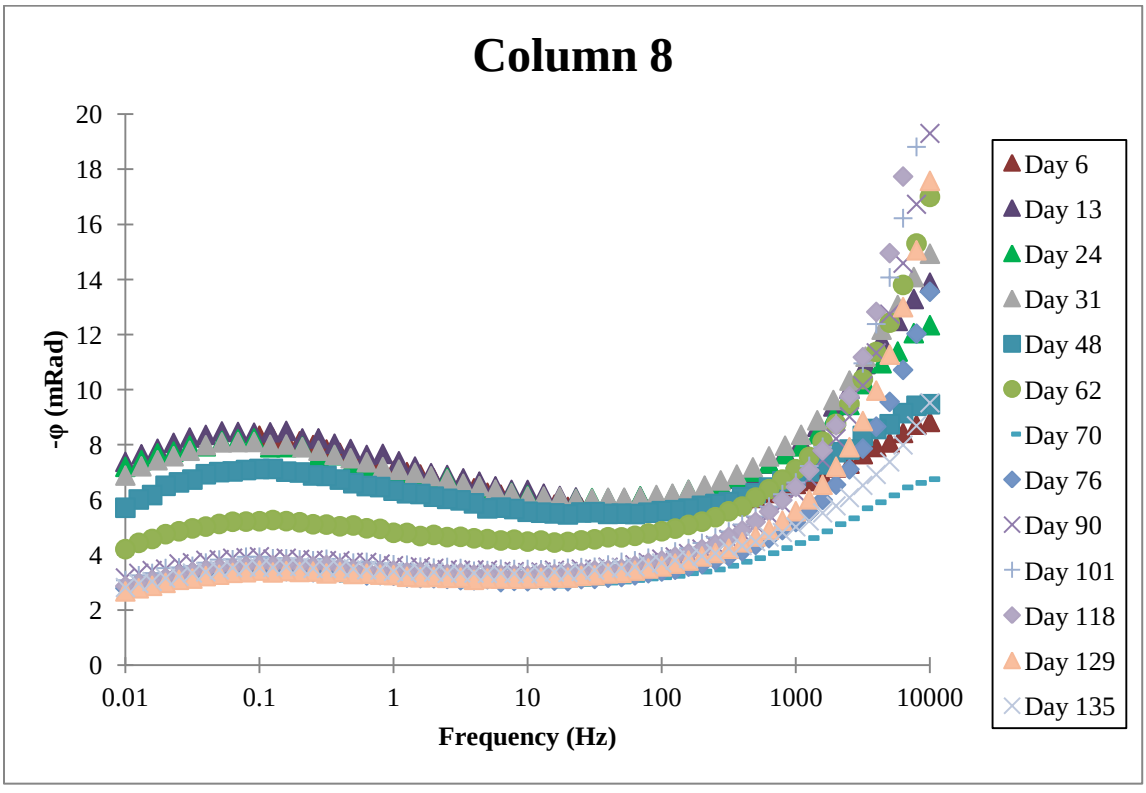
Column 8
-φ (mRad)
20
18
16
14
12
10
8
6
4
2
0
0.01
0.1
1
10
100
1000
10000
Frequency (Hz)
Day 6
Day 13
Day 24
Day 31
Day 48
Day 62
Day 70
Day 76
Day 90
Day 101
Day 118
Day 129
Day 135

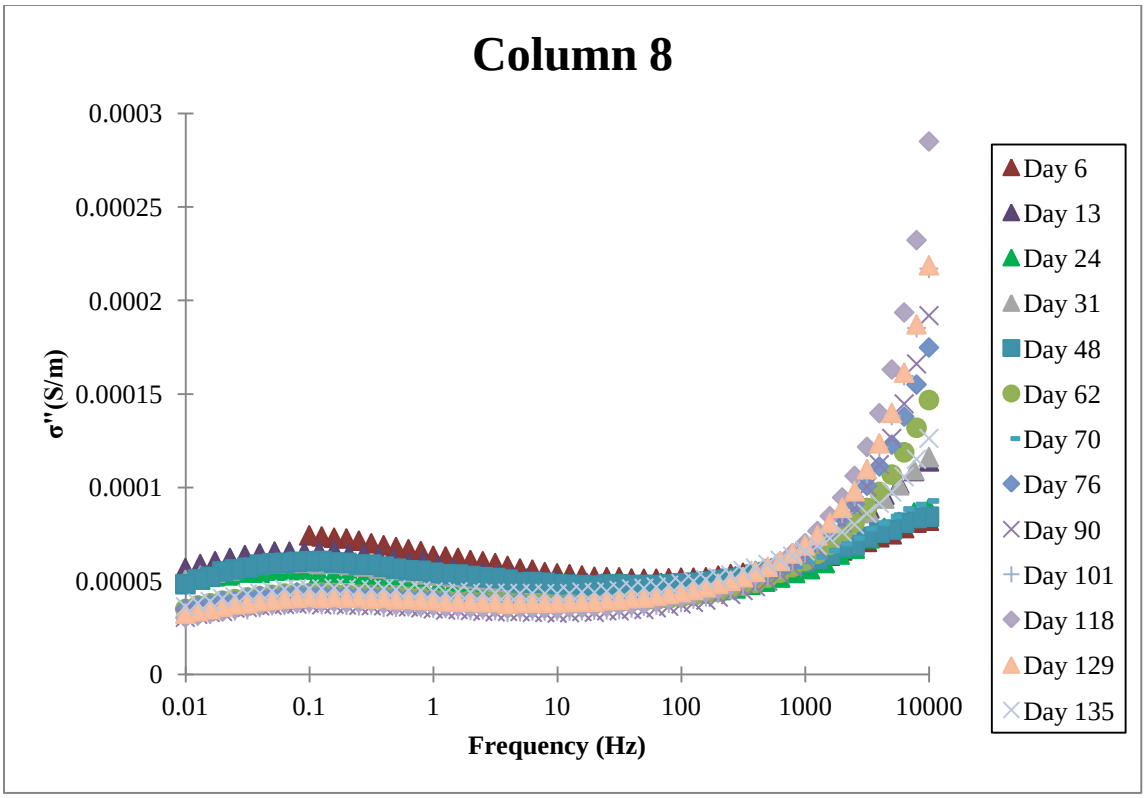

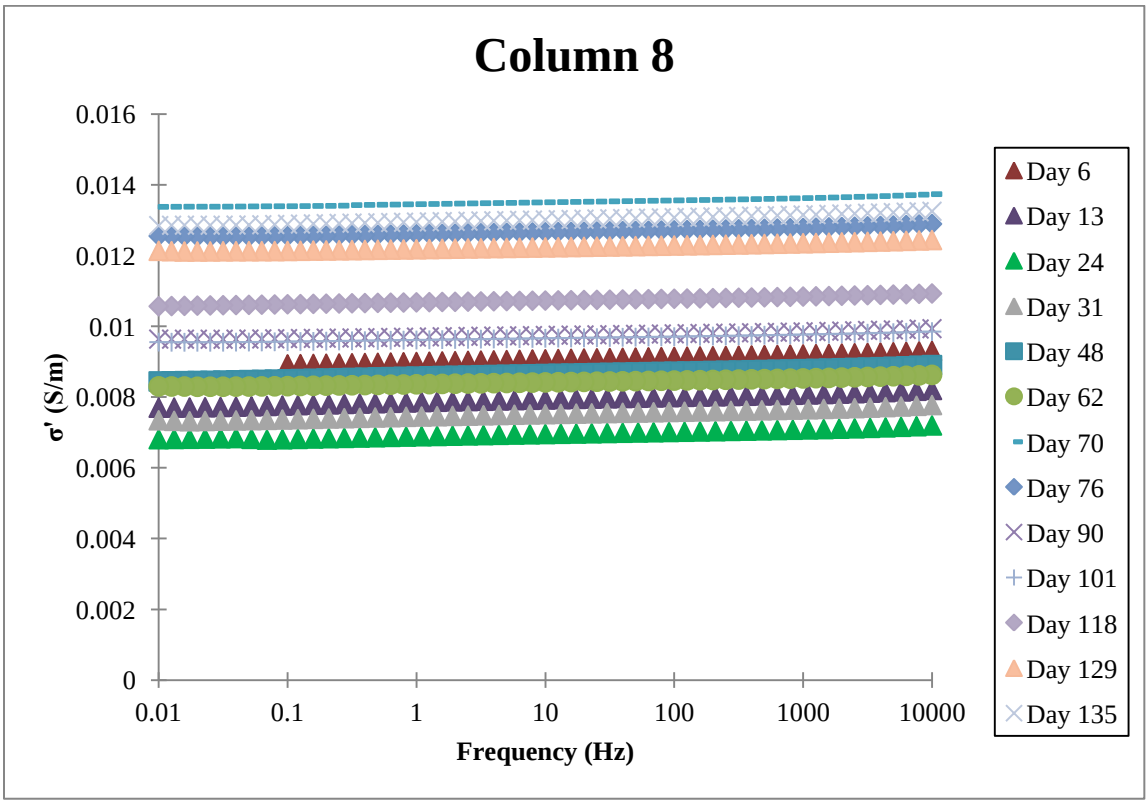

Figure A-2. Resistivity, bulk conductivity, phase response, and real and imaginary conductivity results per column per day over the entire frequency range.

Fluid Geochemistry Results

Table A1. pH values of outflow solution from each column by day

Day	pH							
	C1	**C2**	**C3**	**C4**	**C5**	**C6**	**C7**	**C8**
3	8.6	8.4	8.7	8	8.1	8.5		
6	7.5	7.8	7.6	7.3	7.4	7.3	7.4	7.6
10	8.1	7.7	8.3	7.8	7.3	7.4	6.6	7.7
13	7.5	7.5	7.4	7.1	6.9	7	7.5	7.5
17	8	8.4	8.5	8.2	7.3	7	7.5	6.8
20	7.7	7.7	8	7.9	7.1	7.1	7.5	7.5
24	8.8	8.8	8.9	8.9	7.9	7.9	8.5	8.5
27	8.8	8.9	8.3	8.1	7.6	7.7	8.2	8.5
31	7.9	8.1	8.3	8.3	7.6	7.7	8	8.1
41	7.6	7.4	7.7	7.7	7.3	7.4	7.7	7.5
45	8.2	7.8	8.2	8.1	7.3	7.6	7.9	7.7
48	7.6	7.6	7.7	7.7	7.5	7.8	7.9	7.9
52	7.7	7.7	7.7	7.5	7.2	7.3	7.3	7.5
55	7.5	7.5	7.6	7.4	7	7.1	7.1	7.4
59	7.4	7.4	7.4	7.2	6.8	6.9	6.9	7.2
62	7.3	7.3	7.4	7.2	6.9	6.9	6.7	7.1
66	6.8	6.9	7.1	6.9	6.6	6.7	7.1	7
70	6.9	6.9	6.9	6.8	6.8	6.8	7.1	7.1
73	6.8	6.9	6.9	6.8	6.8	6.8	7.1	7
76	6.9	7	7	7	6.8	6.9	7	7
80	6.8	6.9	7	7	6.6	6.6	7	7
87	6.9	7	7	6.9	6.8	6.8		7
90	6.8	6.9	7	7	6.8	6.8		7
94	6.8	6.9	7	7.1	6.8	6.7		6.8
98	6.9	6.9	7.1	7.1	6.9	6.8		6.6
101	6.8	6.8	7	7.1	6.9	6.9		6.8
104	6.8	6.9	7.1	7.1	6.8	6.8		7
108	6.9	6.9	7.1	7.1	6.9	6.9		6.7
115	6.9	6.8	7	6.9	6.7	6.9		7
118	7.1	7	7		6.9	6.9		7.1
122	7	6.8	6.6		6.9	6.8		6.9
129	7.1	7.1	6.7		6.9	6.8		7
135	7.1	7.1			6.9	6.8		7.1

Note: Blanks correspond to data that were considered outliers or for which there was no outflow sample available for fluid geochemistry analysis.

Table A2. Fluid Conductivity (in µS/cm) of outflow solution from each column by day

Day	Fluid Conductivity (µS/cm)							
	C1	**C2**	**C3**	**C4**	**C5**	**C6**	**C7**	**C8**
3	2350	2430	1530	1410	4540	4520		
6	2700	2380	1410	1120		3940		1357
10	3567	2014	951.8	954.6	3557	3670	1144	1004
13		2170	1040	907.9	3400	3370	1080	986.4
17	3120	2090	946.3	906.8	3470	3600	1080	
20	1930	2020	949.5	894	3330	3600	1000	939.8
24	3030	2100	976.6	925.7	3530	3530	1020	913.9
27	2590	2050	1050	925.6	3510	3670	1170	952.1
31	2230	2050	963.2	885.8	3210	3620	986.1	929.6
41	2310	2270	1010	928.3	3370	3610	1240	918
45	2280	2040	911.6	908.8	3440	3540	954.2	1040
48	2290	2150	994.9	940.8	3690	3630	982.8	906
52	2280	1980	981.8	878.9	3380	3600	946.3	946.8
55	2000	2030	983.7	918.8	3470	3440	906.4	889.9
59	2220	2110	1030	971.4	3590	3650	857.1	933
62	2020	2170	980.3	943.4	3610	3600	781.9	1030
66	2291	1784	1009	933.3	3446	3436	1340	1459
70	2253	2000	1041	943.9	3544	3547	1348	1259
73	2043	2129	1043	948	3611	3586	1152	1210
76	2067	2070	1031	936.8	3446	3523	1066	1204
80	2074	2086	1010	923	3539	3475	1057	1068
87	2076	2069	1073	946.2	3461	3462		1034
90	2256	2105	1013	936.5	3399	3267		969.9
94	2150	2130	994.7	919.3	3415	3419		981.7
98	2107	2104	966.9	949.6	3478	3411		820
101	2006	1992	990.1	955.7	3355	3332		942.6
104	2033	1973	1028	949	3499	3389		905.3
108	2229	2010	1043	954.9	3493	3467		914.5
115	2145	1981	959.8	880.6	3346	3325		1017
118	2246	2027	1012		3405	3333		1022
122	2016	2019	1039		3546	3567		1095
129	1945	1957	989.2		3414	3543		1420
135	1994	1771			3066	3061		1000

Note: Blanks correspond to data that were considered outliers or for which there was no outflow sample available for fluid geochemistry analysis.

Geophysical Data

Figures A-3, A-4, and A-5 show the real and imaginary conductivity results at 0.1, 1, and 10 Hz respectively. Figures A-6 and A-7 show the imaginary and bulk conductivity respectively at the peak frequency for which replicate column data was averaged for each inflow solution. Figure A-8 shows the bulk conductivity data over the entire frequency range and each inflow solution is plotted in the same scale to clearly illustrate the variations in conductivity.

a)

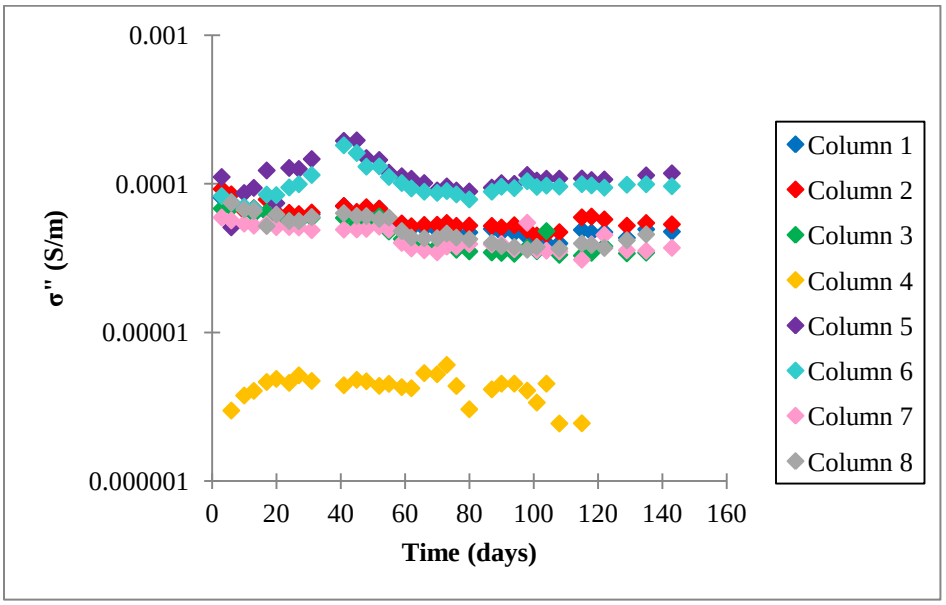

b)

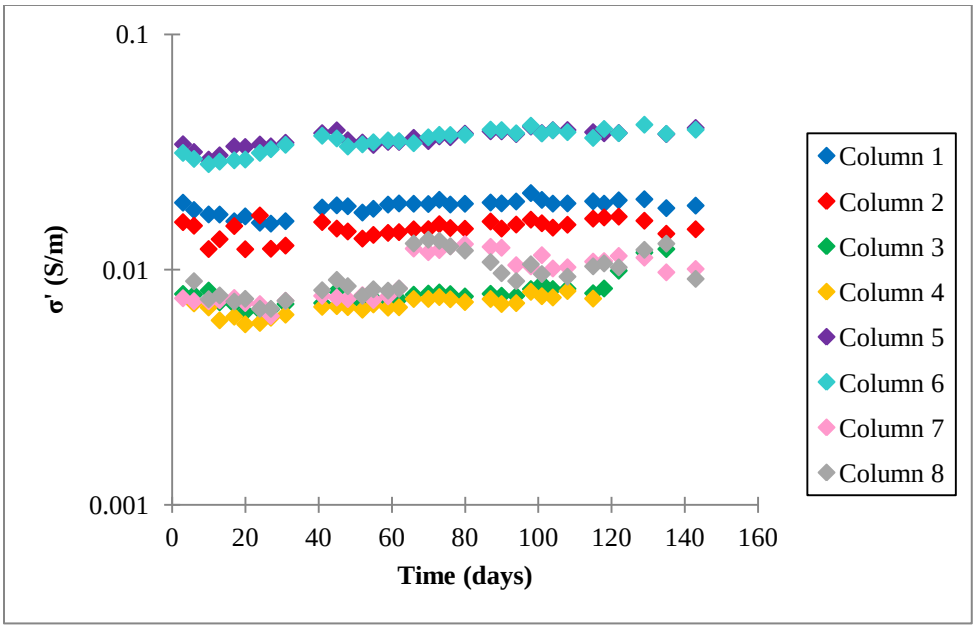

Figure A-3. a) Imaginary and b) Real conductivity at 0.1 Hz. This data is similar to that seen in Figure 5 since the peak frequency was ~0.1 Hz. Columns 5 and 6 show an increase in imaginary conductivity to a peak at day 41 whereas the control columns show no appreciable change in conductivity. Columns 5 and 6 show the most pronounced increase in real conductivity; Columns 1 and 2 show only a slight increase in real conductivity whereas the control columns show no appreciable change in conductivity. Columns 1, 2, 3, 5, and 6 are the Active Columns; Columns 4, 7, and 8 are the Control Columns.

a)

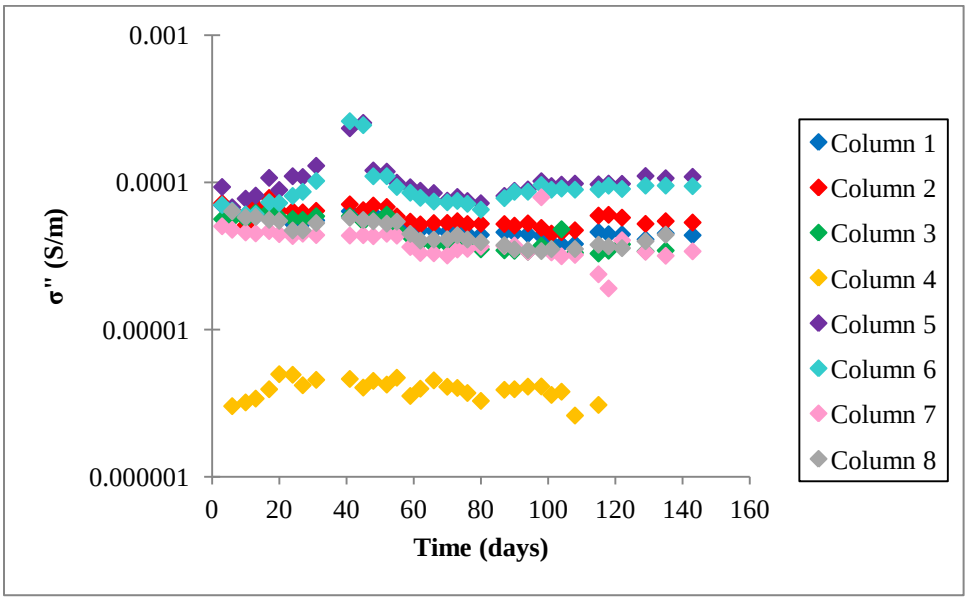

b)

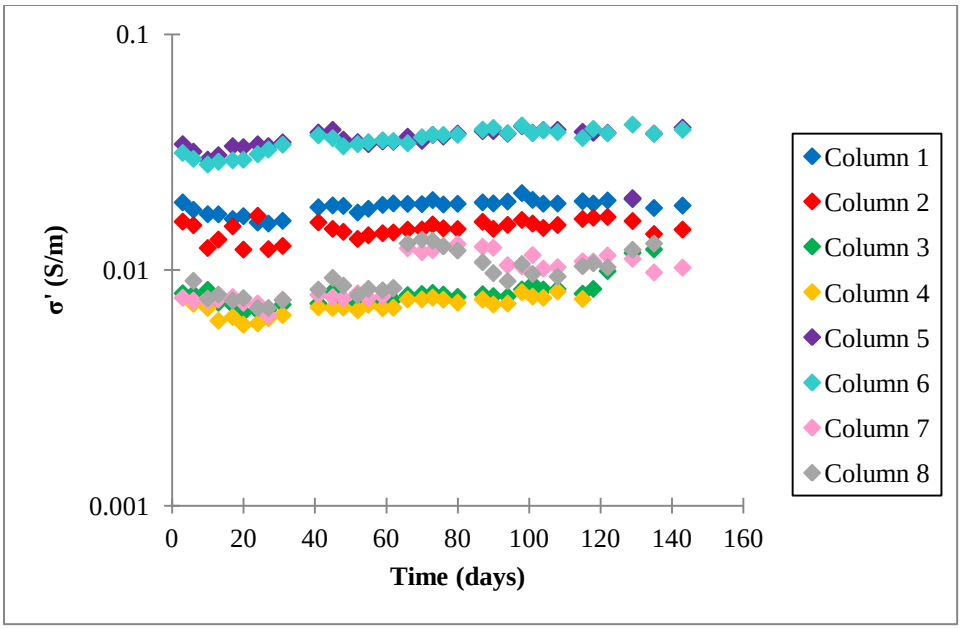

Figure A-4. a) Imaginary and b) Real conductivity at 1 Hz. The overall trends in each column are the same as that seen in Figures 5 and A-3 with a higher peak at the higher frequencies. Columns 1, 2, 3, 5, and 6 are the Active Columns; Columns 4, 7, and 8 are the Control Columns.

a)

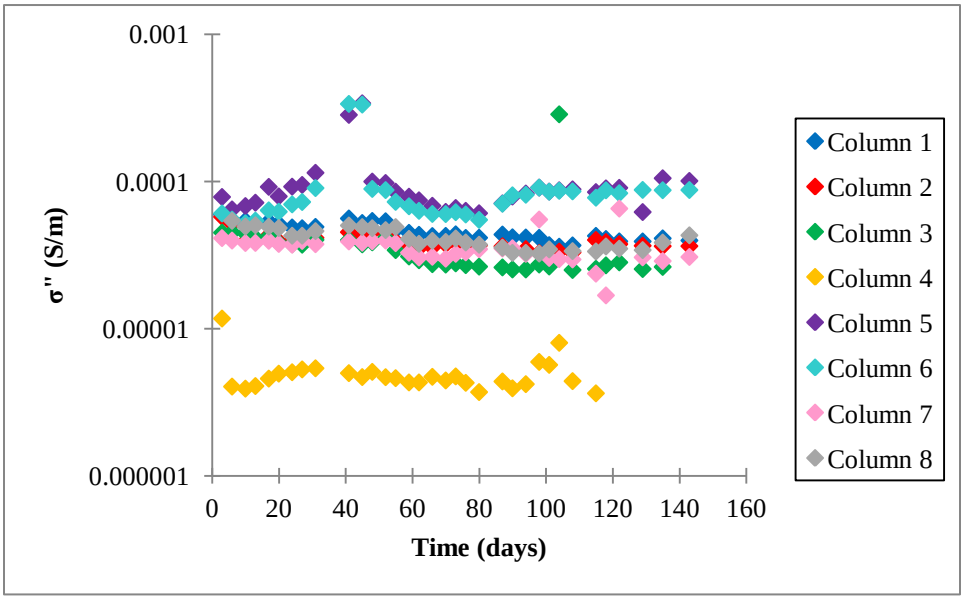

b)

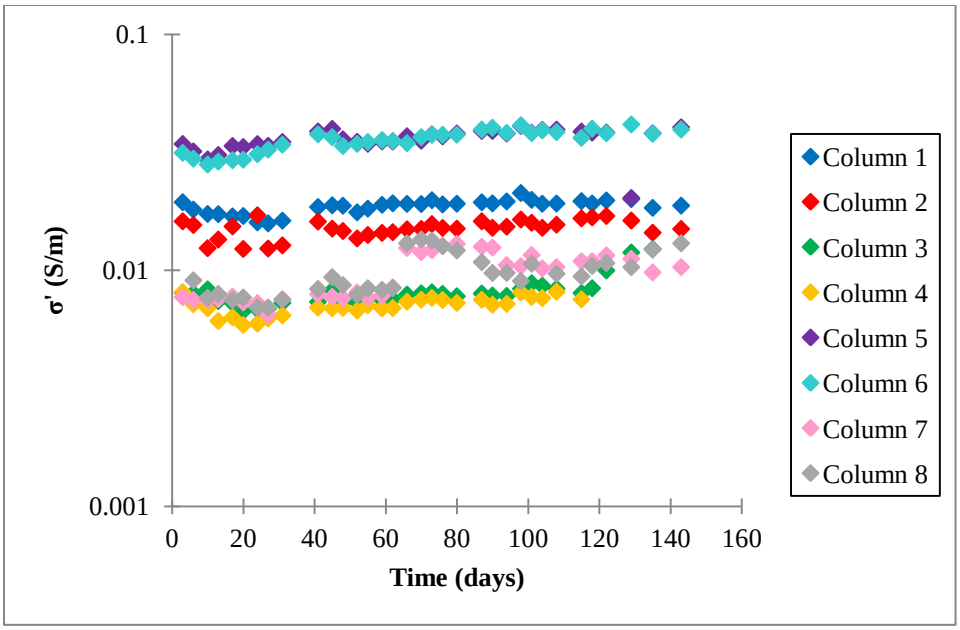

Figure A-5. a) Imaginary and b) Real conductivity at 10 Hz. The overall trends in each column are the same as that seen in Figures 5 and A-3 with a higher peak at the higher frequencies. Columns 1, 2, 3, 5, and 6 are the Active Columns; Columns 4, 7, and 8 are the Control Columns.

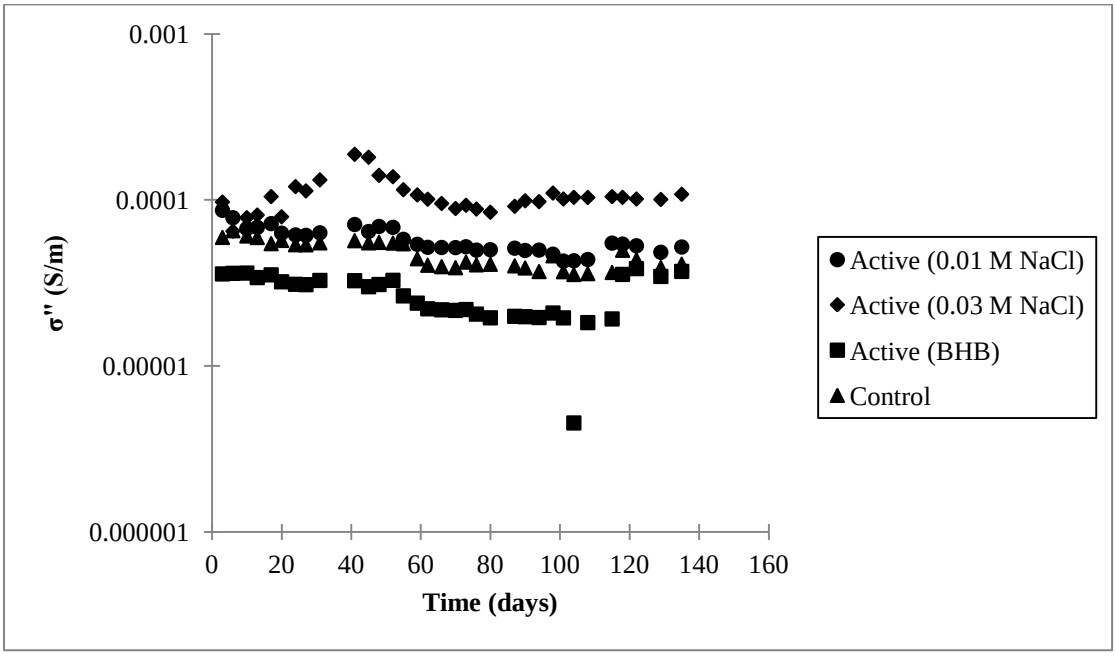

Figure A-6. Imaginary conductivity at the peak frequency (~0.1 Hz) for which replicate column data was averaged for each inflow solution. As shown previously, Columns 5 and 6 show an increase in imaginary conductivity to a peak at day 41 whereas the control columns show no appreciable change in conductivity.

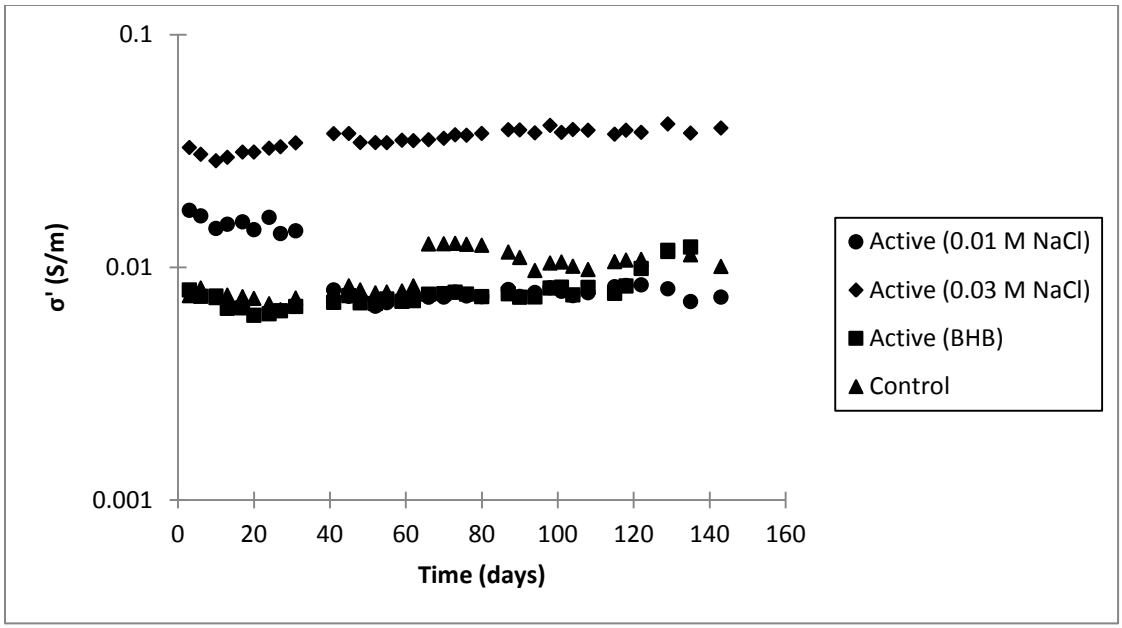

Figure A-7. Real conductivity at the peak frequency (~0.1 Hz) for which replicate column data was averaged for each inflow solution. Columns 5 and 6 show the most pronounced increase in real conductivity; Columns 1 and 2 show only a slight increase in real conductivity whereas the control columns show no appreciable change in conductivity.

a)

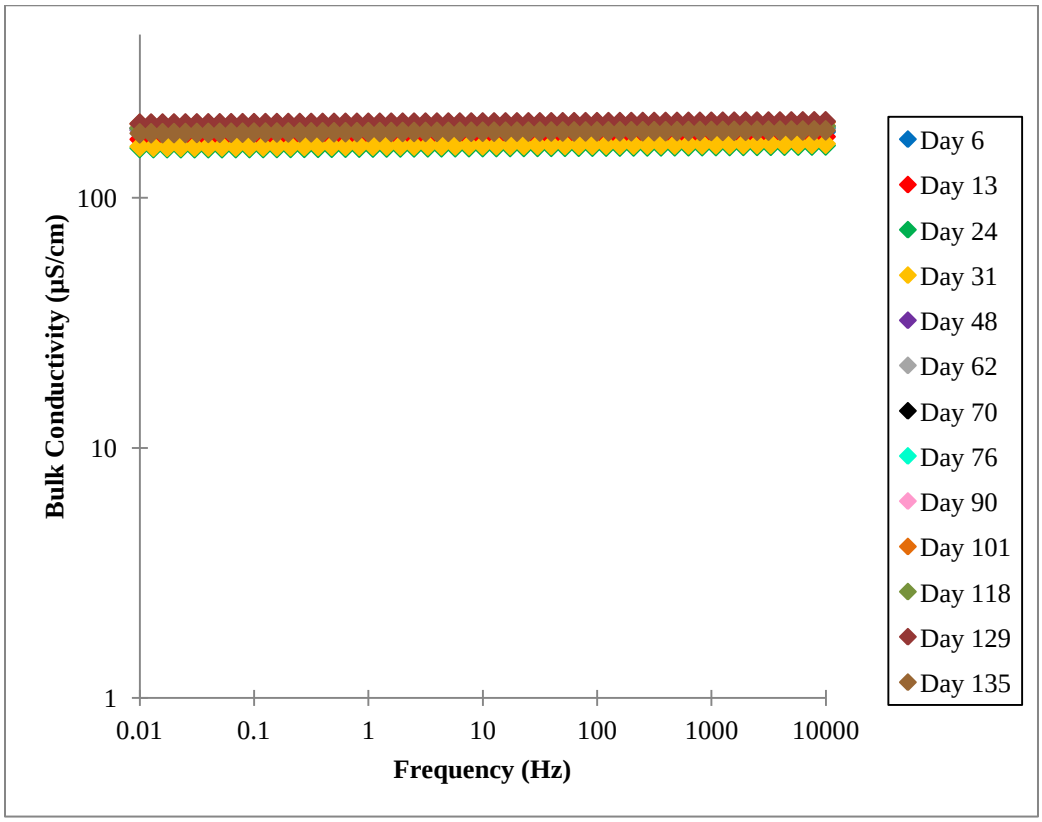

b)

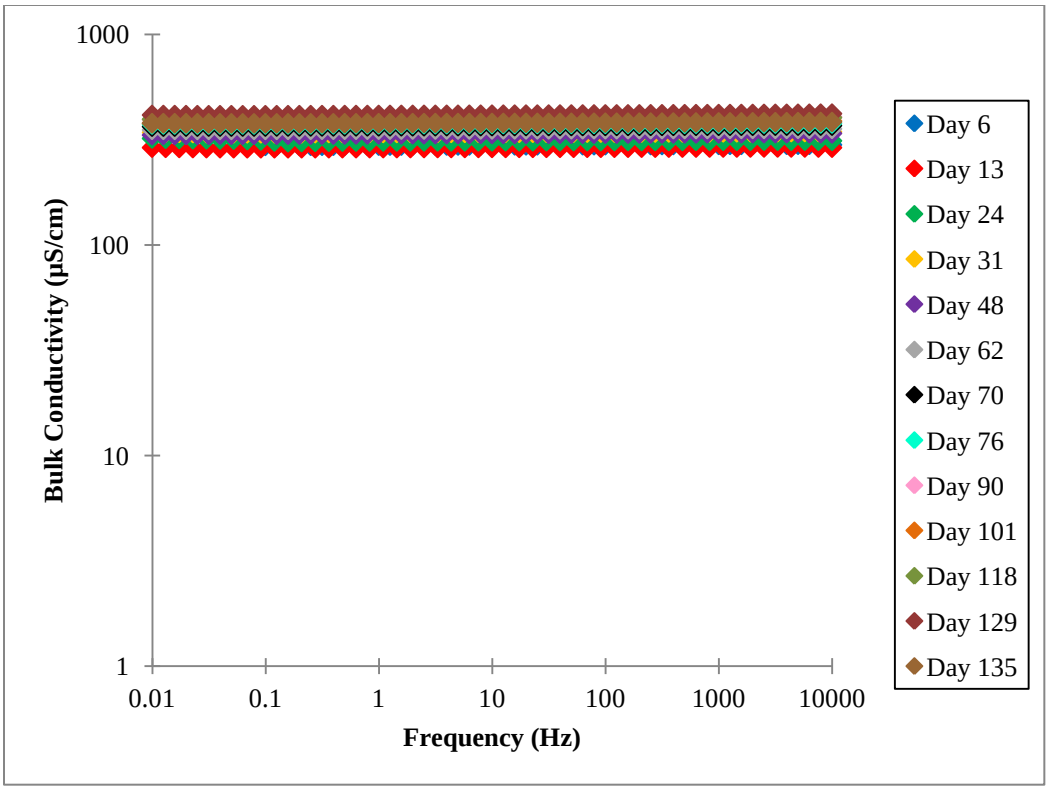
1000
100
10
1
Bulk Conductivity (µS/cm)
0.01
0.1
1
10
100
1000
10000
Frequency (Hz)
Day 6
Day 13
Day 24
Day 31
Day 48
Day 62
Day 70
Day 76
Day 90
Day 101
Day 118
Day 129
Day 135

c)

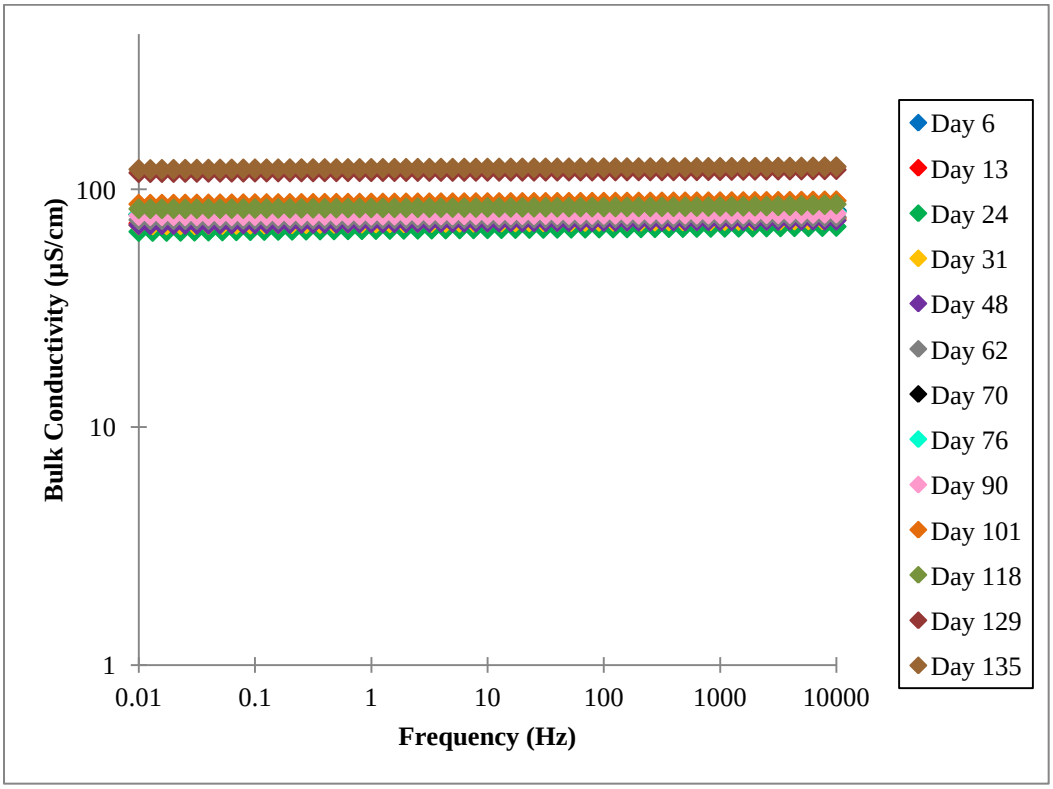
100
10
1
Bulk Conductivity (µS/cm)
0.01
0.1
1
10
100
1000
10000
Frequency (Hz)
Day 6
Day 13
Day 24
Day 31
Day 48
Day 62
Day 70
Day 76
Day 90
Day 101
Day 118
Day 129
Day 135

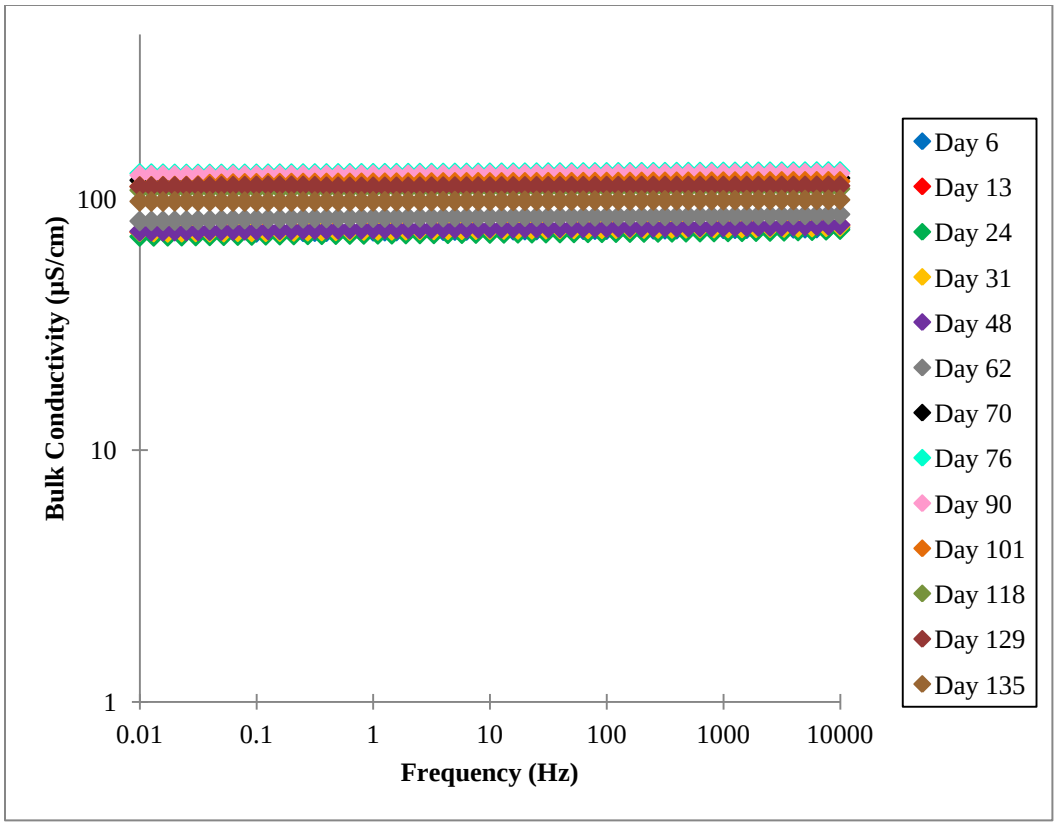

d)

Figure A-8. Bulk Conductivity data for each inflow solution over the entire frequency range. Plot a) is the 0.01 M NaCl and 25% Bushnell Haas broth solution, b) is the 0.03 M NaCl and 25% Bushnell Haas broth, c) is the 25% Bushnell Haas broth, and d) is the 0.1m M $HgCl_2$ and 25% Bushnell Haas broth. Columns 1, 2, 3, 5, and 6 are the Active Columns; Columns 4, 7, and 8 are the Control Columns.

Overall, the phase response at the peak frequency decreased throughout the course of the experiment for Columns 1, 2, 3, 7, and 8. As seen in Figure A-9, the control columns displayed the highest phase response, ~8 mRad, between days 10-27 and a low of ~3 mRad around day 70. The highest phase for Column 3 occurs at day 17 with a value of ~9 mRad and the lowest phase occurred at day 129 with a value of ~3 mRad (both values similar to those in the control columns). Again, Column 4 showed no appreciable change

in the phase response, likely due to the reasons mentioned above. Columns 1 and 2 showed a peak phase of ~5 mRad at day 3 and a low of ~2 mRad at day 101. Columns 5 and 6 however showed a gradual increase in phase response at the peak frequency up to day 41 where it reached ~5 mRad and then decreased throughout the remainder of the experiment reaching its lowest value of ~2 mRad (values similar to those observed in Columns 1 and 2). The peak frequency remained at ~0.1 Hz for all columns throughout the experiment.

Figure A-10 shows the phase response at the peak frequency for which replicate column data was averaged for each inflow solution. Figure A-11 shows the phase response over the entire frequency range and each inflow solution is plotted in the same scale to clearly illustrate the variations in phase data.

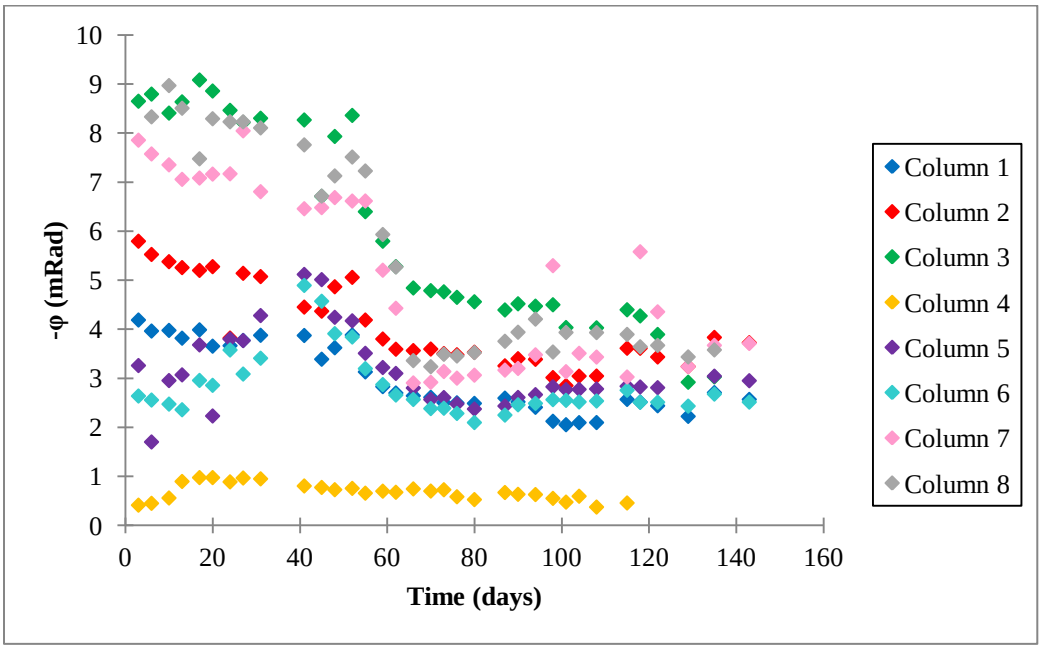

Figure A-9. Phase response at the peak frequency (~0.1 Hz). The phase response at the peak frequency decreased throughout the course of the experiment for Columns 1, 2, 3, 7, and 8 whereas Colum 4 showed no appreciable change in phase. Columns 5 and 6 showed an increase in phase to a maximum at day 41 after which it decreased throughout the remainder of the experiment. Columns 1, 2, 3, 5, and 6 are the Active Columns; Columns 4, 7, and 8 are the Control Columns.

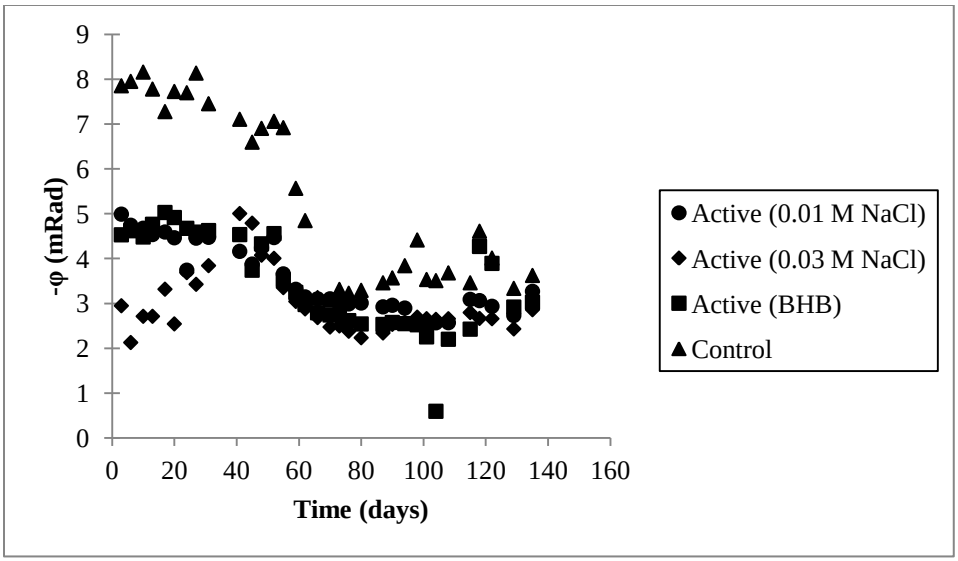

Figure A-10. Phase response at the peak frequency (~0.1 Hz) for which replicate column data was averaged for each inflow solution. Columns 1, 2, 3, 5, and 6 are the Active Columns; Columns 4, 7, and 8 are the Control Columns.

a)

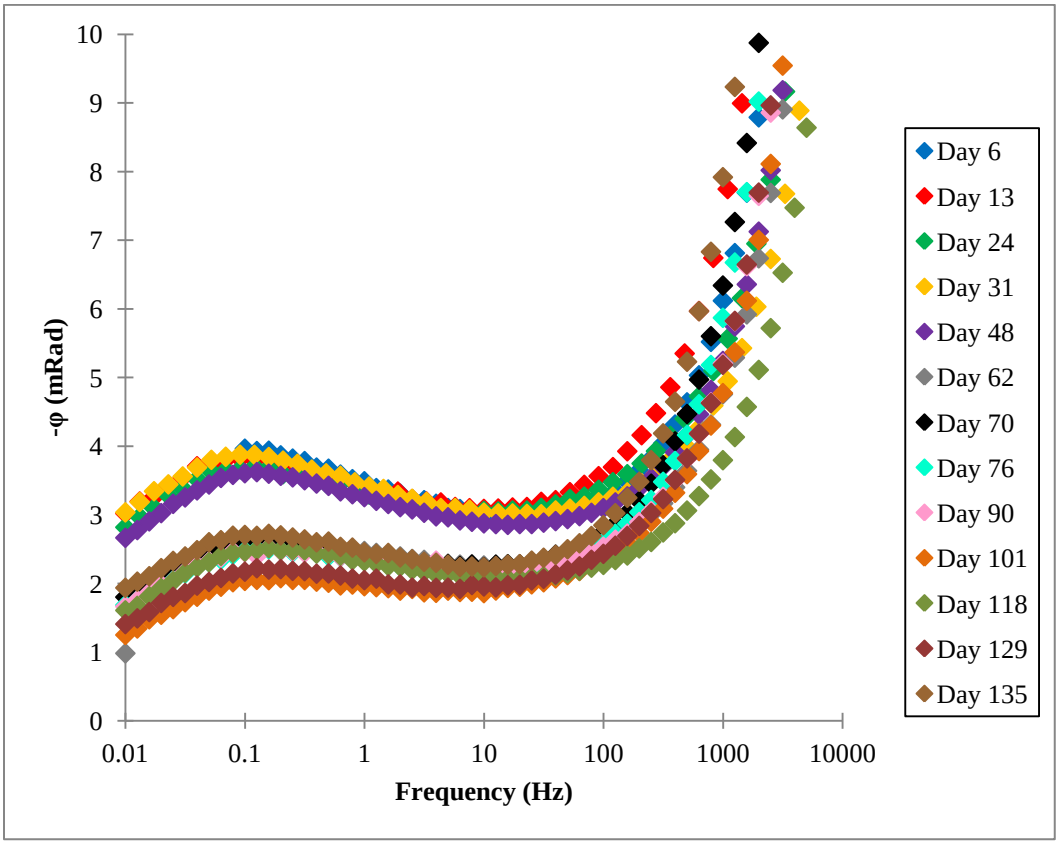

b)

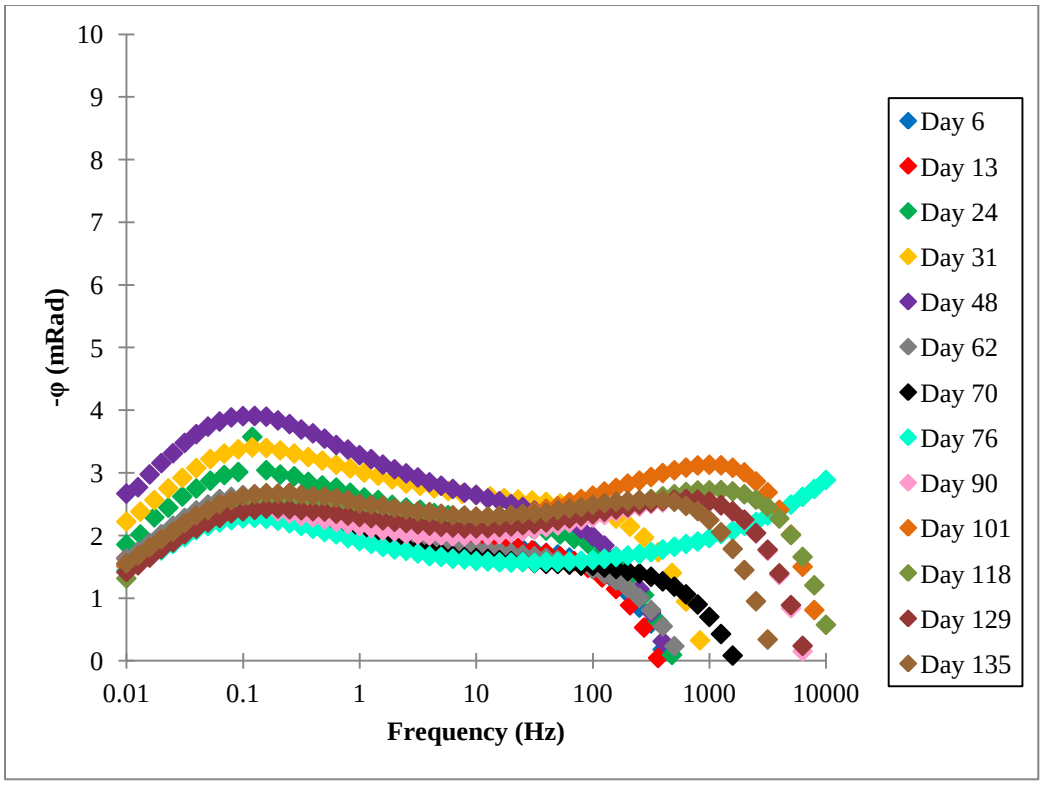
10
9
8
7
6
5
4
3
2
1
0
-φ (mRad)
0.01
0.1
1
10
100
1000
10000
Frequency (Hz)
Day 6
Day 13
Day 24
Day 31
Day 48
Day 62
Day 70
Day 76
Day 90
Day 101
Day 118
Day 129
Day 135

c)

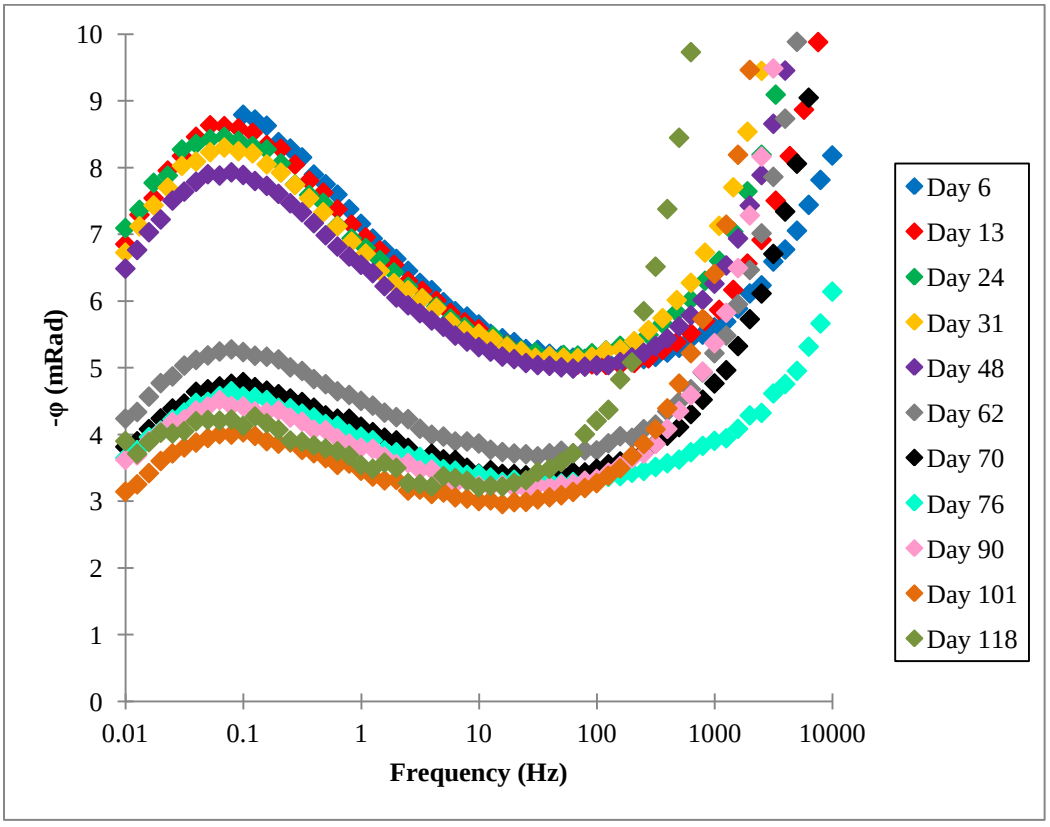
10
9
8
7
6
5
4
3
2
1
0
-φ (mRad)
0.01
0.1
1
10
100
1000
10000
Frequency (Hz)
Day 6
Day 13
Day 24
Day 31
Day 48
Day 62
Day 70
Day 76
Day 90
Day 101
Day 118

d)

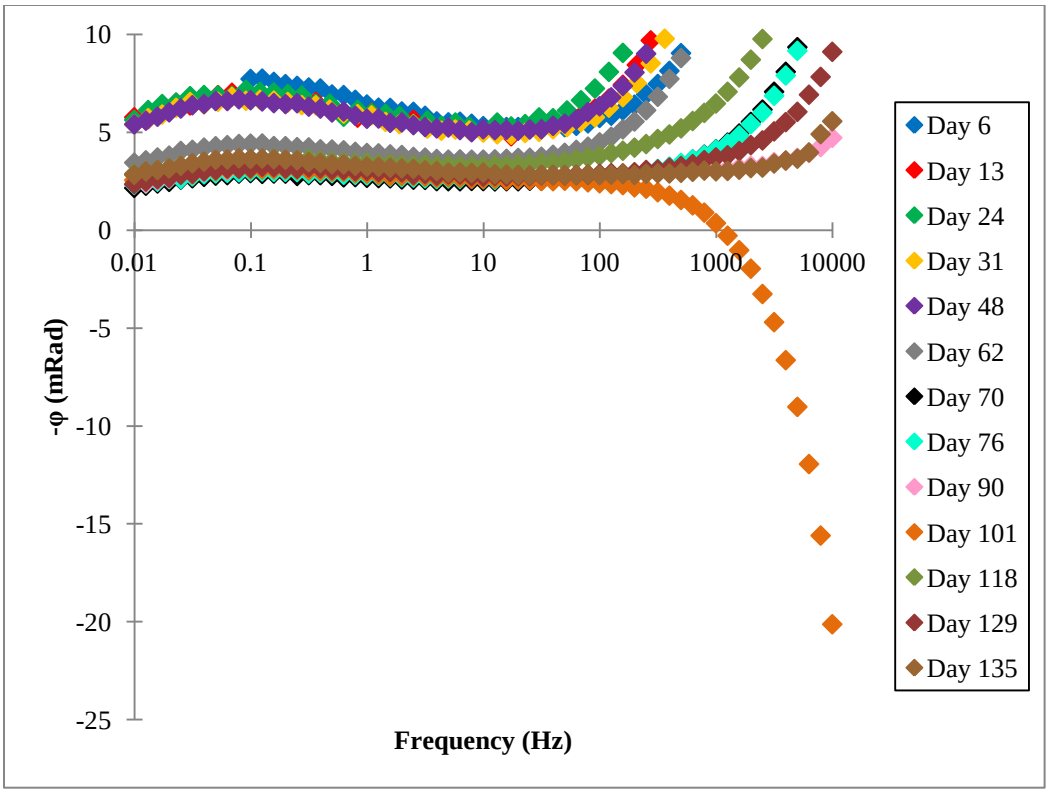

Figure A-11. Phase Response data for each inflow solution over the entire frequency range. Plot a) is the 0.01 M NaCl and 25% Bushnell Haas broth solution, b) is the 0.03 M NaCl and 25% Bushnell Haas broth, c) is the 25% Bushnell Haas broth *(no data available after Day 118 due to measurement difficulties)*, and d) is the 0.1m M $HgCl_2$ and 25% Bushnell Haas broth. Columns 1, 2, 3, 5, and 6 are the Active Columns; Columns 4, 7, and 8 are the Control Columns.